INVESTIGATION OF THE PVDF BASED ENERGY CONVERSION DEVICE

by

Michael Y. Leshchiner

Diploma in Mechanical Engineering
Ukrainian State Marine Tech. University, 1995

Submitted to the Department of Mechanical Engineering
in Partial Fulfillment of the Requirements for the Degree of

Master of Science in Mechanical Engineering

at the

MASSACHUSETTS INSTITUTE OF TECHNOLOGY

June 1998

Signature of Author _____
Department of Mechanical Engineering
May 22, 1998

Certified by _____
Professor John G. Brisson
Department of Mechanical Engineering
Thesis Supervisor

Accepted by _____
Professor Ain A. Sonin
Chairman, Department Committee on Graduate Students

INVESTIGATION OF THE PVDF BASED ENERGY CONVERSION DEVICE

by
Michael Y. Leshchiner

Submitted to the Department of Mechanical Engineering
on May 22, 1998 in Partial Fulfillment of the Requirements for
the Degree of Master of Science in Mechanical Engineering

ABSTRACT

James Scott Strachan, currently a director of Optical Metrology Ltd., located at the University of Edinburgh, Scotland and Harold Aspden, senior research fellow at the University of Southampton, England, have recently reported a polyvinylidene fluoride (PVDF) based energy conversion device that allowed for the thermo-electro-mechanical energy conversion with the efficiencies up to 73 % that of Carnot limit.

An experimental study was performed to determine the possible mechanisms for the energy and entropy transport within the device and explain the existence of the energy conversion effect. For that purpose the replica of the Strachan - Aspden's prototype device was built. It was assembled in series-parallel capacitor arrangement utilizing about two hundred layers of PVDF, coated on one side with nickel and aluminum.

The present study presents the constructional and operational details of the replica device. The single PVDF layer experiments are performed to check the hypothesis of the device operation. The cyanoacrylate bonding technique is developed to construct the PVDF stacks similar to those described by Strachan. A high power electrical drive circuit is designed and series of tests are performed to test the device in various modes of operation.

No anomalous effects related to the energy conversion are observed and none of the Strachan's reported results are confirmed. Possible explanations for the Strachan - Aspden's energy conversion device operation are reviewed, but no satisfactory explanation has yet come to light.

Thesis Supervisor: John G. Brisson

Title: Assistant Professor of Mechanical Engineering

ACKNOWLEDGMENTS

I am sincerely grateful to my advisor, Professor John G. Brisson for his patient guidance of this work, who no matter how busy he was, always had time for me and whose helpful participation in this project is almost impossible to overestimate.

I also want to thank my second advisor, Professor Joseph L. Smith, who could always help with a practical advice in any situation during the course of this research project.

I would like to express my gratitude to Dr. Joseph Gerstmann, who was essentially my third advisor and who provided a necessary experimental base at AMTI.

Special thanks are due to John Cox, electronics engineer at AMTI, who answered a lot of my questions and helped to design and build electrical equipment for testing the device.

I recognize the staff of AMTI for creating a pleasant environment for carrying this work.

Grateful acknowledgment is made to Doug MacBride, who started this project and shared a lot of useful information about his experience with the device.

I am very thankful to Doris Elsemiller for her caring personality and who helped to make my life at MIT a little easier.

Special recognition should be given to Brian Bowers and Ashok Patel, graduate students at Cryogenics Lab, from whom I learned lots of practical and computational engineering tools.

Finally, my wife Natasha deserves the deepest appreciation for her constant support, patience and encouragement throughout this work, and who directly participated in creation of this manuscript.

TABLE OF CONTENTS

LIST OF FIGURES

LIST OF TABLES

NOMENCLATURE

A = area, m^2

b = damping coefficient, $\frac{N \cdot s}{m}$

C = capacitance, Farad

c_{ij} = elastic modulus, N/m^2

D = electric displacement, V/m

d_{ij} = piezoelectric strain or charge constant, m/V

E = electric field, V/m

e_{ij} = piezoelectric strain or charge constant, $\frac{Coul/m}{m/m}$

F = force, N

f = frequency, Hz

g_{ij} = piezoelectric stress constant, $\frac{N/m}{V/m^2}$

h_{ij} = piezoelectric strain constant, $\frac{N/m}{V/m^2}$

i = current, Amperes

k = thermal conductivity, W/m-K; effective spring constant, N/m

K = thermal conductance, W/K

l = thickness, m

L = inductance, Henry

m = mass, kg

N = number of turns

n = refractive index,

p = pyroelectric coefficient, $Coul/m^2$-K

P = pressure, N/m^2; polarization, C/m^2

Q = rate of heat transfer, Watts; acoustic quality factor

q = electric charge, Coul

R = electrical resistance, Ohms

S = entropy, J/K

s_{ij}^{E} = elastic constant short circuit, m^2/N

s_{ij}^{D} = elastic constant open circuit, m^2/N

T = temperature, K

T_m = melting temperature, °C

t = time, sec

V = voltage, V

ν = specific volume, m^3/kg

v_S = speed of sound, m/s

W = work, J

X = strain, m/m

x = spatial coordinate, m

Δx = elongation, m

Y = Young's modulus, N/m^2

Z = thermoelectric figure of merit, K^{-1};

Z_a = acoustic impedance, kg/m^2;

Z_e = electric impedance, Ohm

α = Seebeck coefficient, V/K

β = volume thermal expansion, K^{-1}

ε = dielectric constant, F/m;

ξ = dumping factor

ς = Poisson ratio

μ = Dipole moment, Coul-m

Π = Peltier heat, W/A

η = efficiency, %

ρ = density kg/m^3; resistivity Ohm/m

τ = stress, N/m^2

ω = angular frequency, rad/s

1. INTRODUCTION

James Scott Strachan, currently a director of Optical Metrology Ltd., located at the University of Edinburgh and Harold Aspden, senior research fellow at the University of Southampton have recently reported the development of thermo-electro-mechanical device with the efficiency several times higher then the maximum achievable efficiency of conventional semiconductor thermoelectric devices. [1,2,13,14] The device was assembled in series-parallel capacitor arrangement, utilizing several hundred layers of dielectric sheet substrate polyvinylidene-fluoride (PVDF) coated on one side with nickel and aluminum. Strachan and Aspden claim that PVDF stack can generate electric power, when exposed to a temperature gradient and connected to a properly tuned electrical circuit and conversely can work in a heat pump mode, when subjected to an appropriate AC excitation.

The object of the studies discussed in this thesis was to find evidence for and confirm the energy conversion effects reported by Aspden and Strachan. The effect was discovered serendipitously and it is clear that the inventors are unable to fully explain the behavior of their device. Aspden feels that the thermoelectric effects play the most important role in the energy and entropy transport mechanism. However, since PVDF material itself possesses strong piezoelectric and pyroelectric properties and existence of the bimetallic coating makes it also thermoelectric, the coupling of these three effects may provide an explanation for the observed energy conversion.

Chapter 2 of this thesis is a discussion of the constructional and operational details of three devices reported by Strachan and Aspden in their publications. Their discussions in the literature are often confusing and incomplete. The discussion of Chapter 2 is the result of several conversations and correspondences with Strachan concerning the specifics of three devices he built.

Chapter 3 is an overview of thermoelectricity, piezoelectricity and pyroelectricity. The magnitudes of these energy conversion effects are discussed and compared to the reported performance of Strachan's device. Chapter 4 presents the discussion on piezo- and pyroelectric qualities of PVDF.

The building of the PVDF device was quite challenging. Chapter 5 discusses in detail the development of the recipe to build the multilayer PVDF elements used in the device. Chapter 6 discusses the drive electronics for device and the experiments that were performed on the MIT replica of Strachan's device. In addition the mechanical behavior of the device is modeled and the expected primary resonance frequencies of the stack are found and compared with the measured values. The conclusions of the performed work are presented in Chapter 7.

The replica discussed in this work, to the author's knowledge, is a faithful reproduction of the Strachan's device. In addition the large electrical drive amplitudes that Strachan used in his devices are duplicated in this work. No anomalous behavior in the PVDF stack was observed and no evidence of energy conversion was found.

2. THE STRACHAN - ASPDEN SOLID STATE ENERGY CONVERSION DEVICE

2.1 Introduction

Strachan observed the energy conversion effect with PVDF while he was testing an ultrasonic lithotriptor, a mechanism for shattering kidney stones in human body. At that time, he was working on an idea of a sonic "laser", a device designed to progressively amplify a traveling wavefront, that would allow for a creation of a high intensity ultrasonic pulse. This traveling wave amplifier was constructed of several hundred layers of thin bimetallic coated PVDF film and was driven acoustically by PZT driver. While working on the device Strachan discovered that it would produce a large voltage spike and destroy the drive circuit electronics when a temperature gradient was imposed across the PVDF stack. Such behavior has not been observed before. This led him to suspect that he discovered an unknown energy conversion effect and prompted further research.

This chapter describes the constructional and operational details of the three prototype devices, built by Strachan to study the energy conversion mechanism. It should be noted that most of the information Strachan and Aspden provided about their experiments was incomplete and often inconsistent. The author's best understanding of their experiments and results is presented here.

2.2 Strachan's Prototype Devices

There were three prototype devices built by Strachan. They all operated with different switching techniques and different design frequencies. All three devices performed remarkably well and showed the efficiencies much higher than that of conventional thermoelectric devices.

The first PVDF device constructed by Strachan contained 500 layers of 28 μm thick PVDF film coated on one side with a 2200 angstrom thick nickel layer and a 800 angstrom thick aluminum layer. It was assembled in 25 PVDF elements in a parallel

capacitor arrangement. Each PVDF element was made of approximately 20 PVDF layers.

The PVDF stack was constructed using ethyl cyanoacrylate adhesive to bond all the surfaces. The PVDF layers and BASF iron oxide recording tape were laminated together layer by layer, as shown in Figure 2.1.

PVDF surfaces and recording tape were treated with a 2% solution of tetrabutyltitanate (TBT) in petroleum ether in an arid atmosphere. After the petroleum ether was allowed to evaporate completely, the surfaces were exposed to a 100% humidity atmosphere at 40 °C. The surfaces were then washed with petroleum ether.

The reason for such a thorough surface preparation is that the polymerization of cyanoacrylates, being inhibited by a low pH (high acidity) does not proceed satisfactorily[28], i.e. at pH below 7 the PVDF surface can release free protons and thus prevents secure bonding. As postulated by Strachan,[3] the titanate layer helps to maintain pH above 7 on the surface, allowing the ethyl cyanoacrylate adhesive to cure more easily.

A Teflon coated lamination jig was used in the construction of the stack. As each layer was added, a press was applied to the jig with a force of 1-6 metric tons.[3] The PVDF layers and BASF tape were laminated together layer by layer to reach a thickness of 0.55 mm, an acoustic half-wave resonant thickness at 2 MHz. Each element was subjected to a test voltage of 5000 V to detect errors in fabrication (electrical shorting between layers, improper bonding, etc.).[3] The elements that failed this test were discarded.

Each element was then bonded to a thin copper leads with electrically conductive epoxy and then laminated to a layer of hard acrylic, as shown in Figure 2.2. Acrylic was machined to a thickness, corresponding to a half-wave resonance at 2 MHz. The process continued until a large number of "good " PVDF-acrylic elements were produced.

Following this, about twenty PVDF-acrylic elements were laminated together to form a PVDF-acrylic stack and an acoustical driver, a ceramic PZT type 5-A with silver electrodes was added to the structure as shown in Figure 2.3. The PZT transducer and each PVDF element except one, a "listener", were driven with a conventional high voltage AC signal generator. The listener element was connected across oscilloscope. Strachan observed voltage spikes of several thousand volts superimposed on listener's output voltage, when temperature gradient was applied in the 2.5 mm direction across the

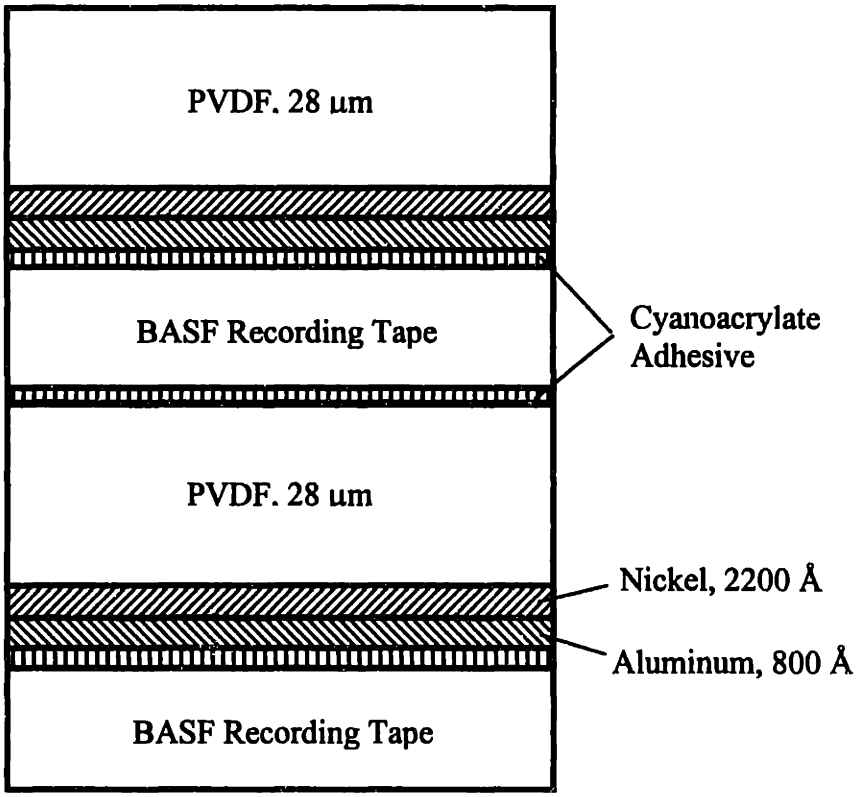

Figure 2.1. The assembly of individual PVDF layers with magnetic tape.

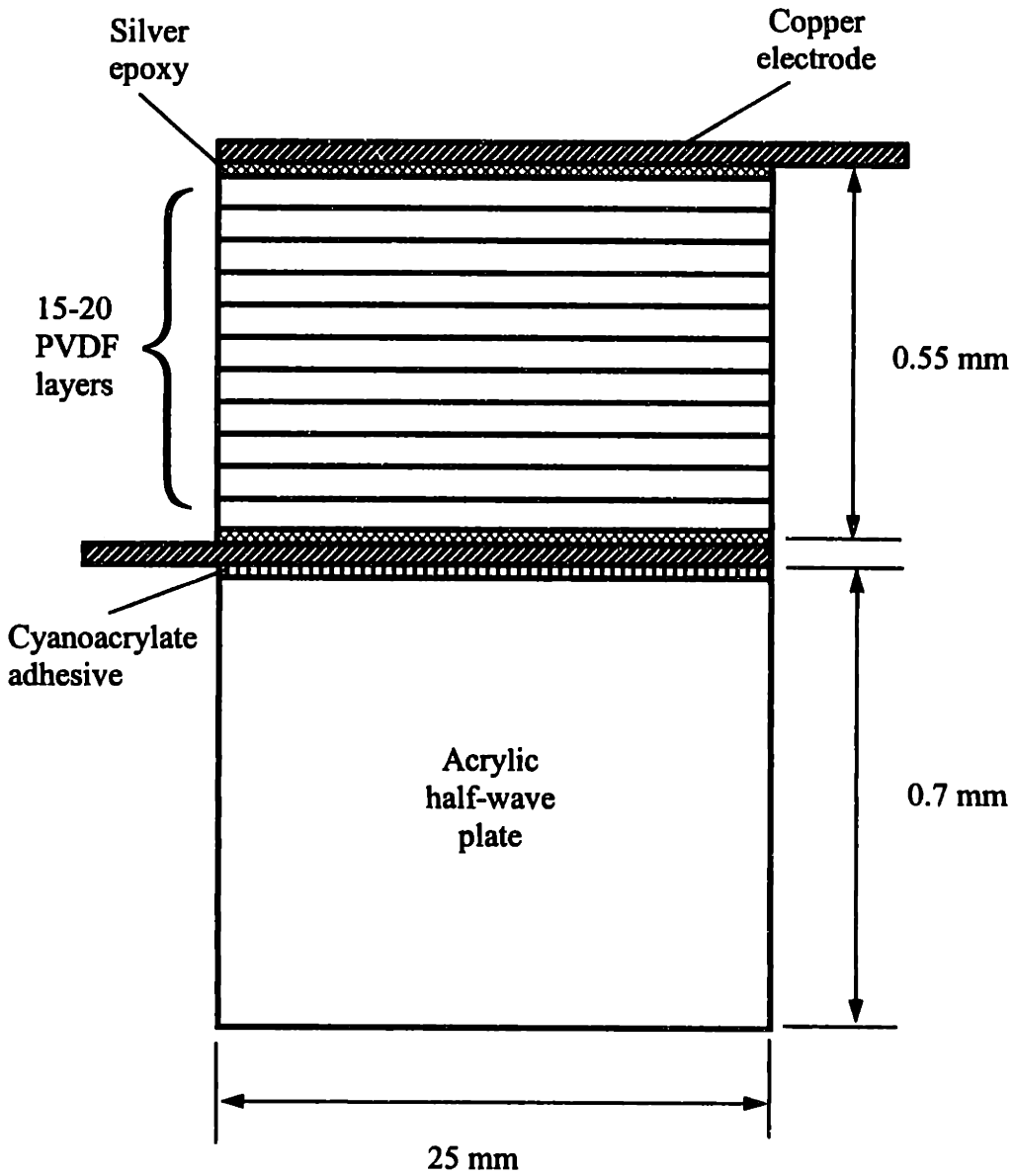

Figure 2.2. Schematic of the PVDF - Acrylic unit cell (not to scale). Thickness is 2.5 mm into the page

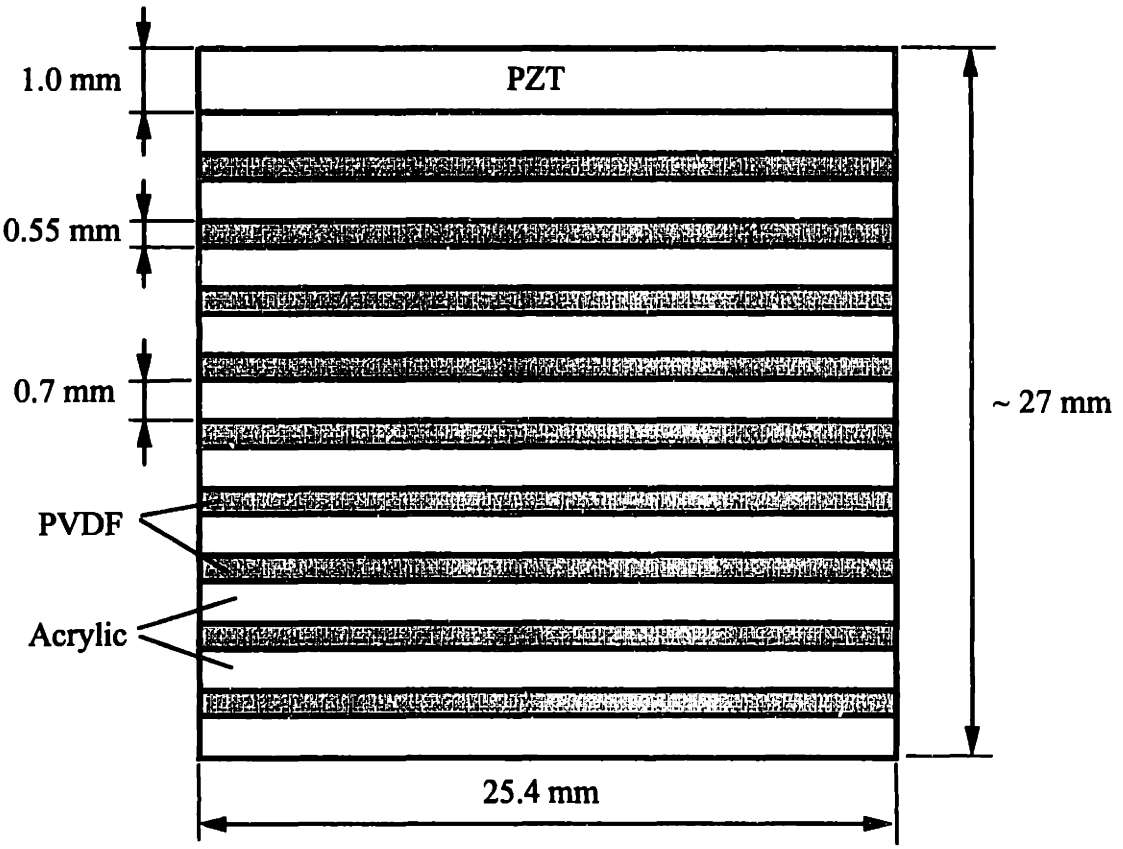

Figure 2.3. Schematic of the prototype device stack layout, incorporating PZT and 20 PVDF - Acrylic unit cells. The thickness of the stack is 2.5 mm into the page.

stack. A sketch of the PVDF output voltage, observed by Strachan, versus time is shown in Figure 2.4.

The spikes would shift phase by 180° when the direction of the temperature gradient was reversed. The time duration of one spike was approximately 20 nanoseconds and the maximum energy output of the spike was measured to be 5×10^{-8} Joules, when a temperature difference of 70°C was applied across the stack. The graph of Figure 2.4 is generated based on Strachan's unpublished written description.[3] No actual data is available on this matter.

The first prototype device was capable of working in both heat pump and power generation modes. When operating in power generation mode, the piezoelectric stack was connected through a transformer to a germanium diode rectifier and a DC load as shown in Figure 2.5. VMOS switch was triggered by Strachan's triggering circuit. When temperature gradient was applied across the stack the device would self-oscillate and DC power could be generated by the circuit.[4] No experimental results are available for the first prototype device. An attempt to chemically unbond the device from the heat sink resulted in corrosion which destroyed the device.

The external circuit for device operating in refrigeration mode is shown in Figure 2.6. The PZT driver and PVDF are coupled both acoustically in the stack and magnetically in the transformer. In addition, the transformer couples the high voltage piezoelectric circuit to low voltage circuit containing 7.2 V battery and VMOS switch GE - F15N05L, triggered by triggering circuit. The circuit would self-oscillate when powered by battery voltage and would cool down one side of the stack. The specifics of triggering circuits used by Strachan is unknown.

The second prototype device was constructed with PVDF elements similar to that of Figure 2.1, except that BASF recording tape was not included and metal layers were 400 and 200 Angstroms thick for nickel and aluminum respectively. In addition, no PZT driver was incorporated into the stack. The SCR switch was driven by externally powered signal generator, so the operating frequency could be controlled. The device contained 300 PVDF layers and was designed to operate in power generation mode only. The experimental setup for the second prototype device is shown in Figure 2.7. Strachan reports[5] that when the device operated between temperatures 47.5 °C and 20.8 °C with a

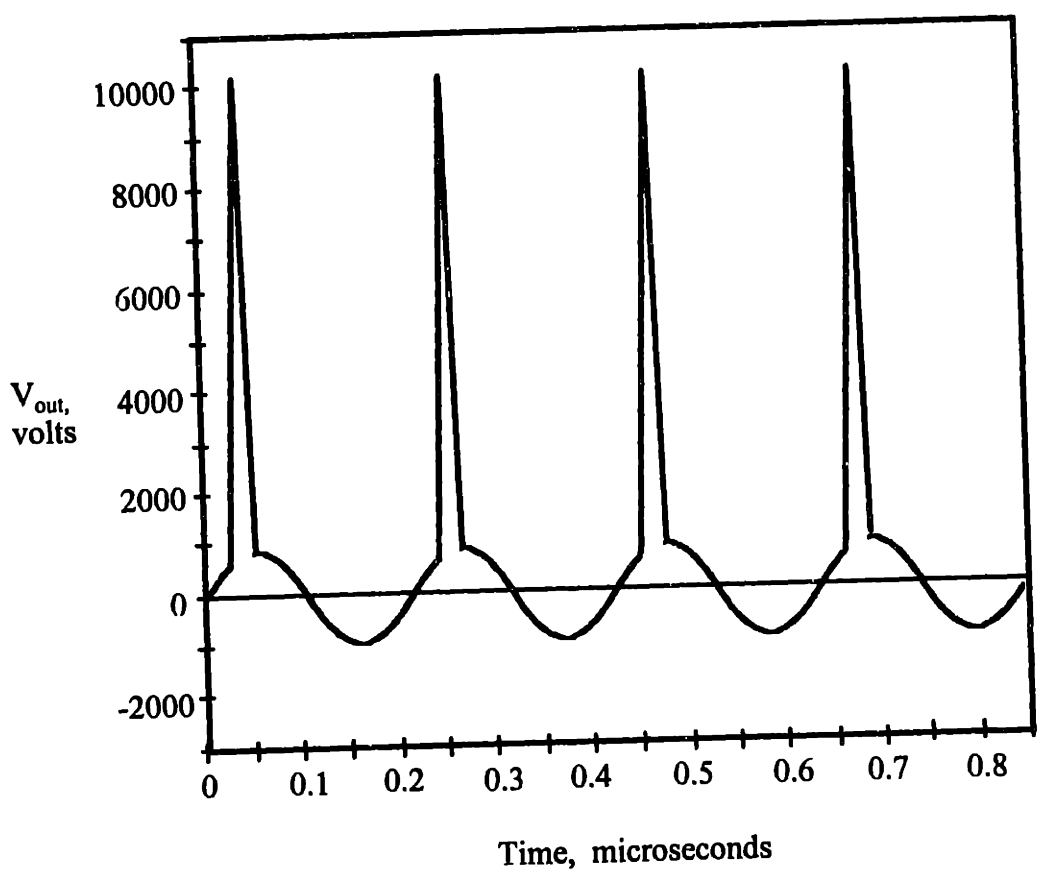

Figure 2.4. Schematic of Strachan's observations of the device voltage output, when a temperature gradient was applied across the stack. Adapted from Strachan [3].

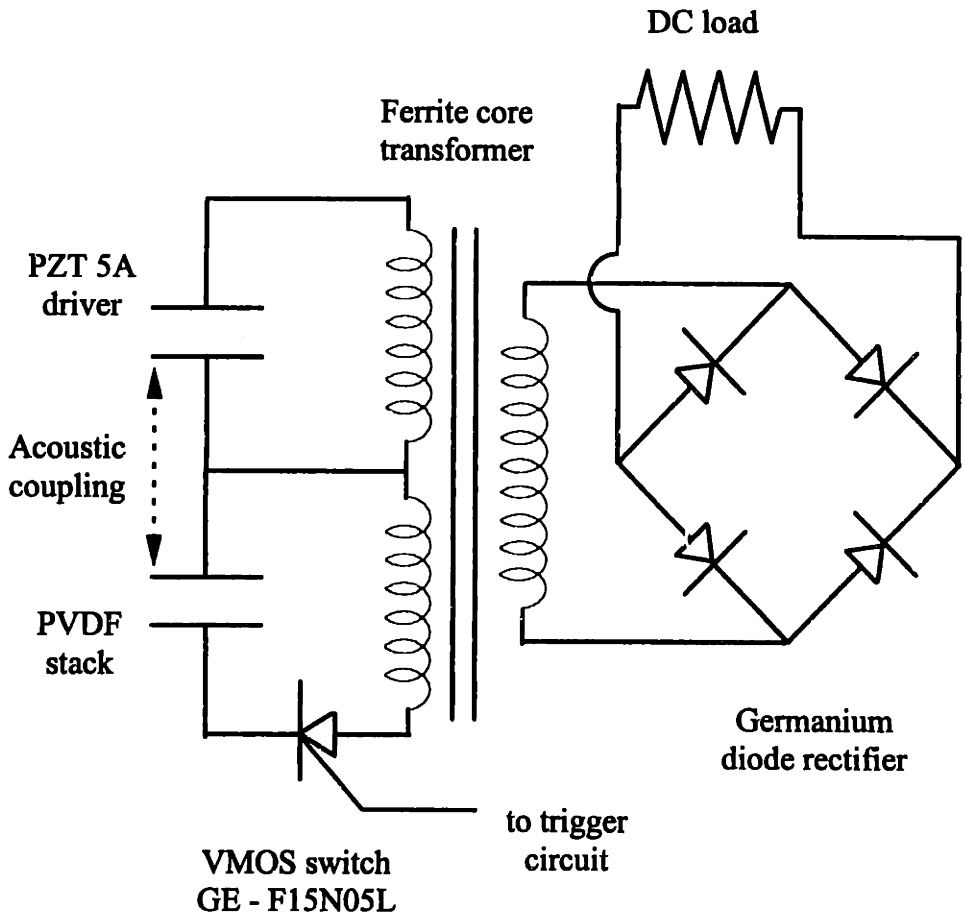

Figure 2.5. Circuit for power generation mode for the first and third prototype devices.

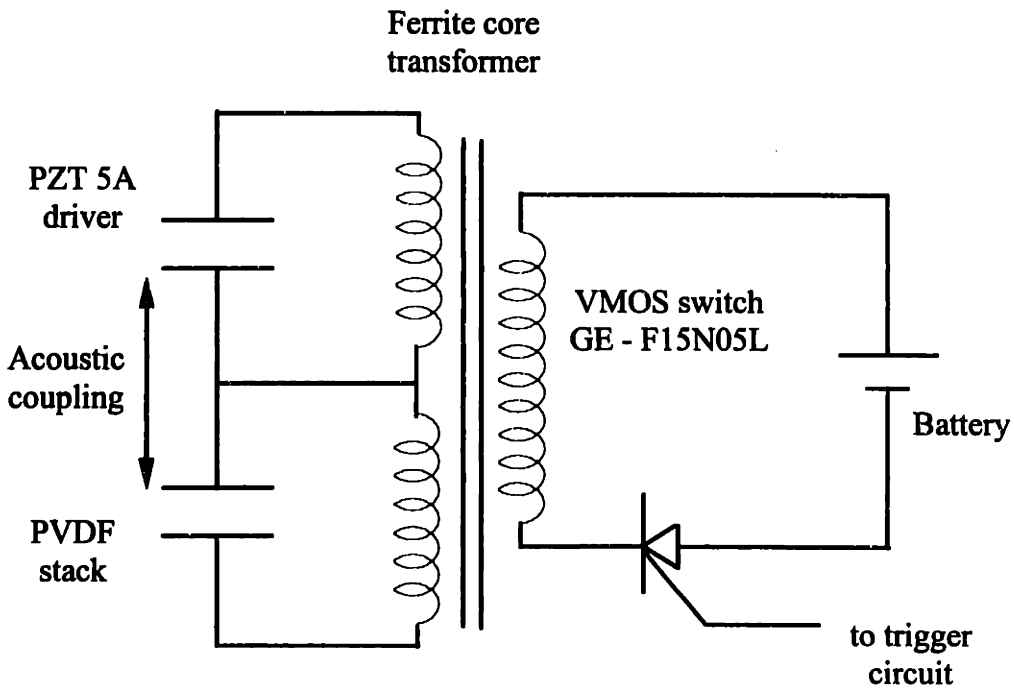

Figure 2.6. Circuit for heat pump mode for the first and third prototype devices.

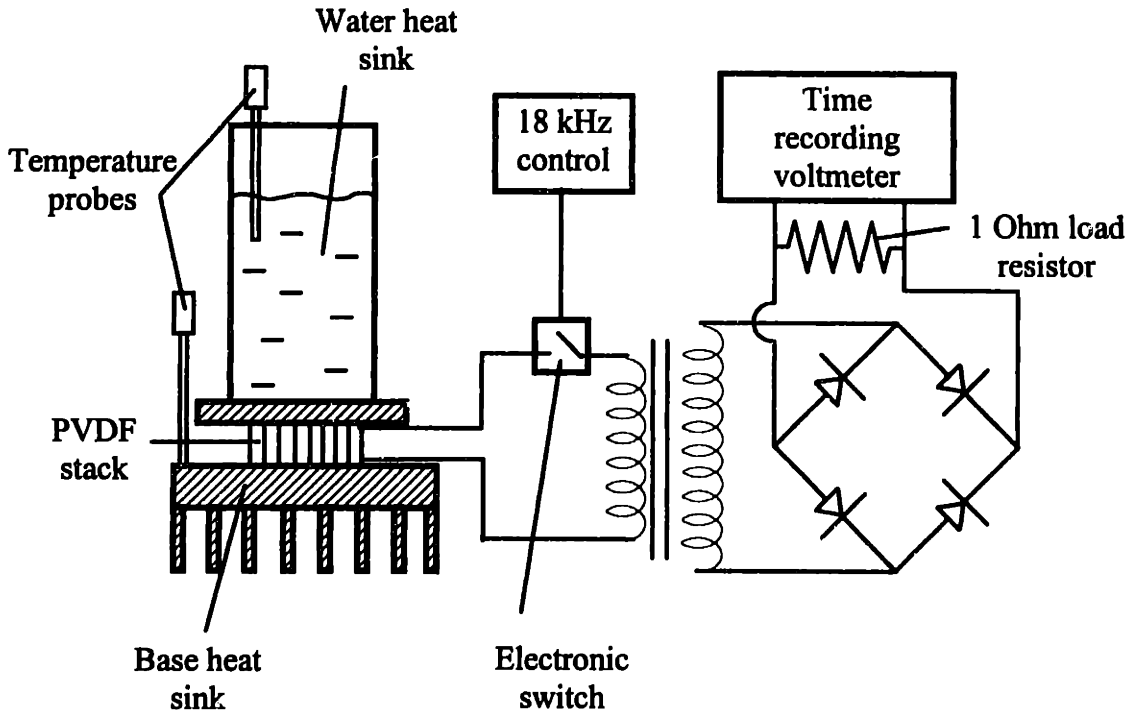

Figure 2.7. Schematic of the experimental setup for the second prototype device. Adapted from Aspden[5].

thermal input power of 3.34 Watts, the net power output into 1 Ohm resistor is 0.202 Watts, which corresponds to efficiency $\eta_{actual} = 0.06$. The Carnot efficiency for the same temperature difference is $\eta_{Carnot} = 0.083$. Therefore the second law efficiency of the device was 72.5 % of Carnot. The second prototype device was the most efficient of the three devices.

The third device was similar in structure to the first device. It had magnetic tape, a PZT driver and it could also operate in both heat pump and power generation modes. Switching between two modes of operation was achieved by exchanging the rectifier circuit leads between DC motor and the battery. The device had an SCR switching circuit which was self-tuning and ran as an oscillator powered by the melting ice in power generation mode or drawing on a battery supply in refrigeration mode.[1] The tests performed on the device indicated the overall performance in refrigeration mode to be 47% of Carnot efficiency and 21% of Carnot efficiency for power generation mode.[1]

In refrigeration mode, 3 milliliters of water froze in the device in 73 seconds[1]. For temperatures of hot and cold heat sinks T_H = 26 °C and T_C = 0 °C respectively and electrical power input of 6.3 Watts the cooling power was 13.7 Watts.[1] This represents a coefficient of performance of 2.17 or 21% of Carnot efficiency for the same temperature limits.

In power generation mode 6 milliliters of water ice was melted on the cold heat sink , while the hot heat sink was kept at T_H = 26 °C. For thermal throughput of 3.7 Watts generated electrical power was 0.15 Watts.[1] This corresponds to overall efficiency of 47% of Carnot value.

2.3 Strachan and Aspden's Explanation for Device Operation

Strachan and Aspden published several hypothesis for possible mechanisms for the energy conversion observed in their device. These hypotheses, in the view of the author, are weak and do not explain the reported effects. They are presented here for completeness and reflect the author's best understanding of their explanation.

The PVDF material that was used for the construction of all three prototype devices was coated with bimetallic coating composed of nickel and aluminum films, thus forming a parallel plate capacitor. The application of the potential difference between the stack's leads will result in AC excitations in the thickness direction. On the other hand the applied temperature gradient will produce some thermoelectric action in nickel and aluminum, metals having opposite polarity Seebeck effects. (For a discussion on thermoelectric effects see Chapter 3.) The temperature differential induced between the edges of PVDF layers will activate the Seebeck effect and produce thermoelectric DC current. This current will cross the bimetallic junctions at the interface in the opposite directions creating a closed circuit within nickel-aluminum interface, as shown in Figure 2.8. The current flow through the metal junctions will result in Peltier cooling on one side and heating on the other. According to Aspden, when AC and DC are superimposed on each other there is cooling due to Peltier action at the cold junction for one half of the AC cycle and heating due to the Peltier effect at the hot junction for other half of the cycle. Aspden suggests that in alternate half cycles of the AC, oscillating current flow operates to block the thermoelectric DC flow at one or another of the thermocouple junctions, therefore separating the Peltier cooling and heating on the respective sides of the device.

Although Aspden postulates that high efficiency energy conversion in the device is possible due to the combination of thermoelectric effects, the calculations based on conventional theory of thermoelectricity show that the maximum achievable temperature difference, that can be supported by a nickel-aluminum thermocouple is less then a degree in the given temperature range. Aspden also suggests the existence of transverse AC excitation will trigger the thermoelectric effects and increase the device efficiency. No indication of this effect is found in literature and no experimental evidence in this study supports this conjecture.

Another of the Aspden's hypotheses postulates the existence of the "cold spots" in the thermocouple junctions[14]. These cold spots can be present in high conductivity materials. In contrast to semiconductors, whose resistivity decreases with increasing temperature, the resistivity of base metals decreases with decreasing temperature. According to Aspden, at some points in the junction interface between two metals at which Peltier cooling is occurring, there is a concentrated cooling action confined to that

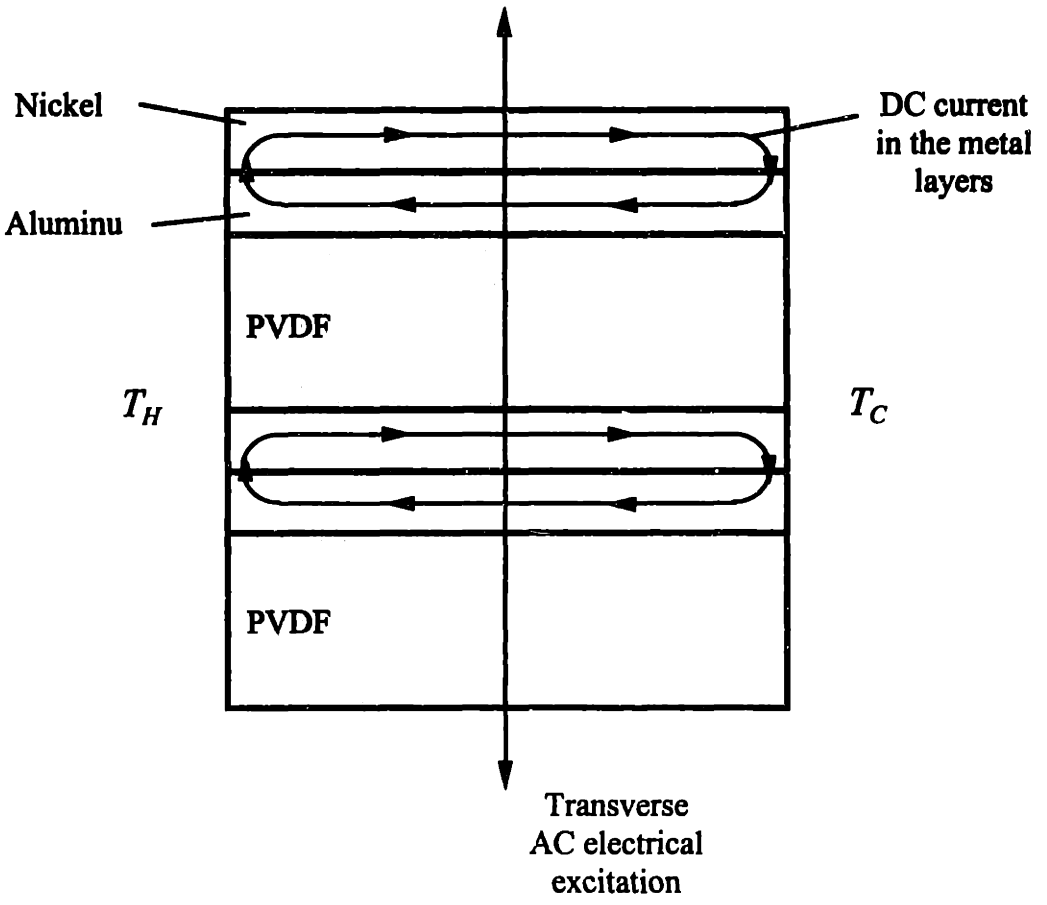

Figure 2.8. The components of the current flow in metal junctions of the stack.

interface. [14] That tends to produce the spots with the lower electrical resistance and the thermoelectric current tends to form a filamentary path and cross the hot junction at a temperature much lower then T_H, reducing the temperature difference between two junctions and therefore, suppressing the thermoelectric cooling action. Aspden feels that Strachan and he avoided the formation of cold spots and increased the device efficiency by means of switching the current on and off so rapidly that the current filaments do not form.[14]

2.4 Summary

Strachan and Aspden, have reported that they built and tested three prototype thermoelectric devices of very high efficiency. The best of those three devices achieved the second-law efficiency of about 73 %. Although Aspden feels that thermoelectric effects play the most important role in the energy conversion, it is a well known fact that the efficiencies of modern conventional thermoelectric devices are less then 20 % of the Carnot value. Strachan-Aspden's devices significantly outperformed the conventional thermoelectric devices.

Strachan's and Aspden's explanations of the device operation based on thermoelectric effects and properties are reviewed and found to be inappropriate from the point of view of the conventional theory of thermoelectricity.

3. THEORETICAL BACKGROUND FOR DEVICE OPERATION

3.1 Introduction

The current research involves processes within thermal, electrical and mechanical systems and various interactions between them. An overview of basic physical processes that might be related to Strachan's reported energy conversion mechanism is presented in this chapter.

Two different possible energy conversion modes will be considered independently. The first one is the possibility of energy and entropy transport by nickel-aluminum coating, composing a thermocouple. The estimate of the thermoelectric efficiency or figure of merit and maximum temperature difference that can be supported by this device are given. As a second possible energy conversion mode, the piezo- and pyroelectric effects in PVDF are investigated.

3.2 Thermoelectric Effects

3.2.1 The Seebeck effect

The definition of Seebeck effect is that a small electric current will flow in a closed circuit composed of two dissimilar conductors when their junctions are kept at different temperatures. For a circuit of two conductors as in Figure 3.1(a) with temperature difference applied as shown, the thermoelectric current will flow in the circuit and the magnitude of the resulting current would depend on the temperature difference. The electromotive force produced under these conditions is known as Seebeck emf. Conductor A is defined as being positive to conductor B if electrons flow from A to B at the colder junction. The Seebeck current is not a unique measure of the Seebeck effect, since it depends on the resistance and therefore the size of the components in the thermocouple. Alternatively, an open circuit as in Figure 3.1(b) may be considered. In that case a potential difference ΔV_{AB} will appear between the terminals which will depend on the junctions temperatures. In other words the thermocouple is a source of

electromotive force which is a function only of temperature difference and of the two conducting materials involved. Where the composition of the two thermoelements may be assumed to remain unchanged, the Seebeck effect is independent of all other variables, including changes in cross section, temperature distributions and temperature gradients.[10] Seebeck effect is the basis for thermoelectric thermometry. Combinations of any of the conducting elements and compounds will give Seebeck currents and voltages.

If, as in Figure 3.1(b), a small temperature difference ΔT is applied between junctions of the couple of conductive materials, the derivative

$$\frac{dV}{dT} \approx \frac{\Delta V_{AB}}{\Delta T} = \alpha_{AB} \tag{3.1}$$

defines the thermoelectric power or the Seebeck coefficient α_{AB} of the thermocouple. If the observed potential difference ΔV_{AB} has the polarity shown in Figure 3.1(b), the absolute thermoelectric power of conductor A is defined as positive with respect to conductor B, i.e. $\alpha_A - \alpha_B = \frac{dV_{AB}}{dT} > 0$.

3.2.2 The Peltier effect

The other thermoelectric effect, the Peltier effect can be observed when an electric current flows across a junction of two dissimilar conductors. Heat can be liberated or absorbed in the junction region, depending on the relative direction of the current flow and the temperature gradient. When an electric current flows in the same direction as the Seebeck current, heat is absorbed at the hotter junction and liberated at the colder junction, Figure 3.2.

The Peltier heat Π_{AB} can be defined as a reversible (in contrast to Joule heating) heat transfer developed in the thermocouple junction per unit time per unit electric current. The rate at which energy is liberated when current i crosses the junction is

$$Q = \Pi_{AB}\, i \tag{3.2}$$

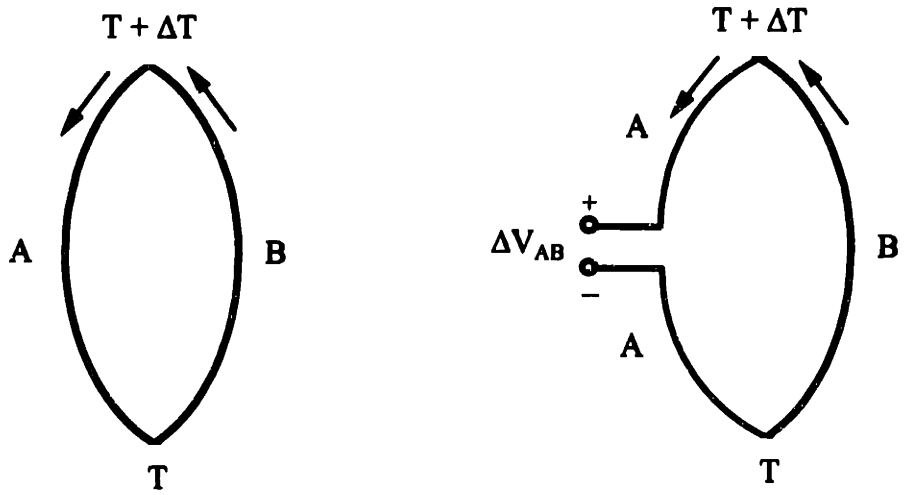

Figure 3.1. The Seebeck effect. (a) *Closed circuit.* If A and B are different conducting materials a thermoelectric current will flow. (b) *Open circuit.* If A and B are different conducting materials a thermoelectric potential difference generated.

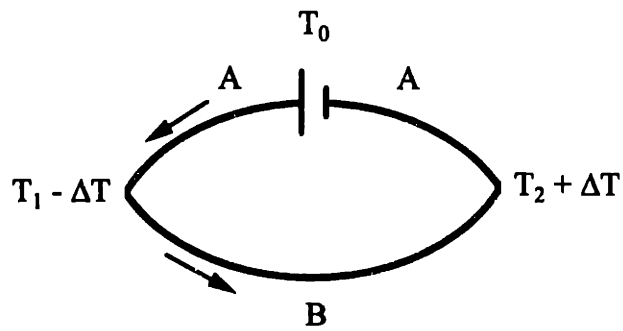

Figure 3.2. The Peltier Effect.

If the current is reversed the energy will be absorbed at the rate $Q = \Pi_{AB}\, i$. It should be mentioned that the magnitude and sign (either heating or cooling) of the Peltier heat Π_{AB} is a function of the junction temperature and composition of two bulk materials. And each material of the couple makes its own contribution to the Peltier heat. The effect is reversible and is independent of the shape or the dimensions of the materials composing the junction[10].

3.2.3 The Thomson effect

The Thomson effect is defined as the change in the heat content of a single conductor of unit cross section when a unit quantity of electricity flows along it through a temperature gradient of 1 K.[10] In other words the Thomson effect is the evolution or absorption of heat when an electric current passes from a material at one temperature to the same material at a different temperature, i.e. in a material with a temperature gradient imposed. For a conductor, shown in Figure 3.3(a) , which has been heated at point O to some temperature T_O, a thermal gradient will exist on either side of the heated point. Two points 1 and 2 of equal temperature $T_1 = T_2 < T_O$ can be found on either side of O. But if current flows in the circuit with the conductor , the temperatures of 1 and 2 will change, Figure 3.3b. These changes are the result of motion of electrons with respect to the direction of the temperature gradient. The electrons flowing from 1 - O will absorb energy moving against temperature gradient and increase their overall internal energy. The electrons flowing in the same direction as the temperature gradient (path O - 1) will give up energy and thus decrease their overall internal energy. Thermal energy will accordingly be absorbed at 1, where the current direction is opposite to the heat flow, and will be liberated at 2, where the current direction is the same as the heat flow.

The rate at which energy is liberated in the conductor is given by

$$Q = \sigma i \Delta T \qquad (3.3)$$

where σ is the Thomson coefficient and the current i in this case passes from the higher to the lower temperature.

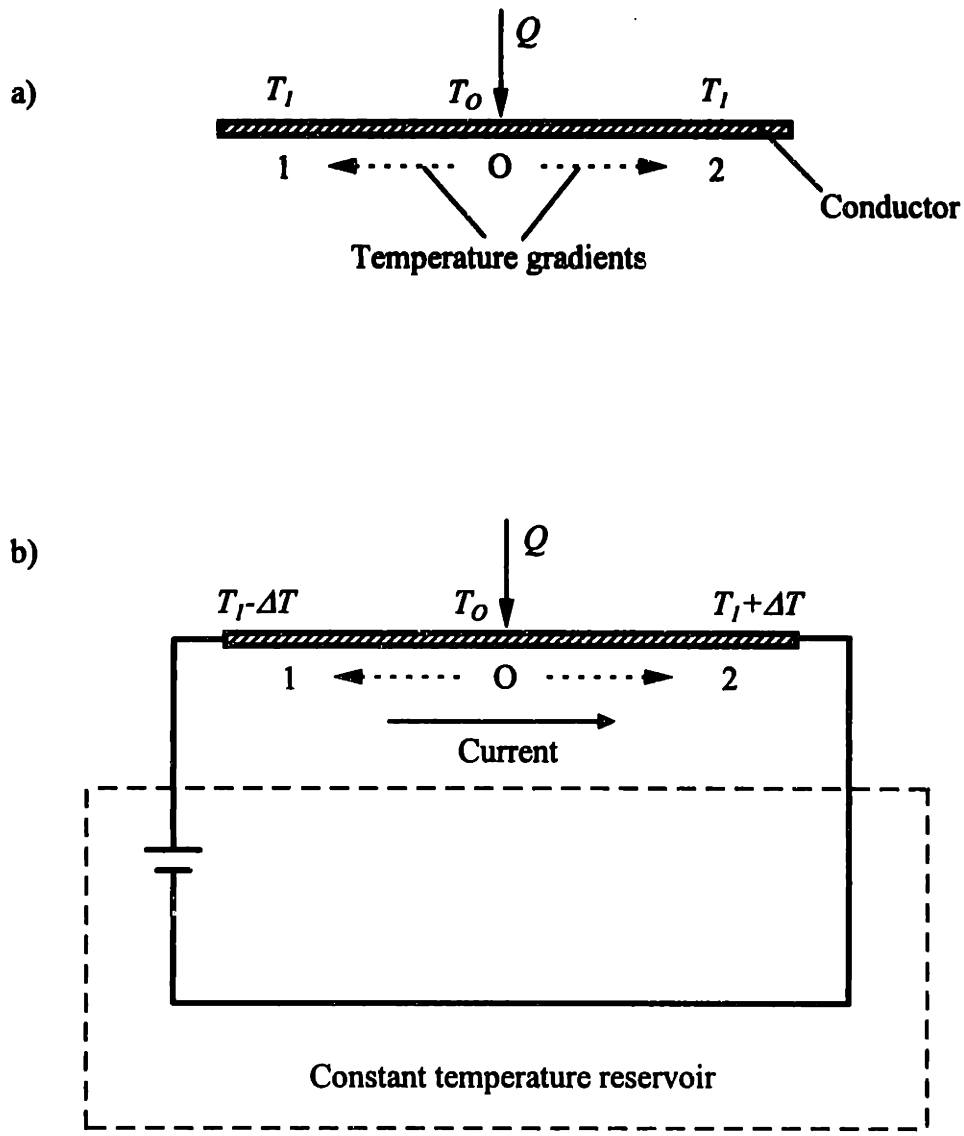

Figure 3.3. The Thomson effect

3.2.4 Relationship of Thermoelectricity to Thermodynamics.

The second law of thermodynamics for the device operating in refrigeration mode requires the entropy to be transported from the lower temperature source to the higher temperature source. It is unclear how the entropy is transported within the Strachan's device.

To produce cooling effect in heat pump operation mode or useful work in power generation mode the entropy and energy must be transported between the heat sources either by means of heat transfer or they must be carried by some working fluid.

Since PVDF is a good electrical insulator, electrons cannot flow freely in the lattice and transport the entropy between the heat sinks. Consequently, it is unlikely that the electrons in the PVDF are the carriers of entropy in Strachan's device. More probably the entropy transport mechanism is by electrons in the nickel-aluminum coating, composing essentially a thermocouple.

In a conventional thermoelectric device, the working fluid is an electron gas, whose entropy depends on the temperature and the crystal lattice structure of the thermoelectric material. The entropy change is associated with movement of electrons from one material to the other.

To clarify the last statement, the energy and entropy transport within the thermoelectric device can be compared with the energy and entropy transport in any ideal cycle working on an ideal gas.

We can compare the operation of the thermoelectric device and an ideal reversible Ericsson cycle with an ideal gas, as the working fluid. Note that the choice of an Ericsson cycle (two isotherms and two isobars) as an example seems natural. The analogy between mechanical work term for an ideal gas (of constant mass) $\delta W_M = \int P dv$, where v is an ideal gas specific volume and an electrical work for electron gas $\delta W_E = \int V dq$, where V is voltage in the thermocouple and q is charge, allows us to treat two seemingly independent and unrelated mechanisms of energy transport in similar manner. The constant pressure processes for an ideal gas in Ericsson cycle are analogous to the constant voltage

processes for an electron gas in the thermocouple. And further, as the processes in an ideal gas cycle can be described using pressure-volume diagram, in the same way the processes within the thermoelectric device can be described using voltage-charge diagram.

As shown in Figure 3.4, the ideal Ericsson cycle working between two heat sources T_H and T_C consists of isothermal compressor, isothermal expander and reversible recuperative heat exchanger. The gas moving up and down has the same temperature, therefore the reversible transport of entropy must be by entropy difference associated with a second thermodynamic property, for example, pressure or specific volume.[7] This means that the working fluid must have non-zero values of Maxwell coefficients. The lower pressure gas leaving the expander carries higher entropy than the higher pressure gas moving towards the expander. This results in a net entropy absorption from lower temperature source T_C. The opposite happens in the compressor. The gas entering the compressor carries more entropy than the leaving gas. That results in net entropy rejection to the higher temperature source T_H. Therefore the expander takes the entropy Q_C / T_C from the cold heat source and converts it into the net entropy flow by mass circulation. The regenerative heat exchanger increases the temperature of the working fluid from T_C to T_H. The compressor converts the entropy flow by mass circulation into Q_H / T_H and rejects it to the hot heat sink. Entropy flow results in energy flow between two heat reservoirs from T_C to T_H.

The similar energy and entropy transport mechanism exists in a thermoelectric device. Two metals composing the PVDF bimetallic coating have different electrical potentials. Nickel is more electronegative metal then the aluminum, so temperature gradient between junctions A and B, see Figure 3.5, will promote thermoelectric current circulation. The difference in electrical potentials result in net entropy flow from the low temperature junction to the high temperature junction, which will cause energy transport between two junctions. In refrigeration mode of operation of the nickel-aluminum thermoelectric device, electrons flowing through junction A from one crystal lattice structure to the other crystal lattice undergo a "compression", therefore reducing their entropy. Junction A in electron gas cycle works as a compressor in an ideal gas cycle,

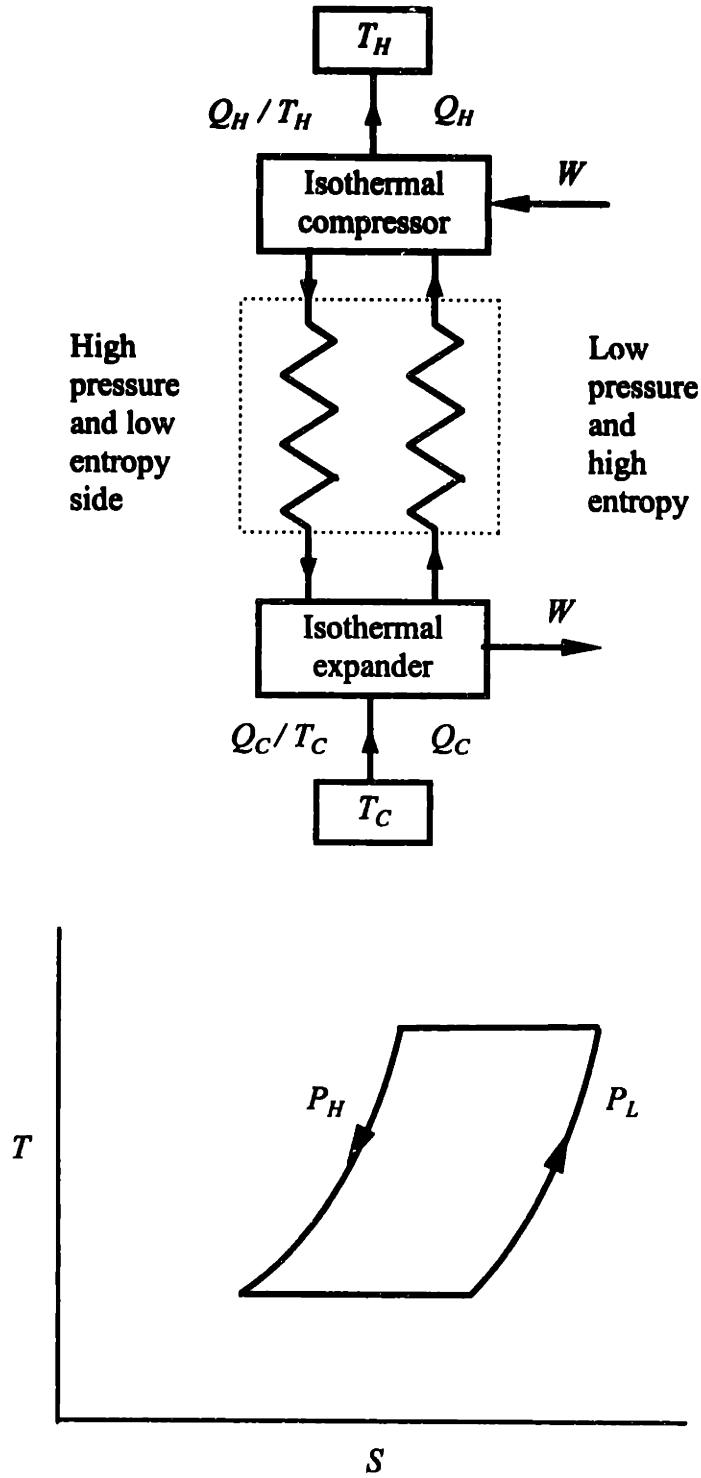

Figure 3.4. Entropy and energy flow in an ideal gas Ericsson cycle.

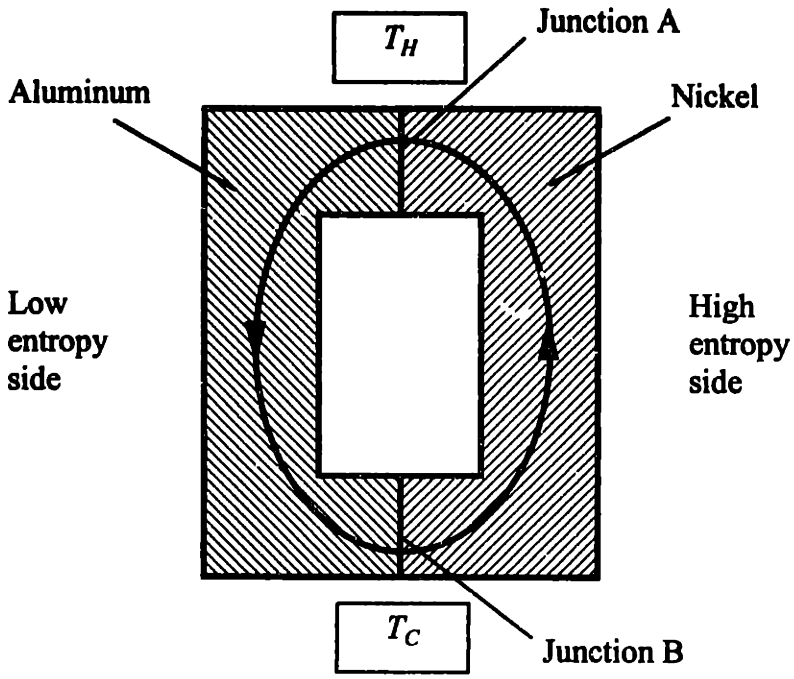

Figure 3.5. Possible entropy transport by electron gas in the nickel - aluminum thermocouple. Comparison with an ideal gas cycle.

converting entropy flow by electron circulation into entropy of the form Q_H / T_H, which is pumped into the hot heat sink. Similarly, in junction B electrons flowing in the opposite direction undergo an "expansion", increasing their entropy. Thus, junction B plays role of the expander, taking entropy from cold sink Q_C / T_C and converting it in the entropy flow by electron circulation. If the direction of the electrons flow is reversed by external source, the "compression" and "expansion" junctions are switched. The entropy flow would be reversed the same way as in ideal gas cycle, where independent of temperature levels the entropy always flows towards the compressor. Thus the thermoelectric device can be reversed and it will generate power.

3.2.5 Thermoelectric Efficiency of the Prototype Device

For the thermoelectric device operating in heat pump mode, i.e. when heat is being absorbed at the lower temperature T_C and liberated at the higher temperature T_H the net rate of heat transfer Q_C can be written as: [11]

$$Q_C = (\alpha_p - \alpha_n)\, T_C\, i \; - \; i^2 R / 2 \; - \; K\,(T_H - T_C) \qquad (3.4)$$

where α is the Seebeck coefficients of the two dissimilar materials designated by the subscripts p and n, in Volts / ^{0}C, i is the direct current flowing in the circuit, in Amperes, R is the total resistance of the two materials, in Ohms, and K is the combined thermal conductance of the thermocouple, in Watts / ^{0}C

The power input required to produce the effect described by Eq. (3.4) is the sum of irreversible Joule heating and Seebeck thermoelectric effect and it may be written in similar terms as follows:[11]

$$W = i^2 R + (\alpha_p - \alpha_n)\,(T_H - T_C)\, i \qquad (3.5)$$

Combining these two terms gives the coefficient of performance of a thermoelectric refrigerating device, which may be written

$$\text{COP} = Q_C / W \tag{3.6}$$

The terms R and K in Eq.(3.4) depend upon the configuration of the thermoelectric device and may be rewritten in terms of the specific electrical resistivity ρ and in terms of the specific thermal conductivity k. Both terms are written with respect to the volume of the sample expressed in terms of length and area. This permits an optimization of the net rate of heat transfer Q by proportioning the areas of the thermoelements, assuming constant length, so that the losses due to electrical resistance and thermal conductance are minimized.[11] With the net rate of heat transfer optimized, the coefficient of performance may also be optimized and written only in terms of the thermoelectric material parameters and the operating temperatures: [11, 17]

$$COP = \frac{T_C}{T_H - T_C} \frac{\sqrt{1 + Z \cdot T_M} - \frac{T_H}{T_C}}{\sqrt{1 + Z \cdot T_M} + 1} \tag{3.7}$$

where $T_M = \frac{T_H + T_C}{2}$ is the mean temperature, K, and (3.8)

$$Z = \frac{(\alpha_p - \alpha_n)^2}{\left(\sqrt{k_p \cdot \rho_p} + \sqrt{k_n \cdot \rho_n}\right)^2} \text{ is the figure of merit, in } K^{-1} \tag{3.9}$$

This equation permits quick evaluation of the operational limits of a particular combination of thermoelectric materials used in the design of a device. The term Z, or figure of merit, when temperature conditions are assumed constant, is the controlling factor of the maximum performance of a thermoelectric device. If Z is raised to infinity, the coefficient of performance approaches that of ideal Carnot efficiency as described by the first term of Eq. (3.7).

The Seebeck coefficients α, the thermal conductivities k, and the specific electric resistivities ρ for nickel and aluminum are shown in Table 3.1.

	α, μV / K	k, W / m · K	ρ, Ω·m
Nickel	-19.5	91	7.8×10^{-8}
Aluminum	-1.66	237	2.8×10^{-8}

Table 3.1. Values of Seebeck coefficients α,[12] thermal conductivities k,[20] and specific electric resistivities ρ[21] for nickel and aluminum.

Using these values, the figure of merit for a nickel-aluminum thermocouple is $Z = 1.159 \times 10^{-5}$ K^{-1}, and the coefficient of performance for the device operating between T_H = 26 °C and T_C = 0 °C has a negative value. That means the device operation cannot be explained solely by thermoelectric effects or properties.

The maximum temperature difference that can be supported by a pair of thermoelectric materials operating in refrigeration mode is[16]

$$\Delta T_{max} = 2T_M \cdot \frac{\sqrt{1+Z \cdot T_M} - 1}{\sqrt{1+Z \cdot T_M} + 1} \tag{3.10}$$

where T_M is the mean absolute temperature as before, and Z is the figure of merit.

For the nickel-aluminum thermoelectric device operating at T_H = 26°C the maximum achievable temperature difference between two junctions is calculated to be 0.58 K, a significantly lower value than that reported by Strachan and Aspden. The thermoelectric effects cannot explain the device operation with given temperature differential.

3.2.6 The Phonon drag effect

To complete the discussion on thermoelectricity, one other effect should be discussed. In certain conductors the Seebeck coefficient becomes much higher then the

values predicted by theory. This phenomenon is attributed to the dragging of electrons by phonons and is known as a phonon drag effect. It is usually assumed that electrons and phonons travel in random directions after collision. However, when the phonon drag effect becomes applicable, this assumption can no longer be made. It is necessary to assume that, after collision with electron, a phonon tends to move in the direction of the electric current.[16] In other words, the momentum of the electrons passed on to the phonons and this leads to an additional flow of energy. The phonon drag effect will contribute to the value of the Seebeck coefficient, which can be calculated as a sum of electrons and phonons contributions. The phonon "portion" of the Seebeck coefficient is[47]

$$\alpha_{ph} = \pm \frac{v_s^2 t_{ph}}{\mu T},$$

where v_s is the average speed of sound, t_{ph} is the relaxation time for the loss of momentum from phonons, μ is the mobility of charge carriers, T is the absolute temperature and the sign is the same as for the electron portion. The phonon-drag effect becomes important at low temperatures and in materials with low values of charge carriers mobility. The effect is the largest at semiconductors at low temperatures. For metals it is usually small. Therefore the phonon drag effect can enhance the thermoelectric energy conversion, but for nickel-aluminum thermocouple at temperature of Strachan's experiments, its impact is negligible.

3.3 Piezoelectricity and Pyroelectricity

Piezoelectricity is a fundamental process of electromechanical interaction and is representative of linear coupling in energy conversion. The piezoelectric effect was discovered in 1880 by Pierre and Jacques Curie. The direct piezoelectric effect is that electric polarization or electrical displacement is produced by mechanical stress. The converse piezoelectric effect is that crystal becomes strained when an electric field is applied. Thus the direct piezoelectric effect is given by

$$D = d \cdot \tau , \tag{3.11}$$

where D is an electrical displacement resulting from the applied mechanical stress τ, and d is a piezoelectric charge constant.

The converse piezoelectric effect is given by

$$X = d \cdot E \tag{3.12}$$

where X is a developed strain, E is an applied electric field and d is a piezoelectric strain coefficient.

It should be noted that d in equations (3.11) and (3.12) is the same coefficient, which is called piezoelectric charge or strain constant, since it defines both direct and converse piezoelectric effects, resulting in developed electrical displacement D (sometimes called electrical charge density) and strain X, respectively.

Pyroelectricity is a linear interaction process between electrical and thermal domains. It refers to the generation of an electrical signal in response to a change in temperature. The pyroelectric coefficient for a mechanically free sample generally consists of two terms[18]:

$$p_3 = \left(\frac{\partial P_3}{\partial T}\right)_{S_i=0} + \sum_{i=1}^{3} e_{3i}\beta_i , \tag{3.13}$$

where p_3 is the pyroelectric coefficient, P_3 is the polarization, T is the absolute temperature, e_{3i} is the piezoelectric stress constant and β_i is the thermal expansion coefficient.

The first term in Eq. (3.13), called the primary effect, expresses the intrinsic pyroelectricity, which appears in a clamped sample. The second term expresses the coupling of piezoelectricity and thermal expansion and is called the secondary effect.[18] In other words, the primary pyroelectricity is that a change in temperature causes a change in polarization of the constant size sample. The secondary pyroelectricity is a change in polarization due to variation of sample dimension when its temperature changed (thermal expansion).

Both piezoelectric and pyroelectric behavior and properties of PVDF will be discussed in greater detail in Chapter 4 and the values of piezo- and pyroelectric coefficients are given in Appendix A.

3.4 Interactions between Thermal, Mechanical and Electrical Domains.

The Strachan-Aspden's replica device represents a multilayer structure composed of polyvinylidene fluoride coated with nickel and aluminum. PVDF is highly piezo- and pyroelectric. The a pair of metals present in the bimetallic coating compose a thermocouple. These thermoelectric, piezoelectric and pyroelectric effects might interact to provide a mechanism for power conversion.

The earlier sections of this chapter considered the effects that occur strictly in bimetallic coating. In this section we concentrate our attention on processes in the PVDF film, essentially neglecting the interactions in nickel-aluminum coating for now.

Assuming that thermal, mechanical and electrical effects and properties are present in homogeneous dielectric, its behavior can be fully described by six fields: temperature T, entropy S, stress τ, strain X, electric field E and polarization P or electric displacement D. According to the first law of thermodynamics the change in internal energy of unit volume of dielectric is

$$dU = \delta Q - \delta W, \tag{3.14}$$

where dU is the change in internal energy of the system, δQ is the heat transfer added to the system and δW is the work done by the system.

Assuming only reversible changes in the system the second law relates the δQ to the temperature and entropy as

$$\delta Q = T \cdot dS. \tag{3.15}$$

The work done on the system can be found as a sum of mechanical and electrostatic terms, given as volume integrals: [35]

$$\delta W_M = -\int_{\upsilon} (\tau_i \cdot dX_i)\, d\upsilon, \tag{3.16}$$

and

$$\delta W_E = -\int_{\upsilon} (E_i \cdot dD_i) \cdot d\upsilon \tag{3.17}$$

where υ is volume of dielectric and minus sign in equations (3.16) and (3.17) by thermodynamic sign convention indicates that the work is done on the system.
Then the first law per unit volume of dielectric can be written as

$$dU = T \cdot dS + \tau_i \cdot dX_i + E_i \cdot dD_i \ . \tag{3.18}$$

So the change in internal energy of dielectric depends on changes in thermal, mechanical and electrical domains. In other words these effects are coupled and should be considered jointly.

Based on fact that thermal mechanical and electrical effects are coupled in polyvinylidene fluoride, as indicated by Eq. (3.18), the PVDF based engine or heat pump seems at least theoretically possible, since the change of film temperature, will result in change of its polarization.

Once again the analogue of the ideal gas cycle can be realized. A simple configuration of the proposed PVDF based engine is shown in Figure 3.6(a).

Referring to Figure 3.6(a) the sequence of processes in the proposed energy production cycle is following:

1. PVDF is at $T = T_H$. The thermal switch A is closed, switch B is open. The film is discharged producing electric power, while absorbing heat from the heat source, resulting in reversible isothermal "expansion" at $T = T_H$.
2. Both thermal switches are open. PVDF is discharged adiabatically, reducing its temperature from T_H to T_C. This process is analogous to reversible adiabatic expansion in ideal gas cycle.
3. When the PVDF temperature reaches $T = T_C$ the thermal switch B is closed. The film is charged by externally applied voltage, while rejecting heat to the lower reservoir, resulting in reversible isothermal "compression" at $T = T_C$.

4. Both thermal switches are open. PVDF is charged adiabatically, increasing its temperature from T_C to T_H. This process is analogous to reversible adiabatic compression in ideal gas cycle.

By sequence of these four processes a pyroelectric Carnot cycle is executed resulting in electrical energy production. The cycle can be reversed to provide refrigeration.

Using the same principles, the "cascaded pyroelectric engine" can be proposed, as shown in Figure 3.6(b). In this engine left and right thermal switches are closed and opened alternately resulting in energy and entropy flow from the heat source at T_H to the heat sink at T_C and thus producing electrical energy output.

Unfortunately, the pyroelectric energy conversion efficiency [40] for most of the ferroelectric materials is measured to be much lower then 1 %. The best ferroelectric materials can achieve the efficiencies of about 3%. It can be increased by heating the material to the temperature of ferroelectric to paraelectric transition[26]. The theoretical studies show that the ideal efficiencies on the order of 10-15 % could be attained if the proper materials are developed to be used in pyro-ferroelectric converters.[40] For copolymer vinylidene-fluoride trifluoroethylene (PVDF-TrFE) the pyroelectric energy conversion efficiency can be increased using this method, but for homopolymer PVDF this temperature is higher then the temperature at which PVDF film looses its polarization and even higher than its melting point, which makes it useless for such applications.

In addition, it should be mentioned that this Carnot cycle is not entirely appropriate for the stack geometry that Strachan used. The direction of the temperature gradient for the Strachan's stack is parallel to the individual PVDF layers, whereas for this cycle it is perpendicular. However, this cycle gives an estimate for the efficiency of the pyroelectric device and indicates what energy conversion efficiencies might be expected from the pyroelectric material. From these arguments, we believe that the pyroelectric properties of the PVDF do not provide a mechanism that explains Strachan's observations.

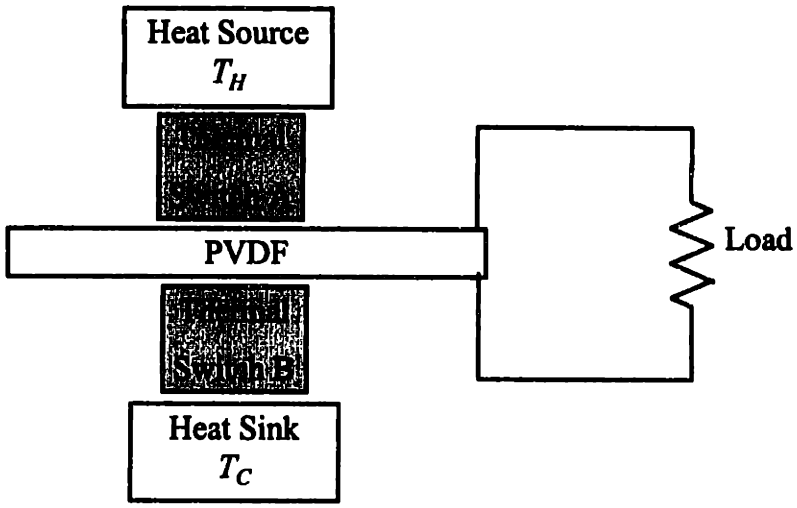

a)

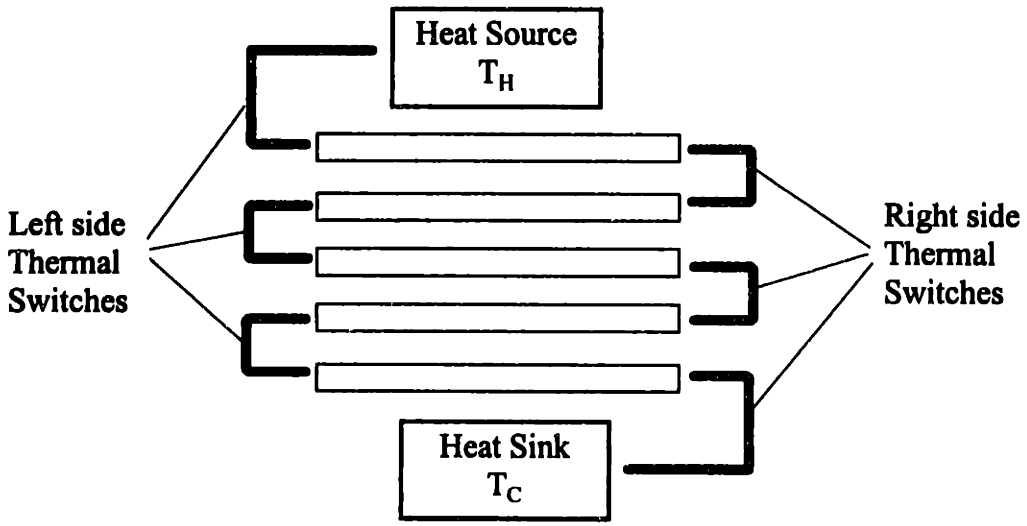

b)

Figure 3.6. Schematic of possible PVDF based engine. (a) One PVDF layer engine. (b) Multilayer "cascaded" engine. Electrical circuit is not shown.

3.5 Summary

The physical phenomena that are possibly involved in the energy conversion and the entropy transport mechanisms are reviewed. The possibility of energy conversion by thermoelectric effects in nickel-aluminum thermocouple and by piezo- and pyroelectric effects in PVDF are considered separately.

The theoretical coefficient of performance and the maximum temperature difference that can be supported by the thermoelectric device are calculated. The obtained values do not agree with the values measured by Strachan for three prototype devices. The temperature difference that can be supported by nickel-aluminum thermocouple is 0.58 K. The figure of merit for this device is two orders of magnitude lower then that of conventional semiconductor thermoelectric devices. And the coefficient of performance for experimental conditions reported by Strachan and Aspden is negative. All that suggest that thermoelectric effects can not provide an explanation for the energy conversion mechanism.

The energy conversion can be realized in PVDF, based on its pyroelectric properties. But the efficiency of such device would be extremely low and would not provide a mechanism that explains Strachan's observations.

4. PIEZOELECTRICITY AND PYROELECTRICITY IN PVDF

Polyvinylidene fluoride is a polymer of repeated unit CH_2 - CF_2 . It has become an important material for transducer applications. It has high mechanical flexibility, low acoustic impedance and low density. PVDF possesses large ferroelectric, piezoelectric and pyroelectric properties. The piezoelectric and pyroelectric coefficients of the material are higher then for the other piezoelectric polymers.

In this work the PVDF film, provided by AMP Inc., was used as a base material. The production process included the mechanical orientation of the extruded resin by stretching, followed by a treatment under intense electric field to electrically polarize the material. A metal film was coated onto the PVDF to provide electrical contact. The metallic coatings were applied by vacuum deposition. Stretching and poling the film results in anisotropic piezoelectric properties. The coordinate system, shown in Figure 4.1 is generally used to characterize the film.

By convention the (1) axis identifies the stretch direction. The (2) axis indicates the transverse direction. Usually, for a PVDF film, the axis of polarization is the (3) axis, so the electrical field axis is in the (3) direction.[25] Positive mechanical action is defined as tensile, negative mechanical action as compressive. Positive electrical action results in an increase in the polarization.

The piezoelectric strain constant d and piezoelectric stress constant g are defined as follows:

$$d = \left(\frac{X}{E}\right)_{\tau} = \left(\frac{\text{Strain developed}}{\text{Applied field}}\right)_{\text{Constant stress}} = (d_{31},\ d_{32},\ d_{33})$$

$$g = \left(\frac{E}{\tau}\right)_{D} = \left(\frac{\text{Electrical field developed}}{\text{Applied mechanical stress}}\right)_{\text{Constant electric displacement}} = (g_{31},\ g_{32},\ g_{33})$$

The main modes and boundary conditions are[25]:

d_{31} - the piezo element is free to move in the (2) and (3) directions and a charge is developed on the surface of the film, (3) direction, for a change in stress in the longitudinal (1) direction.

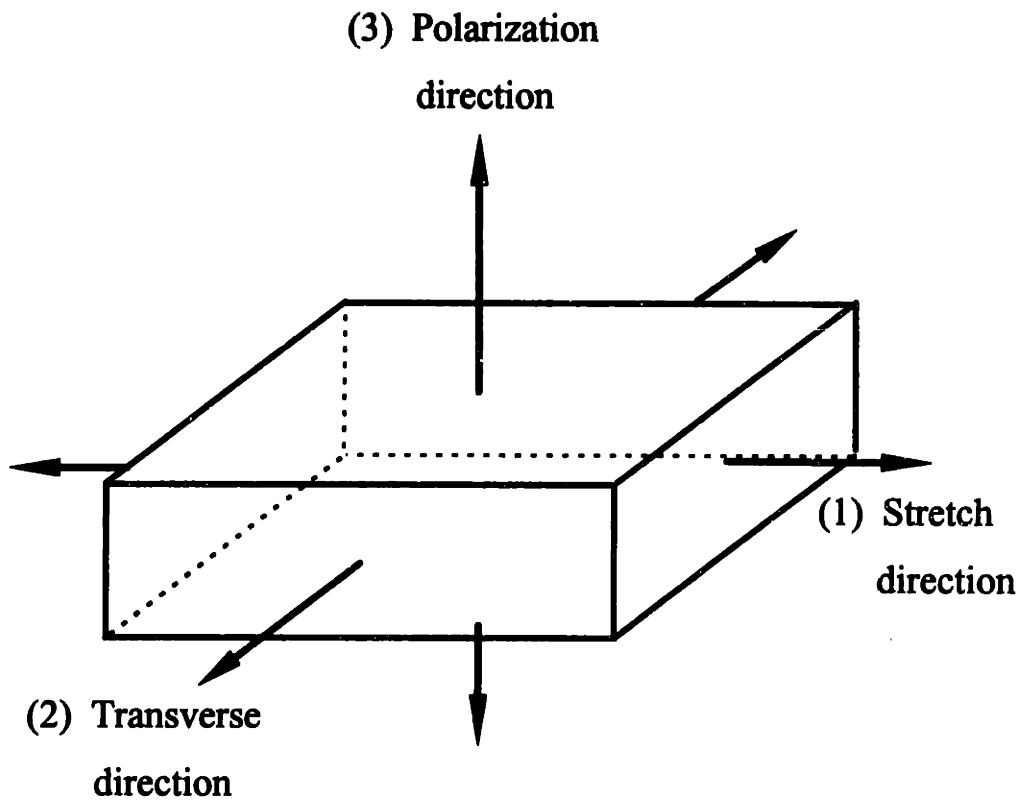

Figure 4.1. Coordinate system for identifying the directions of piezoelectric action in PVDF

d_{32} - the piezo element is free to move in the (1) and (3) directions and a charge is developed on the surface of the film (3) for a change in stress in the transverse (2) direction.

d_{33} - the piezo film element is free to move in the (1) and (2) directions, and a charge is developed in the thickness (3) direction for a change in stress in the (3) direction (normal to the plane of the film).

For the inverse effects, applying a field in the (3) direction to an unconstrained PVDF film element results in a strain along the (1), (2) and (3) directions, and the corresponding strain is obtained by d_{31}, d_{32} and d_{33} respectively.

g_{31} - the piezoelectric constant for mechanical stress (tensile or compressive) applied in the (1) longitudinal direction resulting in an electrical field developed in the (3) direction.

g_{32} - the piezoelectric constant for mechanical stress applied in the (2) transverse direction resulting in an electrical field developed in the (3) direction.

g_{33} - is the applicable constant for mechanical stress applied in the (3) direction, normal to the plane of the film, resulting in an electrical field developed in the (3) direction.

The first numerical subscript in piezoelectric coefficients indicates the axis of polarization or applied electrical field. The second subscript identifies the direction of the mechanical stress or strain.

Typically for PVDF film, the sign of d_{31}, d_{32}, g_{31} and g_{32} is positive, but for d_{33} and g_{33} is negative.

Two additional piezoelectric constants occasionally used , e and h are defined as follows:

$$e = \left(\frac{\tau}{E}\right)_X = \left(\frac{\text{Stress developed}}{\text{Applied Electrical field}}\right)_{\text{Constant strain}}$$

$$h = \left(\frac{E}{X}\right)_D = \left(\frac{\text{Electrical field developed}}{\text{Applied Strain}}\right)_{\text{Constant electric displacement}}$$

The piezoelectric constants are temperature dependent. Figure 4.2 shows the temperature dependence of the piezoelectric constants d_{31}, d_{33}, e_{31}, e_{33} in PVDF.

The pyroelectric tensor for PVDF is

$$p = \begin{bmatrix} 0 \\ 0 \\ -p_3 \end{bmatrix}$$

An increase in temperature of the film will increase its volume, resulting in decrease of polarization. Thus pyroelectric coefficient of PVDF is negative. The temperature dependence of PVDF pyroelectric constant is shown in Figure 4.3.

The utilization of the PVDF material is limited by temperature of about 85-90 °C, since at that temperature PVDF losses its polarization, as can be seen from Figure 4.3.

The pyroelectricity in PVDF is of secondary nature. It has been shown that only 50% of the total pyroelectric response can be contributed by secondary pyroelectricity.[24] Recent investigations of PVDF behavior showed that a larger contribution can arise from the secondary pyroelectricity.[26]

Based on the observations of pyroelectric and piezoelectric constants behavior, it has also been shown that p_3 and d_{31} in PVDF are linearly related.[24] Therefore both piezoelectricity and pyroelectricity in PVDF are not independent of each other and should be considered jointly in energy conversion device.

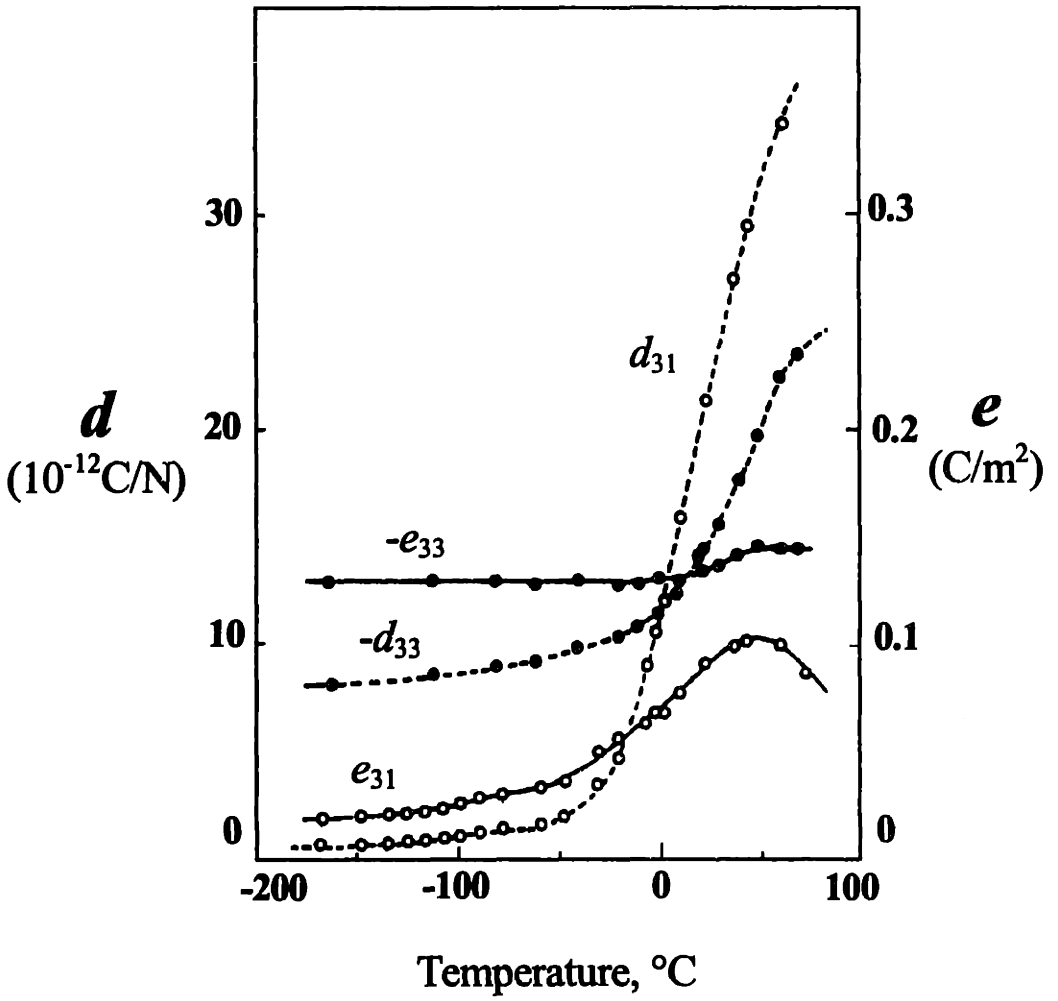

Figure 4.2. Temperature dependence of the piezoelectric constants d_{31}, d_{33}, e_{31}, e_{33} in PVDF. Adapted from Ohigashi [22].

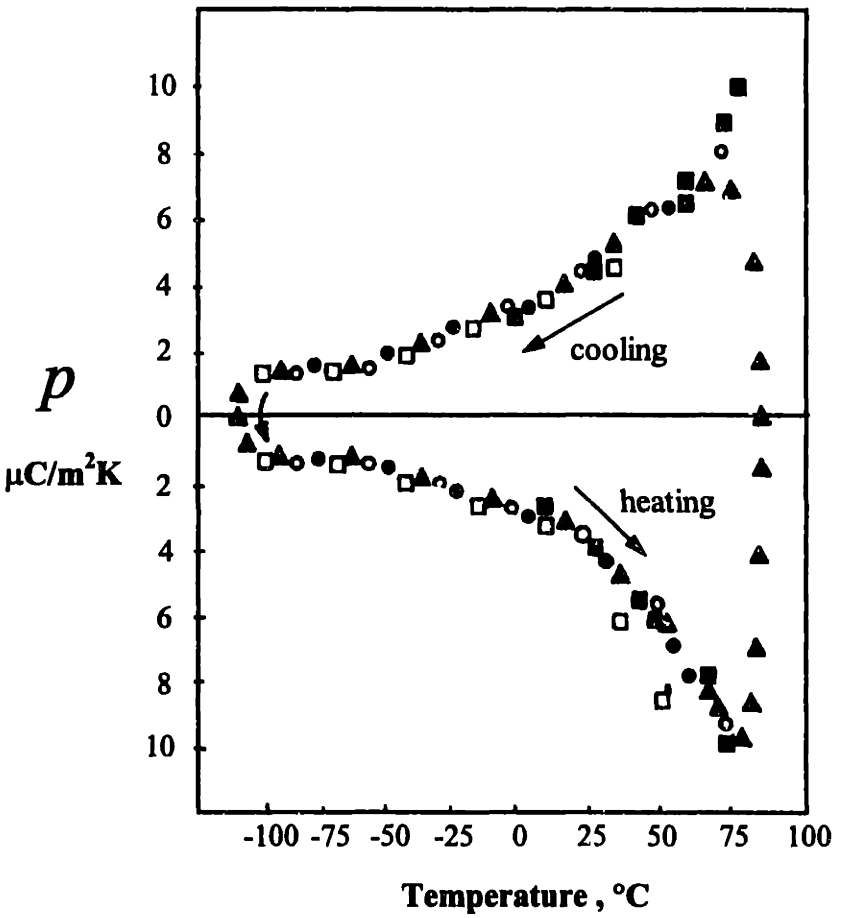

Figure 4.3. PVDF pyroelectric coefficient versus temperature. Adapted from Burkard and Pfister [23].

5. CONSTRUCTION OF THE REPLICA DEVICE

5.1 Introduction

During the course of this project we attempted to make a faithful reproduction of the Strachan - Aspden device. Strachan believes that the choice of materials for the stack as well as constructional details were crucial to the successful operation of his three devices.

Because of difficulties in construction of the stack and gluing the PVDF in particular, three different PVDF materials and more than ten different types and brands of cyanoacrylate adhesives were tested using several bonding and surface preparation techniques. Two auxiliary devices were designed for laminating and cutting the PVDF multilayer assemblies. The best results in the stack lamination were achieved with ZAP CA (super-thin penetrating formula) ethyl cyanoacrylate adhesive, provided by Pacers Technology, Inc. The description of the bonding techniques and constructional details are presented in this chapter.

In order to reproduce the results obtained by Strachan and Aspden, the replica device was built, following Strachan's recipes outlined in Chapter 2. The PVDF stack, was built utilizing eleven PVDF elements, twelve Acrylic plates and a PZT driver. The dimensions of the stack are 155 × 25 × 2.5 mm. This stack differed from the first and third Strachan's prototype devices in that it did not have recording tape between PVDF layers. However, it was not expected that this would be a problem because Strachan's second prototype device did not have recording tape and could still operate as an energy converter.

5.2 Bonding Experiments

The purpose of bonding experiments was to choose the adhesive and adhesion method that would provide good mechanical strength and high quality acoustic coupling between PVDF surfaces and the elements of the device.

The previous work of MacBride[34], found that bonds to PVDF with cyanoacrylate adhesive were of difficult and of inferior quality. Consequently instead of cyanoacrylate, MacBride used a high-temperature-setting, low viscosity strain-gauge epoxy, which allowed him to get very thin (submicron) and strong bonds. Unfortunately MacBride's device didn't show the energy conversion effect.

Therefore, to duplicate results reported by Strachan and Aspden, it was necessary to duplicate the Strachan's cyanoacrylate bonding method. In addition, it was postulated by Strachan that the cyanoacrylate adhesive could be contributing to the energy conversion through some chemical means. So, the effort was concentrated on producing strong and thin glue lines with cyanoacrylate.

Three different PVDF materials were used for bond strength and quality tests. One type is a uniaxially stretched PVDF film coated on both sides with 2200 angstroms nickel and 800 angstroms aluminum. Following the Strachan's advice, the metallization on one side was removed with pencil eraser. The second and the third types of PVDF material is the same uniaxially stretched PVDF film, but coated with nickel and aluminum on one side. These two types differed from each other in that they had different directions of polarization, i.e. one of them had metallization on positive side and the other material had metallization on the negative side. All three types of material are provided by AMP, Inc.

The procedure for the cyanoacrylate bonding tests was very close to that used by Strachan [3]:

1. PVDF film is cut to a face dimension of 25 mm × 5 mm using sharp razor blade or scalpel.
2. 2% solution of tetrabutiltitanate in petroleum ether is prepared. The TBT is needed to produce the alkaline PVDF film surfaces. Otherwise, if the surfaces have pH < 7 the cyanoacrylate will not cure properly [28].
3. Both PVDF surfaces are treated with solution of TBT in petroleum ether in a dry atmosphere. For that purpose a glove box is constructed and the process is carried on in a nitrogen atmosphere. Strachan suggests[3,6] that the desire for a dry atmosphere is due to the fact that the negative polarization side of PVDF tends to attract positive ions H^+ from the environment and that, in turn, would prevent cyanoacrylate from

secure bonding to the surfaces. After that treatment the surfaces of the film appear iridescent, that indicates successful titanate adhesion.

4. After allowing PVDF to dry, the surfaces are exposed to 100% humidity atmosphere at 40°C for a period of time from 1 - 30 minutes.
5. The layers, one by one, are assembled with ethyl cyanoacrylate adhesive and put into press between two polyethylene plates. The range of pressure applied is from 0.19 - 197 MPa.
6. The stack is inspected for the mechanical strength and for the absence of voids on PVDF surfaces after peeling the layers apart.

There were several variations in step 5. Initially the PVDF assembly was allowed to cure in air. The second experimental stack was allowed to cure in presence of ammonia, yet another stack was allowed to cure in humid atmosphere. Also several types of cyanoacrylate adhesives are tested. But all the attempts resulted in a poor bond, an unsatisfactory bond line thickness (12 - 40 μm), and numerous voids in a glue line.

The time interval between initial contact of two PVDF layers with the glue and application of the press force was too long to allow for the effective use of the fastest and strongest cyanoacrylate adhesives with the curing time ranging from 1 - 10 seconds. All attempts resulted in a very thick and uneven bond. In order to improve the bonding technique the die set is assembled with two steel blocks, used as supports for the PVDF stack, as shown in Figure 5.1. The edges of each following PVDF layer are taped to the upper half of the die set. The spring is incorporated between two die halves to prevent the PVDF layers from the premature contact, when the press force is not applied to the top die half. Such construction allowed to apply press and make contact between adherent surfaces simultaneously, which resulted in better adhesive spreading and wetting the surfaces. Using the die set, much thinner glue lines could be achieved, when applied pressure in the stack was high enough.

To optimize the applied press force, required to achieve the thinnest and the strongest glue line, series of tests are performed. For that purpose the arbor press is used in the range of applied force from 24 - 3260 N and the hydraulic press in the range from 2900 - 25000 N. For 25 mm × 5 mm PVDF strips that corresponds to pressure ranges in

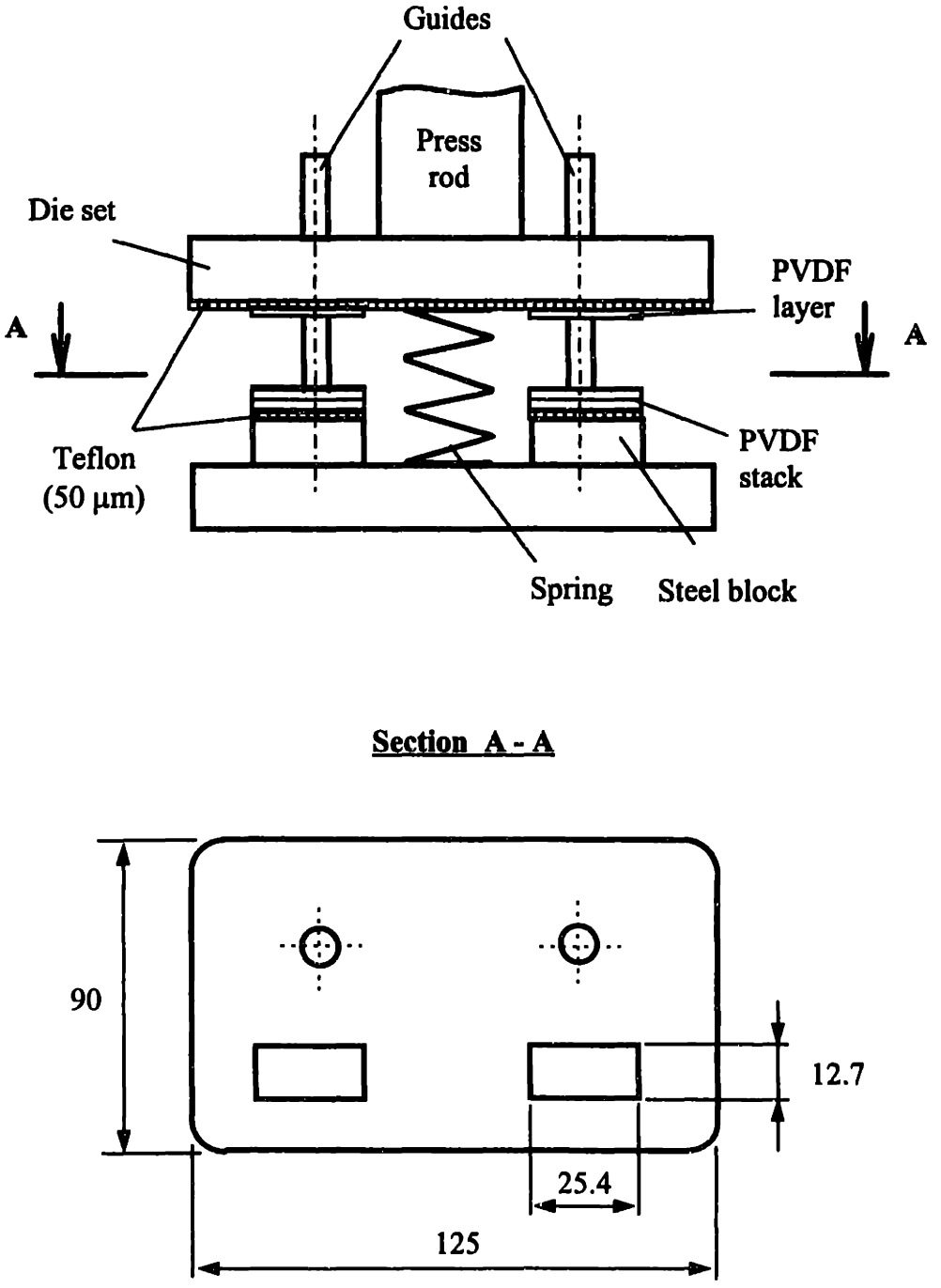

Figure 5.1. Schematic of the cyanoacrylate bonding setup. Die set, assembled with two steel blocks for supporting PVDF stack during adhesion. All dimensions in millimeters.

the stack of 0.19-25.6 MPa and 22.8-197 MPa respectively. The results of measurements of pressure in the stack versus bond line thickness and peel strength for ZAP CA ethyl cyanoacrylate adhesive is shown in Figure 5.2 .When the applied pressure was higher then 0.55 MPa the glue line thickness stayed approximately constant. However, the increase in applied force resulted in rapid drop of mechanical strength of the PVDF assembly. The measured peel strength for two best cases, when the applied pressure was 0.55 and 0.7 MPa respectively was in the range from 6 - 7 N/cm. The corresponding average bond line thickness of 4 - 4.5 μm is obtained. This mechanical strength of PVDF elements considered inappropriate. However, contacting Strachan, it was discovered that mechanical strength of his stacks was of the same order of magnitude. In addition, testing the produced stacks on Hipotronic HD 100 series AC/DC Hipot tester with voltage up to 3000 V did not result in stacks delamination. Thus the procedure described above was considered adequate.

5.3 Construction of the PZT-PVDF-Acrylic Stack

When Strachan observed the effect, he was working on building a lithotriptor. He tried to construct a piezoelectric stack that would work as a traveling wave amplifier. The maximum power transmission mode of such devices occurs at the frequency corresponding to the resonance frequency of the acoustical driver. In Strachan's devices the PZT driver's resonance frequency was 2 MHz. Consequently, PVDF elements were built to thickness corresponding to this resonance frequency. To match the phase of all PVDF elements Strachan interleaved them with acrylic spacers, machined to the dimension to support the same resonance frequency.

For a given thickness l and clamped boundary conditions, the principal resonance occurs at half-wave resonance frequency:

$$f = \frac{v_s}{2l}, \tag{5.1}$$

where v_s is sound velocity.

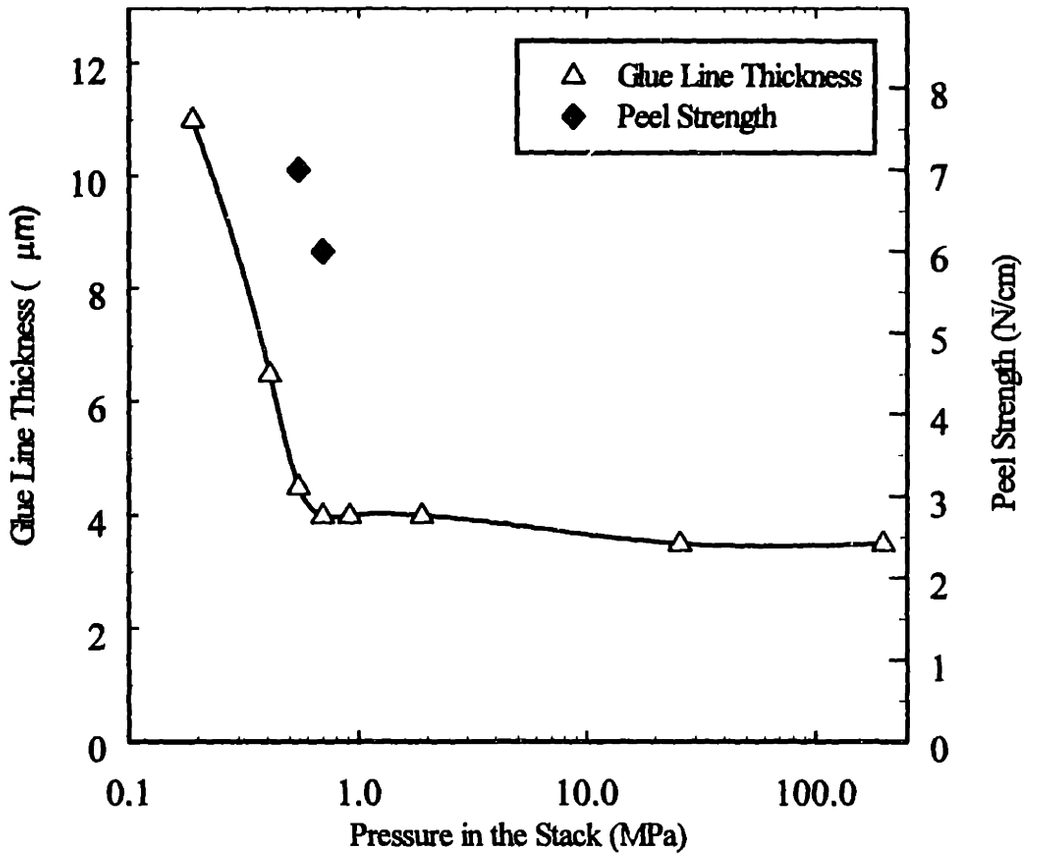

Figure 5.2. Measured applied pressure versus glue line thickness and peel strength for ZAP CA cyanoacrylate adhesive. The peel strength is measured for two best cases corresponding to the applied pressure in the stack of 0.55 and 0.7 MPa.

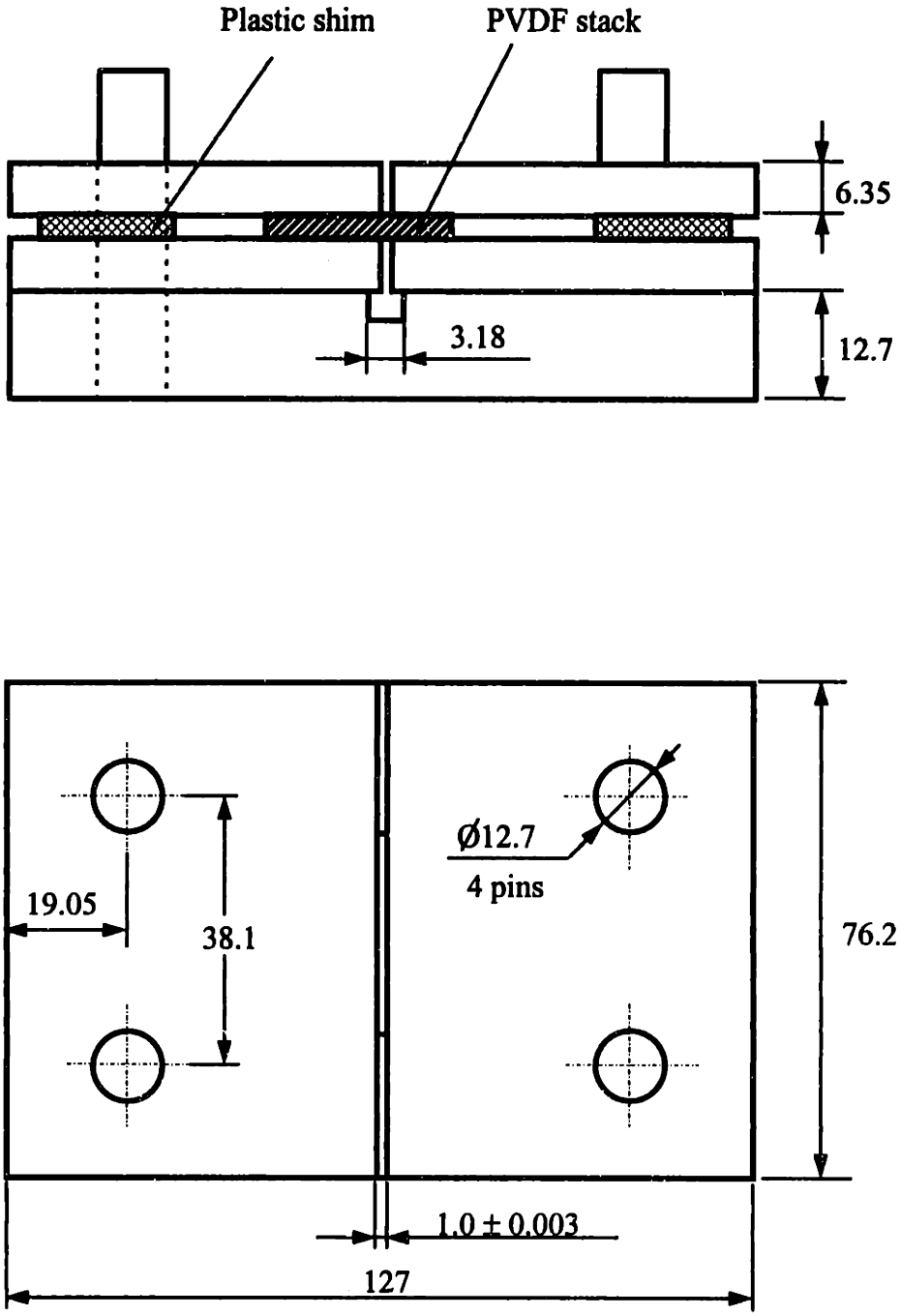

Figure 5.3 Auxiliary device for cutting the PVDF stacks. All dimensions in millimeters

Then the thickness corresponding to the half-wave resonance is

$$l = \frac{v_s}{2f}. \tag{5.2}$$

5.3.1. PVDF elements

The speed of sound in the PVDF film is 2200 m/s.[25] Then the thickness of the PVDF element corresponding to 2 MHz half-wave resonance is 0.55 mm.

The PVDF elements similar to those shown in Figure 2.2 but with no magnetic tape interleaving each PVDF layer were constructed. The PVDF film was cut to size 25.4 mm × 12.7 mm (the dimensions of the steel blocks from Figure 5.1). Both sides of each strip were subjected to the surface preparation as described in section 4.2. Two stacks were laminated simultaneously, layer by layer, in the die set with the ZAP CA cyanoacrylate adhesive. The pressure in the stack was adjusted during the adhesion process to be approximately 0.65 MPa. The process continued until the thickness of the PVDF stacks reached 0.55 mm. The top and the bottom layers of each stack was cut to size 40 × 12.7 mm and were used as leads for electrical wiring connections. In this way two PVDF multilayer assemblies were produced at a time. Those stacks had face dimensions of 25.4 mm × 12.7 mm , thickness 0.55 mm and had leads for electrical connections on both sides.

The next step was to cut the 12.7 mm wide stacks to the size of 2.5 mm. The scalpel was used for this purpose. An attempt to cut the first laminated stack led to it's failure because of the excessive shear stress acting on PVDF during the cutting. The areas of the stack closely adjacent to the cutting edges completely delaminated and had the damaged and torn PVDF layers. In order to prevent the stacks from delamination during cutting, an auxiliary device was designed, shown in Figure 5.3. The device consists of aluminum baseplate 12.7 mm thick with four stainless steel pins pressed into it. The pins are used as guides for the four aluminum plates, which are designed to clamp the PVDF stack on both sides and to leave only a small slot between the plates with enough space

just for the scalpel blade. In this way only a portion of the stack approximately 0.5 mm was delaminated or damaged, and that portion was easily removed on table grinding machine. Using the procedure described above, each laminated stack was cut into three elements, about 4 mm wide each. Total number of 16 PVDF elements was produced this way and each element was ground to the dimension of 2.65 mm on a table grinding machine using the aluminum oxide grinding wheel. During grinding each element was clamped in a precision machinist's vise and was ground in the direction parallel to individual PVDF layers in very small (2.5 micrometers) increments to prevent the material overheating.

5.3.2 Acrylic plates

The thickness of the acrylic plate corresponding to the half wave resonance is determined by Eq. (5.2) and is calculated to be 0.7 mm. The sheet of cast acrylic 2.54 mm thick was cut to strips with dimensions 25.4 × 2.65 × 0.7 mm on milling machine. Each acrylic plate was then assembled with PVDF using ZAP CA cyanoacrylate adhesive following the procedures close to that of assembling the PVDF layers, outlined in section 5.3.1. Each PVDF element was taped to the top half of the die set (Figure 5.1) and acrylic plate was mounted on the steel block and the cyanoacrylate adhesive applied to the acrylic surface. A total number of sixteen PVDF-acrylic elements were produced. They differed from Strachan's, shown in Figure 2.2, in that instead of copper electrodes, the top and bottom PVDF layers were made longer and used as leads for electrical connection.

5.3.3 PZT driver

PZT plates type 5A with silver electrodes on the surfaces were provided by American Piezo Ceramics, Inc. Each plate have dimensions 38.1 × 2.5 × 1 mm. A 30 gauge Teflon coated copper wires were soldered to silver electrodes on both sides of the plate across 1 mm dimension.

5.3.4. Assembly of the stack

As described in section 5.3.2 sixteen PVDF-acrylic elements were produced. Each PVDF-acrylic element is a structure composed of seventeen 28 μm thick PVDF layers and 0.7 mm thick acrylic plate. The face dimensions of each element was 25 mm × 2.65 mm and a thickness of 1.25 mm.

Each PVDF-acrylic element is then subjected to 2500 V test voltage on Hipotronic HD100 Series AC/DC Hipot tester. Those elements that failed are discarded. Fourteen "good" stacks were left and eleven of them were chosen to be used in construction of the device.

Using the die set (Figure 5.1) as before, eleven PVDF-acrylic elements were assembled one by one using ZAP CA cyanoacrylate adhesive. The twelfth acrylic plate was added to the structure in order to have a layer of acrylic between PZT and first PVDF element. The stack is ground on the table grinder with aluminum oxide wheel to the dimension of 2.5 mm and assembled with PZT driver.

5.3.5 Electrical connections

After the assembly, the stack consisted of eleven PVDF elements, twelve acrylic plates and PZT driver. A 30 gauge wire with Teflon insulation was attached to each PVDF electrical lead tab, using BA-2905 electrically conductive epoxy, provided by TRA-CON, Inc. A schematic of the stack with electrical connections is shown in Figure 5.4.

After the wires were connected the stack's lead tabs were electrically insulated from each other with two thin layers of paper and cemented with Resin Technology Group, Inc., Epon 828 epoxy resin to prevent them from being torn or damaged during the device operation.

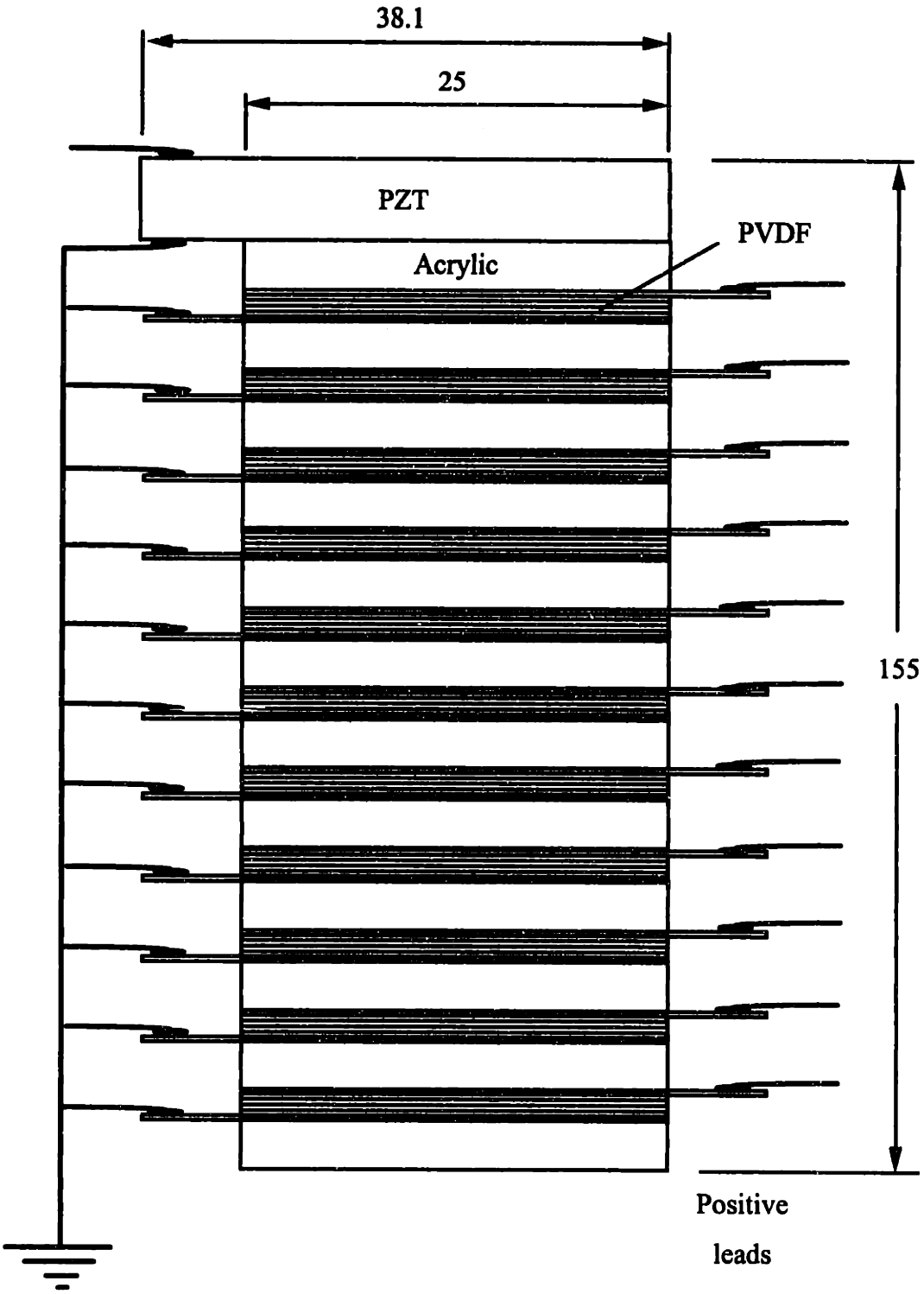

Figure 5.4. Schematic of the stack with electrical connections. Stack composition: 11 PVDF elements, 12 acrylic plates and a PZT driver.

5.4 Measurement of the Stack Capacitance and Dissipation Factor

To ensure the good quality of PVDF elements and detect the errors in fabrication (improper bonding, electrical shorting between PVDF layers, etc.) the capacitance and dielectric factor of each PVDF element were measured using General Radio model 1615-A capacitance bridge. The schematic of the measurement setup is shown in Figure 5.5. The PVDF stack electrical leads were connected to the capacitance bridge using two-terminal connection. The stack was driven by General Radio type 1311-A oscillator at a frequency 1 kHz. An EG&G Princeton Applied Research model 128A lock-in amplifier was used to balance the bridge. Grounded aluminum foil was used to shield the stack from the external noise. All electrical connections were made using shielded coaxial cable.

The measured values of capacitance and dissipation factor for each PVDF element are shown in Table 5.1.

PVDF element No.	Capacitance, pF	Dissipation factor (tan δ)
1	10.98	0.0263
2	10.95	0.0252
3	12.55	0.0266
4	13.22	0.0236
5	12.63	0.025
6	11.69	0.0256
7	11.41	0.0294
8	13.16	0.025
9	3.17	0.033
10	12.25	0.0263
11	17.82	0.0369

Table 5.1. Measured values of capacitance and dissipation factor for each PVDF element in the stack.

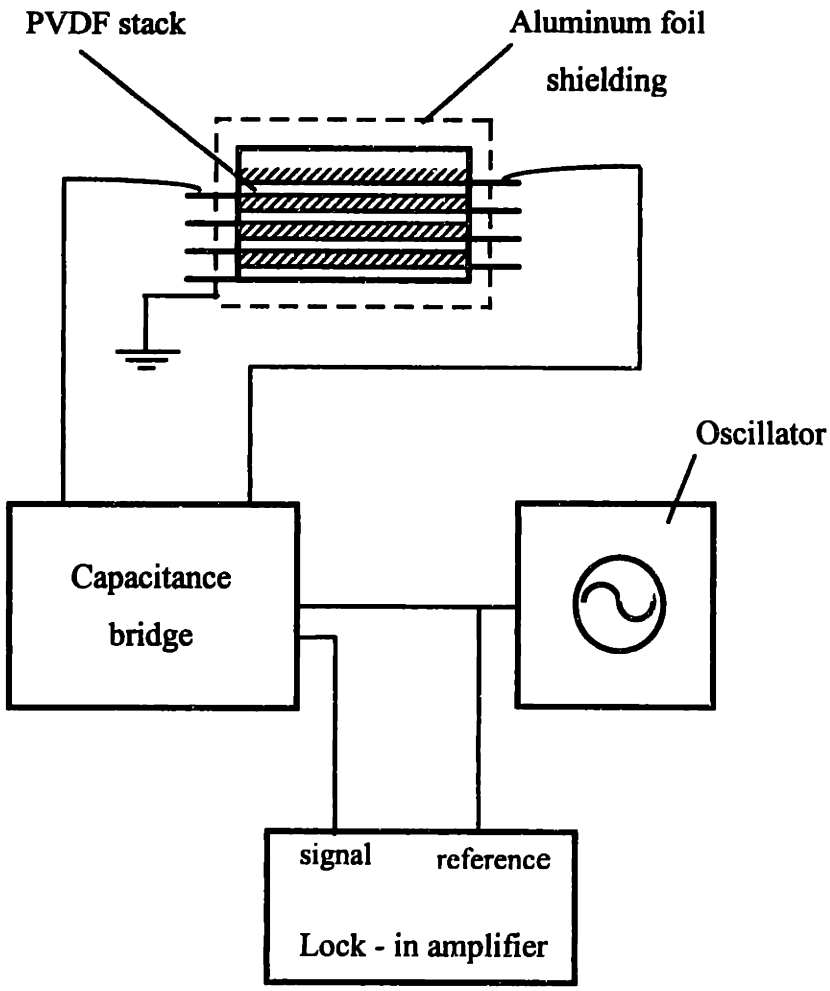

Figure 5.5. Schematic of the setup for the PVDF stack capacitance and dissipation factor measurements.

The PVDF elements are numbered from top to bottom, corresponding to Figure 5.4, so the PVDF element that is the closest to PZT driver is referred as No. 1.

The theoretical value of the PVDF element capacitance C is

$$C = \frac{\varepsilon \varepsilon_0 A}{l} \quad , \qquad (5.1)$$

where ε is relative dielectric permittivity of PVDF, $\varepsilon_0 = 8.854 \times 10^{-12}$ F/m is a dielectric permittivity of free space, A is the capacitive area, and l is the thickness of the PVDF element

Using the appropriate dimensions and a value of a relative dielectric permittivity the capacitance of each PVDF element was calculated to be 12.07×10^{-12} Farads and is in good agreement with measured values.

The capacitance of one of the PVDF elements, element 9 in particular, is smaller then the expected value, that probably means there is electrical shorting between the PVDF layers or other defect in its fabrication. This element was not included in the drive circuit and was grounded during the device testing and operation.

Both dielectric permittivity and dissipation factor of PVDF are frequency dependent. In addition, dissipation factor is highly temperature dependent. The temperature dependence of PVDF dissipation factor is shown in Figure 5.6. As follows from that graph the values of the dissipation factor corresponding to 1 kHz and $T = 25$ °C (the conditions for PVDF capacitance and dissipation factor measurements) are in the range from 0.02 - 0.03. This is in good agreement with the measured values, which tells about good acoustical coupling of the produced PVDF elements.

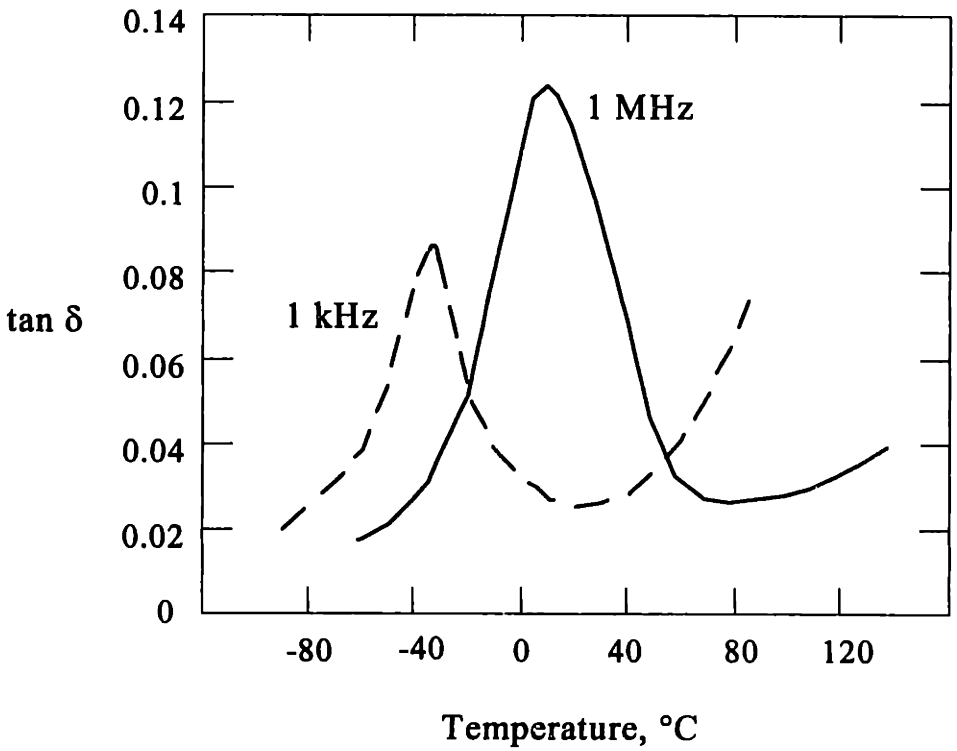

Figure 5.6. Temperature dependence of PVDF film dissipation factor at 1 kHz and 1 MHz. Adapted from Andreev *et al.* [29]

5.5 Summary

A replica of the Strachan-Aspden prototype device was constructed. The PVDF stack was constructed utilizing about 200 layers of 28 μm thick layers of polyvinylidene fluoride film assembled in 11 PVDF elements 0.55 mm thick each. PVDF elements were interleaved with acrylic plates of thickness corresponding to half-wave resonance at 2 MHz. Hard ceramic driver PZT type 5A was incorporated to the stack. All connections in the stack were made with ZAP CA cyanoacrylate adhesive. The stack produced in this way had dimensions 155 × 25 × 2.5 mm.

The capacitance and dissipation factor of each PVDF element were measured on General Radio model 1615-A capacitance bridge. The measured capacitance values of PVDF elements is in a good agreement with values calculated from Eq. (5.1) and the values of dissipation factor agreed with the values measured by Andreev et al.[29] That ensures a good electrical and acoustical coupling in the PVDF stack.

6. TESTING THE REPLICA DEVICE

6.1 Piezoelectric Model and Single PVDF Layer Experiments

It is likely that the explanation of the Strachan device is related to the thermal, electrical and mechanical coupling in the PVDF. Strachan's device operates with large electric and acoustic fields. In order to understand the response of the device a model that incorporates only the electro-mechanical aspects of the device's behavior was made. The model has utility in that it is relatively simple. Unfortunately, it does not include thermal effects necessary for a complete model of Strachan's device; however, it does provide a baseline from which to judge the experimental performance of the PVDF device. Experimental deviations from the electro-mechanical model would signal possible effects linked to Strachan's energy conversion phenomenon.

Considering electro-mechanical interactions in material with piezoelectric characteristics, mechanical variables are generally strain X and stress τ. For electrical variables, either polarization P or electric flux density D can be selected as the extensive variable, although the intensive variable is always electric field E.

Fundamental piezoelectric relations with stress τ and electric field E taken as independent variables are given by[15]

$$X = s^E \cdot \tau + d \cdot E, \tag{6.1}$$

$$D = d \cdot \tau + \varepsilon^\tau \cdot E, \tag{6.2}$$

where s^E is an elastic compliance coefficient, ε^τ is a dielectric constant and $d = \frac{X}{E}$ is a piezoelectric strain coefficient.

For simplest one dimensional case with two piezoelectric elements, as shown in Figure 6.1, the strains in driver and listener are:

$$X_l = s_l^E \cdot \tau_l + d_l \cdot E_{in} \tag{6.3}$$

for the driver,

$$X_2 = s_2^E \cdot \tau_2 + d_2 \cdot E_{out} \qquad (6.4)$$

for the load or listener.

Boundary conditions for that model:

$$\tau_1 = \tau_2 = \tau \qquad (6.5)$$

$$l_1 X_1 = - l_2 X_2 \qquad (6.6)$$

where l_1 is the driver thickness, l_2 is the thickness of the listener .

Combining Equations 6.3 - 6.6 and recalling that $E = \frac{V}{l}$, where V is an appropriate voltage drop, we obtain:

$$l_1 \cdot s_1^E \cdot \tau + l_1 \cdot d_1 \cdot \frac{V_{in}}{l_1} = -l_2 \cdot s_2^E \cdot \tau - l_2 \cdot d_2 \cdot \frac{V_{out}}{l_2} \qquad (6.7)$$

or rearranging,

$$V_{out} = -\frac{d_1}{d_2} \cdot V_{in} - \frac{1}{d_2} \cdot \left(l_1 \cdot s_1^E + l_2 \cdot s_2^E \right) \cdot \tau . \qquad (6.8)$$

Using Eq. (6.2) the stress τ for the listener is

$$D_2 = d_2 \cdot \tau + \varepsilon_2^\tau \cdot E_{out} , \qquad (6.9)$$

Since there is no free charge in the listener, $D_2 = 0$ and

$$\tau = -\frac{\varepsilon_2^\tau}{d_2} \cdot \frac{V_{out}}{l_2} . \qquad (6.10)$$

Substituting Eq. (6.10) into (6.8), the output voltage is found as a function of the drive voltage:

$$\frac{V_{out}}{V_{in}} = -\frac{\frac{d_1}{d_2}}{1 + \frac{\varepsilon_2^{\,r}}{d_2} \cdot \frac{l_1 \cdot s_1^{\,E} + l_2 \cdot s_2^{\,E}}{l_2}} \cdot \tag{6.11}$$

The combined thickness of driver and listener in single layer model is much smaller than the wavelengths corresponding to the operational frequency range. The single PVDF layer behavior will be tested at frequencies below 100 kHz. The first primary (half-wave) resonance for PZT-PVDF single layer assembly occurs at approximately 1.6 MHz and the half-wave resonance for PVDF-PVDF single layer assembly corresponds to 19.6 MHz. Therefore the output voltage from PVDF listener is frequency independent and is only a function of the driver's voltage and properties of two materials involved.

In this model the piezoelectric response is calculated for single 28 μm thick PVDF layer, driven by 1 mm thick PZT type 5-A driver, and also for two PVDF layers (PVDF driver - PVDF listener) setup.

To measure the PVDF layer piezoelectric response a 38.1 mm × 5.08 mm × 1 mm PZT type 5-A piezoelectric element with silver electrodes on both sides, from American Piezoceramics, Inc., is driven with Hewlett Packard 33120A signal generator in frequency range from 10 - 90 kHz. A single PVDF layer 28 μm thick, coated on one side with 2200 angstroms Nickel and 800 angstroms Aluminum, is used as a listener. The bare PVDF side is electroded with the thin copper tape, which is also used as a common ground for both PZT and PVDF. The electrical connections for PVDF layer are made using electrically conductive BA-2902 epoxy, provided by TRA-CON, Inc.

PVDF listener is connected to Tektronix 475 digital oscilloscope using shielded coaxial cable. Both Driver and listener are thermally and electrically insulated from the metal vise with the 3.5 mm thick glass spacers.

In addition, the piezoelectric response measured for single PVDF layer model with imposed temperature gradient. The schematic of temperature gradient setup is shown in Figure 6.2. A Minco HK 5255R31.6 thermofoil heater, powered by DC power supply,

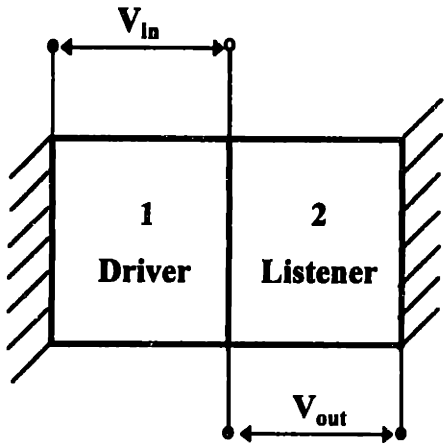

Figure 6.1 One dimensional piezoelectric model, clamped boundary conditions.

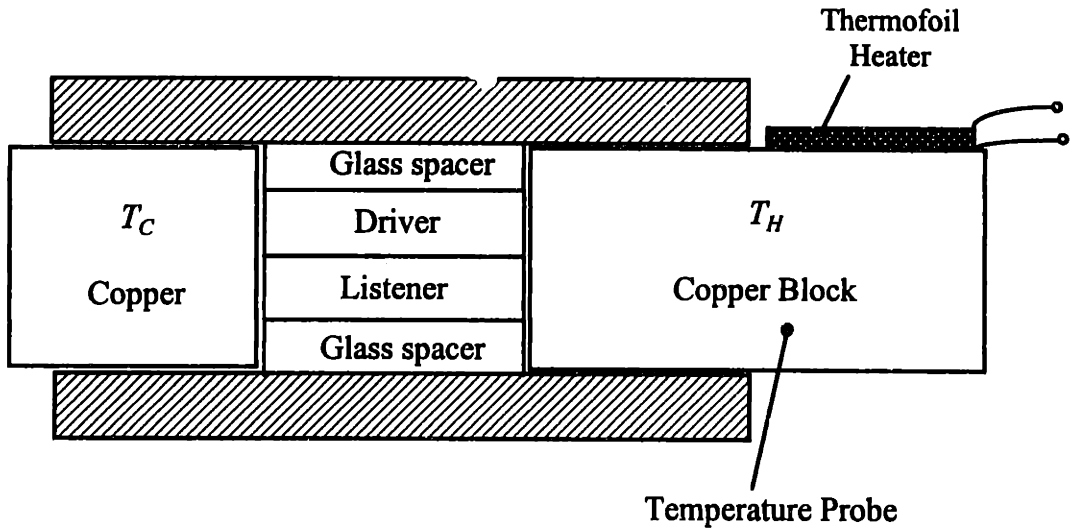

Figure 6.2 Schematic of temperature gradient setup for piezoelectric single layer experiments.

is mounted on one side of the copper block and used as a high temperature source. The temperature of the copper block is measured with the Type T (copper-constantan) thermocouple. Along with PZT-PVDF piezoelectric response experiments, PVDF-PVDF tests are performed, with the only difference that the same as the listener, 28 μm thick PVDF layer, is used as a driver instead of a PZT element.

The measured piezoelectric response of single PVDF layer is shown in Figures 6.3 and 6.4, combined with the predicted response calculated from Eq.(6.11). The measured V_{out}/V_{in} ratio as a function of frequency is given for measurements performed at T = 23 °C (isothermal conditions) and with 50 °C/cm temperature gradient applied along PVDF layer and is compared to the expected response of electro-mechanical model. Both experimental data and the predicted response follow the similar pattern behavior and lay within 25 % difference, which indicates no or insignificant influence of either frequency or temperature gradient on the listener PVDF layer behavior. Slightly higher output voltages corresponding to non-isothermal conditions can be explained by temperature dependence of PVDF piezoelectric strain coefficient d_{33}.

6.2 Mechanical Model for the Drive Experiments

The replica of the Strachan-Aspden's prototype device is a multilayer structure that contains eleven PVDF elements, twelve acrylic plates and PZT. The components of the device posses different properties and characteristics. To find the dynamic response of such complicated system the one dimensional mechanical model of the stack is produced. The schematic of the stack corresponding to that mechanical model is shown in Figure 6.5.

Each PVDF element is modeled as a two mass-spring-damper combination driven by an electrical input signal (analogous to the external force). The model for an acrylic plate consists of a mass and two springs. The PZT is modeled as a mass, a spring and an electrical driver. The corresponding models are shown in Figure 6.6. The PVDF element, due to its multilayer structure, has the lowest acoustic quality factor Q, which is much lower than that of Acrylic and several orders of magnitude lower than the Q for PZT.

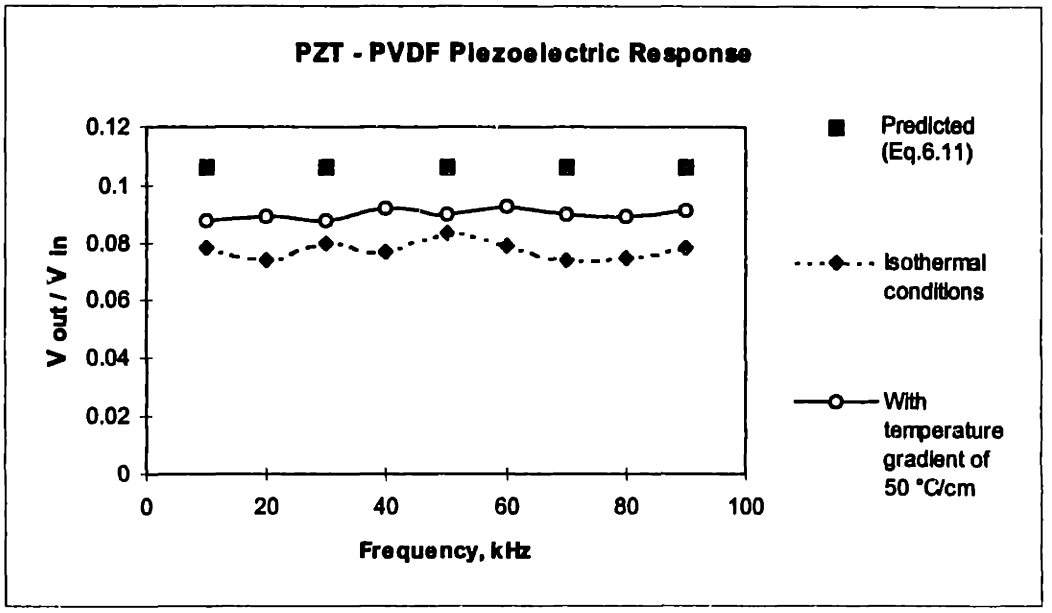

Figure 6.3. Piezoelectric response from single PVDF layer, driven by PZT

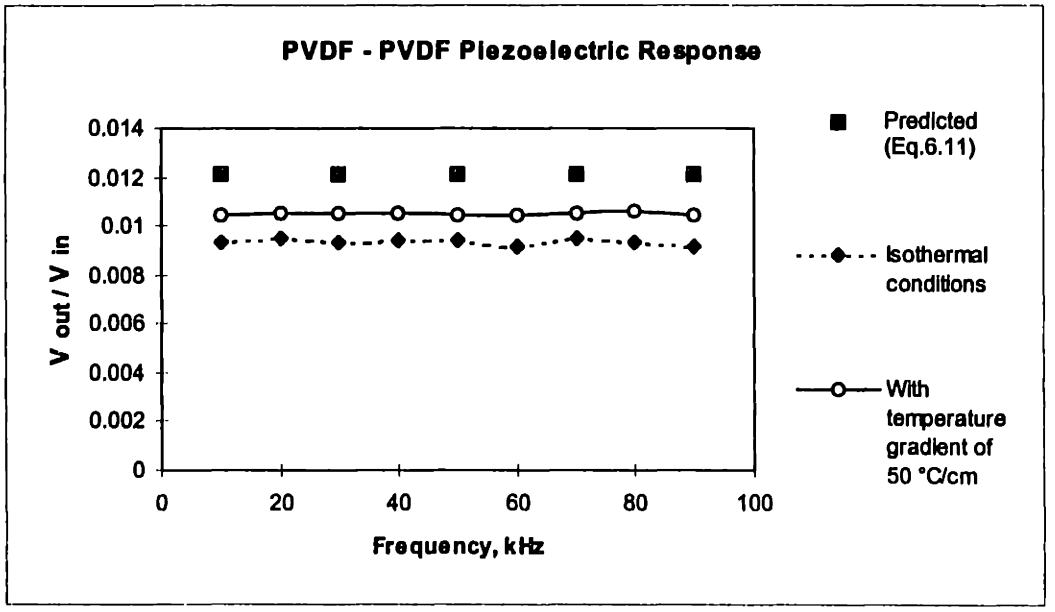

Figure 6.4. Piezoelectric response from single PVDF layer, driven by PVDF

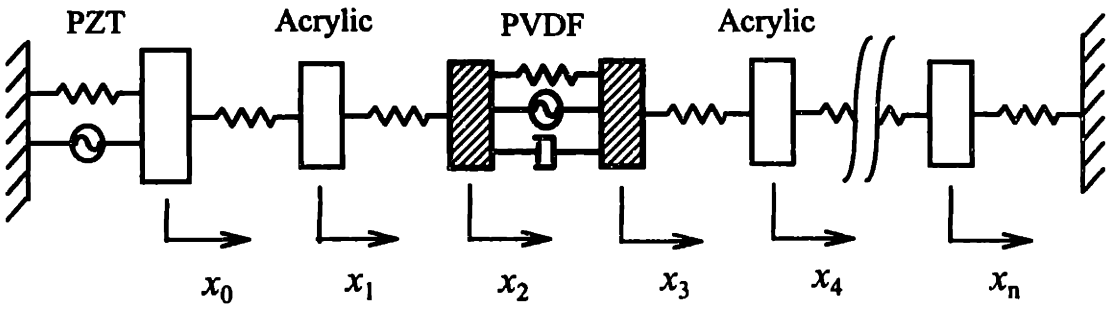

Figure 6.5. Stack model for the mechanical drive experiments.

Therefore most of the losses are essentially in PVDF. So only PVDF element includes damping effects.

The damping coefficient b can be expressed as[46]

$$b = 2\zeta \cdot m \cdot \omega_n \tag{6.12}$$

where ζ is the damping factor, m is the mass and ω_n is the natural frequency of oscillations. The damping factor is related to the quality factor[46] $\zeta \approx \frac{1}{2Q}$ and the natural frequency is $\omega_n = \sqrt{\frac{k}{m}}$, where k is the spring constant. Then Eq. (6.12) becomes

$$b = \frac{1}{Q} \cdot \sqrt{k \cdot m} \tag{6.13}$$

The quality factor of the PVDF elements built by MacBride[34] was 5.6. So for this model the PVDF elements quality factor is assumed to be $Q \cong 5$.

The effective spring constants can be obtained from the stress - strain relationship:

$$\tau = Y \cdot X, \tag{6.14}$$

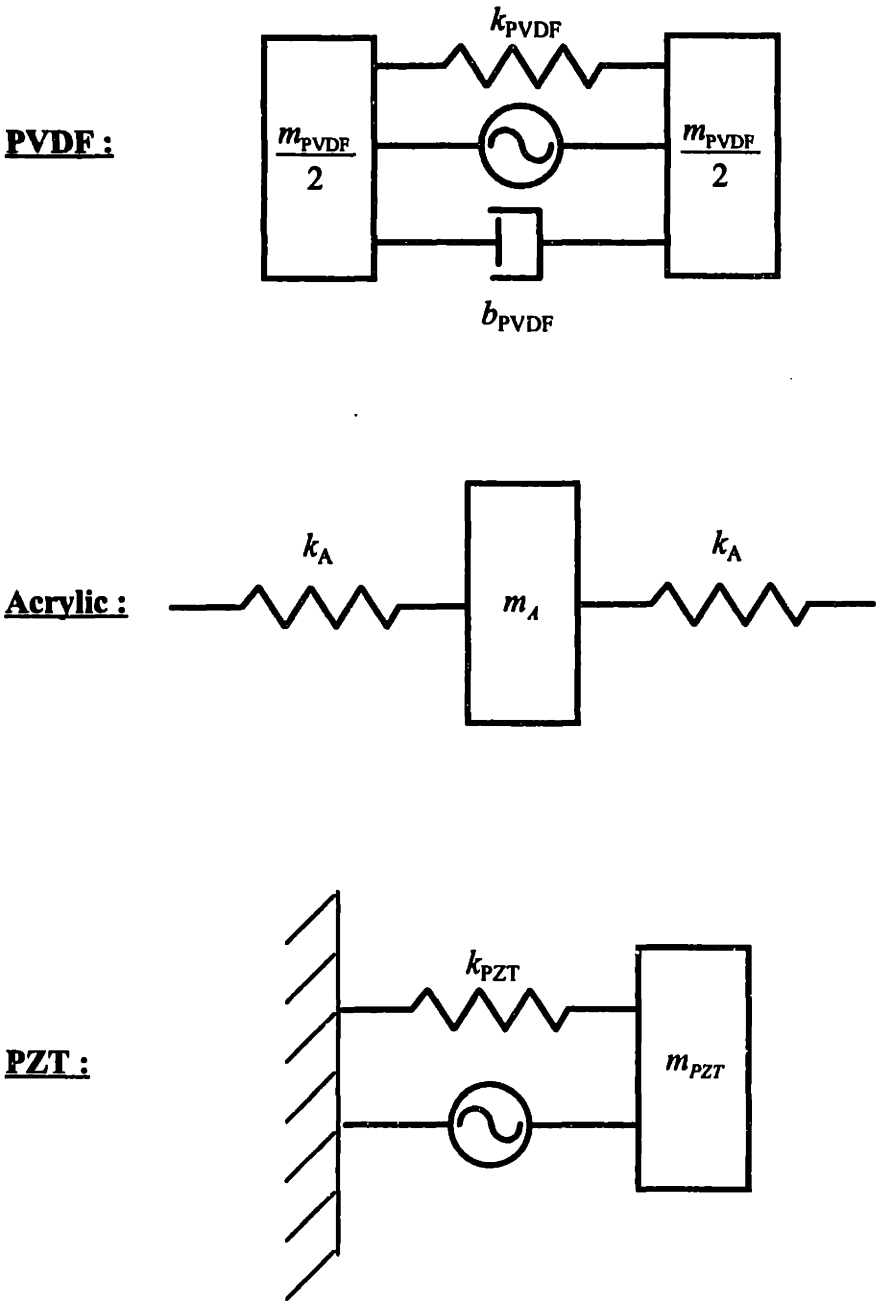

Figure 6.6. PVDF, Acrylic and PZT one dimensional models for the mechanical drive experiments.

where τ is the stress, X is the strain and Y is the Young's modulus.

The definitions of stress and strain are

$$\tau = \frac{F}{A}, \quad X = \frac{\Delta x}{l} \tag{6.15}$$

where F is the force component in the x direction, A is the cross section area, l is the element thickness and Δx is the elongation.

Then for each element modeled as a one dimensional mass - spring combination

$$k_{eff} = \frac{F}{\Delta x} = \frac{Y \cdot A}{l}. \tag{6.16}$$

The effective spring constant and mass for each PVDF element are found to be:

$$k_{PVDF} = \left(\frac{Y \cdot A}{l}\right)_{PVDF} = 2.27 \times 10^{8} \ \frac{\text{N}}{\text{m}}$$

$$m_{PVDF} = (\rho \cdot A \cdot l)_{PVDF} = 6 \times 10^{-5} \text{ kg}.$$

Using these values the damping coefficient for PVDF is $b_{\text{PVDF}} = 23.34 \frac{N \cdot s}{m}$. For computation purposes the value $b_{\text{PVDF}} = 25 \frac{N \cdot s}{m}$ is used.

The similar way the effective spring constant and mass for Acrylic are

$$k_A = \left(\frac{Y \cdot A}{l/2}\right)_A = 5.54 \times 10^{8} \ \frac{\text{N}}{\text{m}},$$

$$m_A = (\rho \cdot A \cdot l)_A = 5.2 \times 10^{-5} \text{ kg},$$

where for each acrylic element half-thickness is taken into account for calculation of the spring constant.

For PZT:

$$k_{PZT} = \left(\frac{Y \cdot A}{l}\right)_{PZT} = 1.72 \times 10^{10} \ \frac{\mathrm{N}}{\mathrm{m}}$$

$$m_{PZT} = (\rho \cdot A \cdot l)_{PZT} = 1.9 \times 10^{-4} \ \mathrm{kg}.$$

The equations of motion for elements of the device are:

$$\begin{aligned}
m_{PZT}\frac{d^2x_0}{dt^2} &= -k_{PZT}x_0 + k_A(x_1 - x_0) + (\psi V)_{PZT} \\
m_A\frac{d^2x_1}{dt^2} &= -k_A(x_1 - x_0) + k_A(x_2 - x_1) \\
m_{PVDF}\frac{d^2x_2}{dt^2} &= -k_A(x_2 - x_1) + k_{PVDF}(x_3 - x_2) + b\frac{d}{dt}(x_3 - x_2) - (\psi V)_{PVDF} \\
m_{PVDF}\frac{d^2x_3}{dt^2} &= -k_{PVDF}(x_3 - x_2) - b\frac{d}{dt}(x_3 - x_2) + k_A(x_4 - x_3) + (\psi V)_{PVDF} \\
m_A\frac{d^2x_4}{dt^2} &= -k_A(x_4 - x_3) + k_A(x_5 - x_4) \\
&\cdots \quad \cdots \quad \cdots \\
&\cdots \quad \cdots \quad \cdots \\
m_A\frac{d^2x_n}{dt^2} &= -k_A(x_n - x_{n-1}) - k_A x_n
\end{aligned} \tag{6.17}$$

where V is the input (drive) voltage and ψ is a constant relating the voltage to the resulting force, $\frac{\mathrm{N}}{\mathrm{V}}$. This constant can be determined by using the zero frequency relation between displacement and voltage

$$\psi V = kx$$

or

$$\psi = \frac{kx}{V} = kd_{33} \ , \tag{6.18}$$

where $d_{33} = \frac{x}{V}$ is a piezoelectric strain coefficient.

Then can find values of ψ for PZT and PVDF.

$$\psi_{PZT} = k_{PZT}\, d_{33,PZT} = 6.43 \ \frac{\mathrm{N}}{\mathrm{V}} \ ,$$

$$\psi_{PVDF} = k_{PVDF}\, d_{33,PVDF} = -\ 0.0075 \ \frac{\mathrm{N}}{\mathrm{V}}$$

Assuming the solution of (6.17) has the form:

$$x_i = x_{i,0}\, e^{j\omega t} \ ,$$

where ω is the system angular frequency.

The system of equations (6.17) becomes

$$\begin{aligned}
&\left(-m_{PZT}\omega^2 + k_{PZT} + k_A\right)x_0 - k_A x_1 = \left(\psi V\right)_{PZT} \\
&-k_A x_0 + \left(-m_A\omega^2 + 2k_A\right)x_1 - k_A x_2 = 0 \\
&-k_A x_1 + \left(-m_{PVDF}\omega^2 + k_A + k_{PVDF} + j\omega b\right)x_2 + \left(-k_{PVDF} - j\omega b\right)x_3 = -\left(\psi V\right)_{PVDF} \\
&\left(-k_{PVDF} - j\omega b\right)x_2 + \left(-m_{PVDF}\omega^2 + k_{PVDF} + j\omega b + k_A\right)x_3 - k_A x_4 = \left(\psi V\right)_{PVDF} \\
&-k_A x_3 + \left(-m_A\omega^2 + 2k_A\right)x_4 - k_A x_5 = 0 \\
&\quad \ldots \quad \ldots \quad \ldots \\
&\quad \ldots \quad \ldots \quad \ldots \\
&-k_A x_{n-1} + \left(-m_A\omega^2 + 2k_A\right)x_n = 0.
\end{aligned} \tag{6.19}$$

Solving the system of equations (6.19) the displacement or strain of each element can be found as a function of frequency. This is done in matrix form, using Matlab.

The predicted dynamic response of the stack as a function of driving frequency is shown in Figure 6.7. The driving voltage on PZT driver in the model is assumed to be V_{PZT} = 500 V and the PVDF driving voltage V_{PVDF} = 1000 V. The predicted primary half wave resonance is found numerically to correspond to frequency f_{res} = 46 kHz. The calculated oscillation amplitude in the PZT-PVDF-acrylic stack corresponding to the half wave resonance frequency as a function of the rest position in the stack is shown in Figure 6.8.

To verify the analytical results obtained from mechanical model and measure the device resonance frequencies, the stack is driven by ceramic driver and its response is measured as a function of driving frequency.

The stack is clamped in the precision machinist's vise. All PVDF elements are grounded except listener, which is connected to the oscilloscope for measurement of the output signal amplitude and phase angle. The stack is driven by PZT driver with voltages varying from 10 - 120 V and driving frequency below 100 kHz. The response is measured for isothermal conditions T = 23 °C.

Testing the device and measuring its dynamic response discovered few resonances in the frequency range from 20 -75 kHz. In particular, the strongest resonance is found at 45 kHz and two resonances, weaker then the primary one are found at 22 kHz and 71 kHz. The 45 kHz resonance is in very good agreement with the value of resonance frequency obtained from mechanical model. The 71 kHz resonance is presumably corresponds to the experimental setup structure including PVDF, PZT, insulating glass and vise. The amplitude and phase of the listener output signal relatively to the input signal are shown in Figures 6.9 and 6.10 respectively.

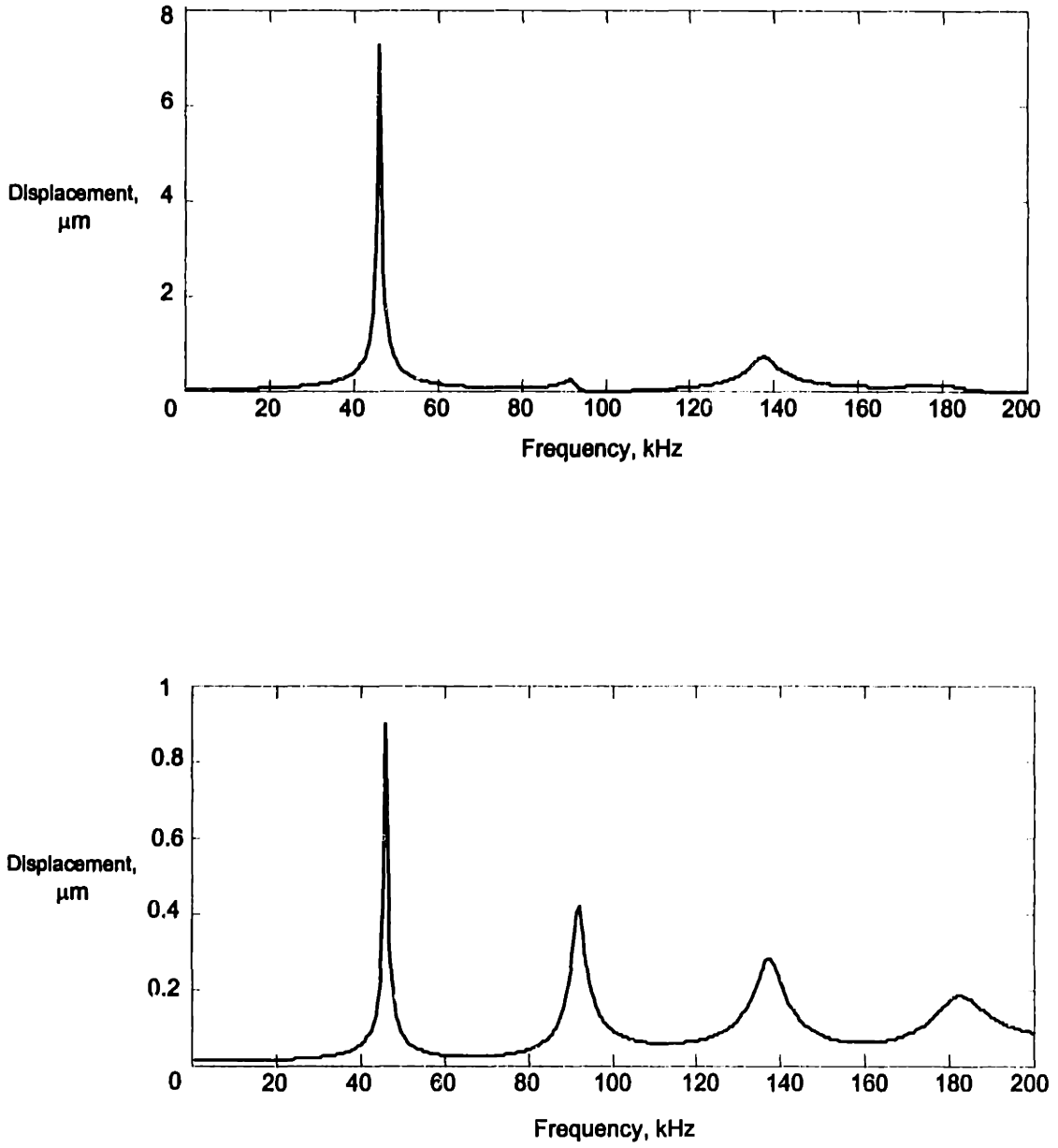

Figure 6.7. The predicted dynamic response of the stack as a function of driving frequency for two locations in the stack. The top graph represents the response of the middle of the stack, the bottom graph, at the stack edge.

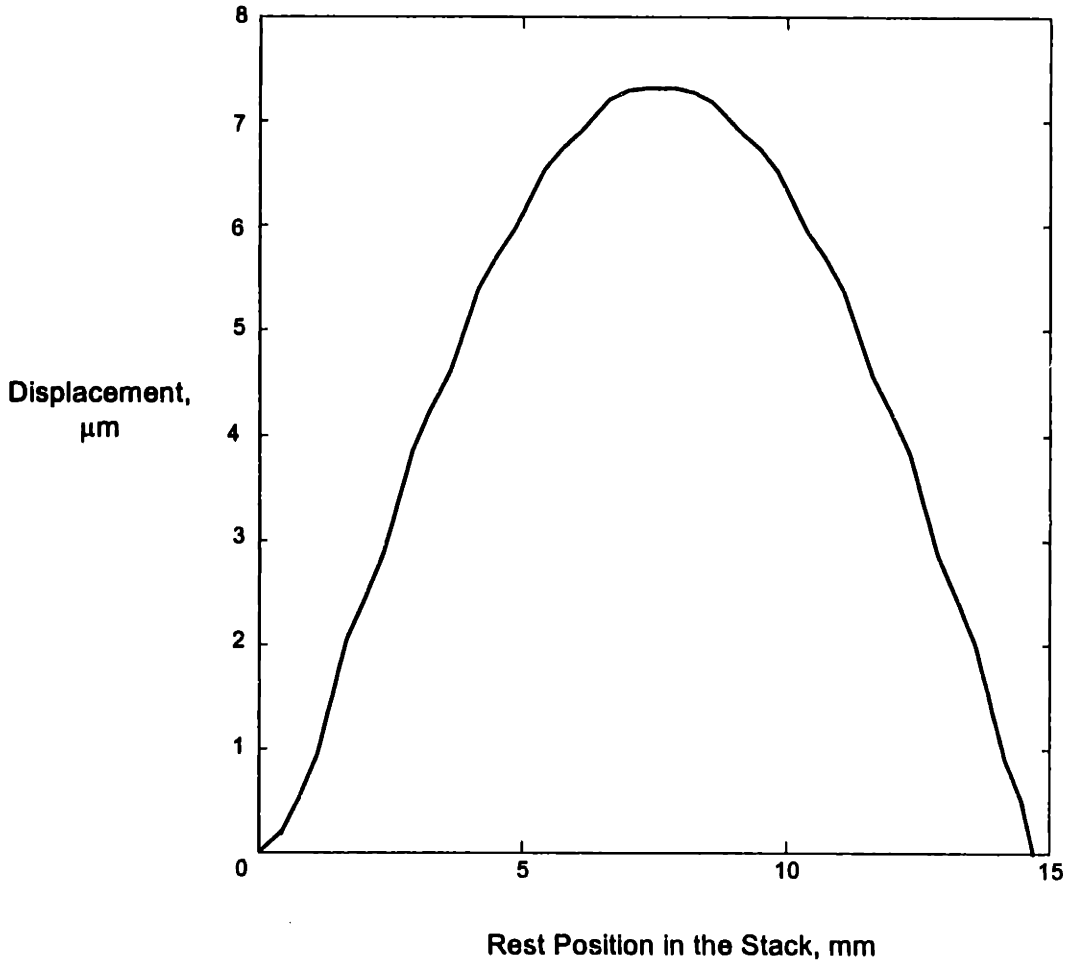

Figure 6.8. The predicted amplitude of oscillation in the stack corresponding to the half wave resonance. Driving frequency is 46 kHz.

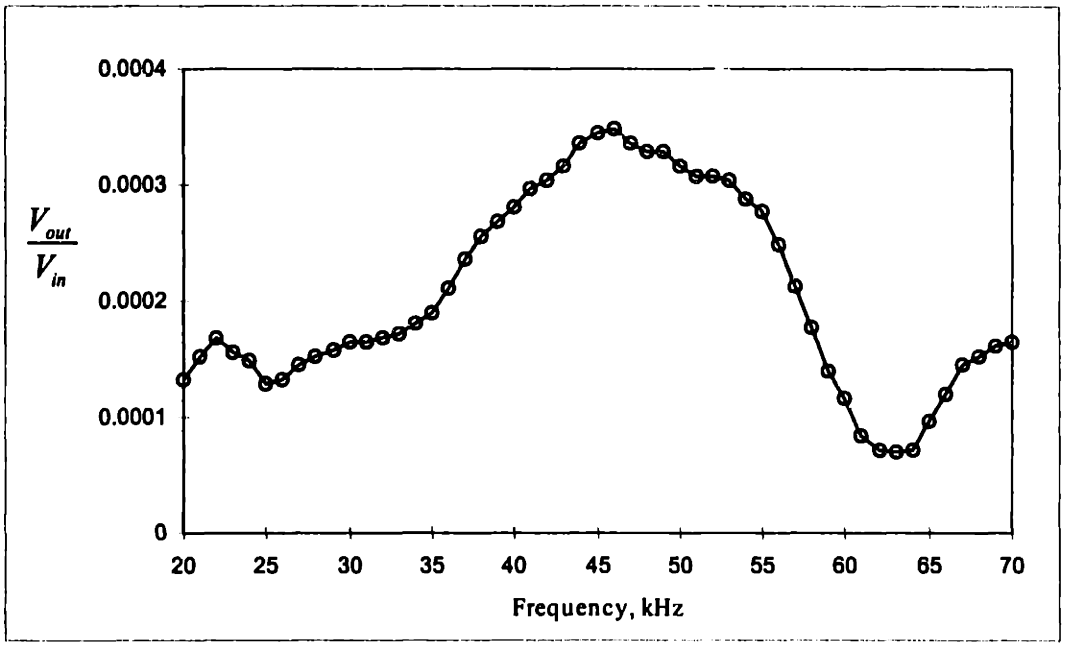

Figure 6.9. Measured V_{out} / V_{in} for isothermal stack driven by PZT only.

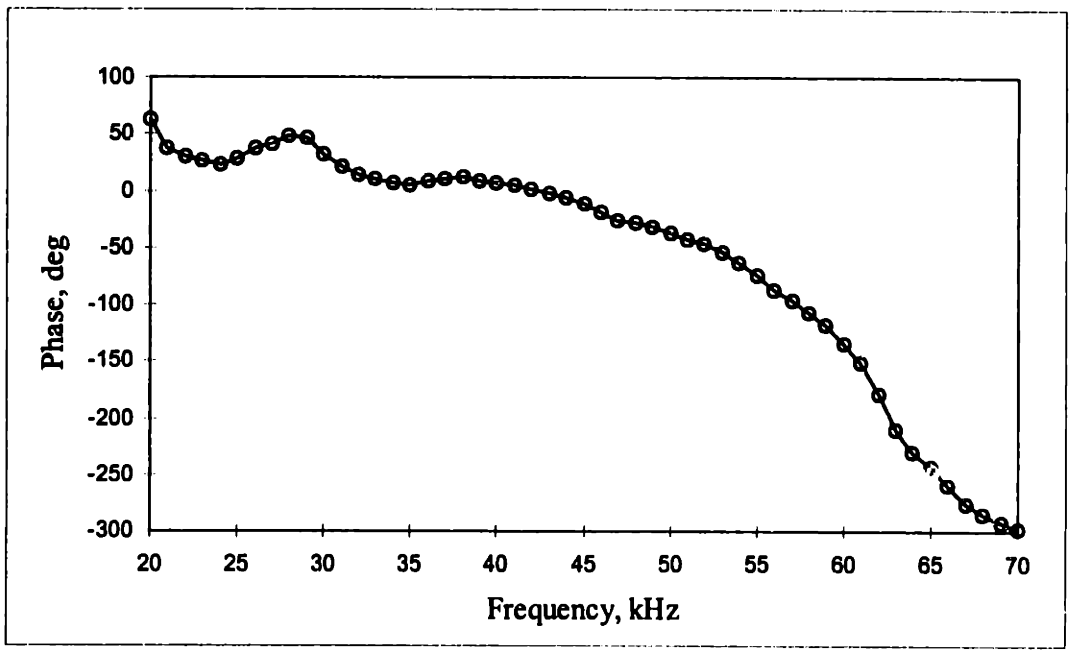

Figure 6.10. Measured phase difference between input and output signals versus frequency for isothermal stack driven by PZT only.

6.3 Resonance Electrical Circuit

Strachan claims that the driving voltage level required to see the effect has to be fairly high. In his experiments the voltage driving the stack was of the order 1000 V or higher, see Figure 2.4. In this work the circuit driving replica device is designed to separately control the gain of PZT and PVDF driving voltages and if needed to drive the stack with the PZT only or the PVDF.

The schematic of the electrical circuit is shown in Figure 6.11. The circuit is driven by HP 33120 function generator. A two channel Crown model DC 300A audio amplifier is connected to the function generator and provides the amplification of the signal for two separately regulated circuits, one with the PZT driver and the other with PVDF stack.

Both PZT and PVDF circuits are connected to a Crown audio amplifier through two custom made transformers with 1 : 24 and 1 : 5 ratios respectively. In order to raise the driving voltage on PVDF, an adjustable L-C resonance circuit is designed, as shown in Figure 6.11. For that purpose, twenty capacitors type P 3508-ND 0.0082 microfarad each are connected in series, parallel to the PVDF stack. Any number out of 20 capacitors can be shorted to make coarse step adjustment of the resonance frequency. The steps in capacitance are 410, 630.8, 820, 1171.4, 1366.7, 1491, 1640, 1822 and 2050 picofarad. The fine adjustment is made by incorporating into the circuit the adjustable parallel plates tuning capacitor with the capacitance range from 30 - 270 picofarad. The tuning capacitor is connected in parallel with the PVDF stack and 20 capacitors for coarse adjustment. The inductance is designed and adjusted by increasing the air gap between the core material to have the inductance of 8×10^{-3} Henry, see Appendix B. The L-C resonance circuit designed this way has the minimum resonance frequency of 33.0 kHz, when only four capacitors out of twenty included in the circuit. The maximum achievable resonance frequency is 74.2 kHz with all twenty capacitors in series. The quality factor of the L-C resonance circuit not including PVDF stack is found using half power method to be 49.6.

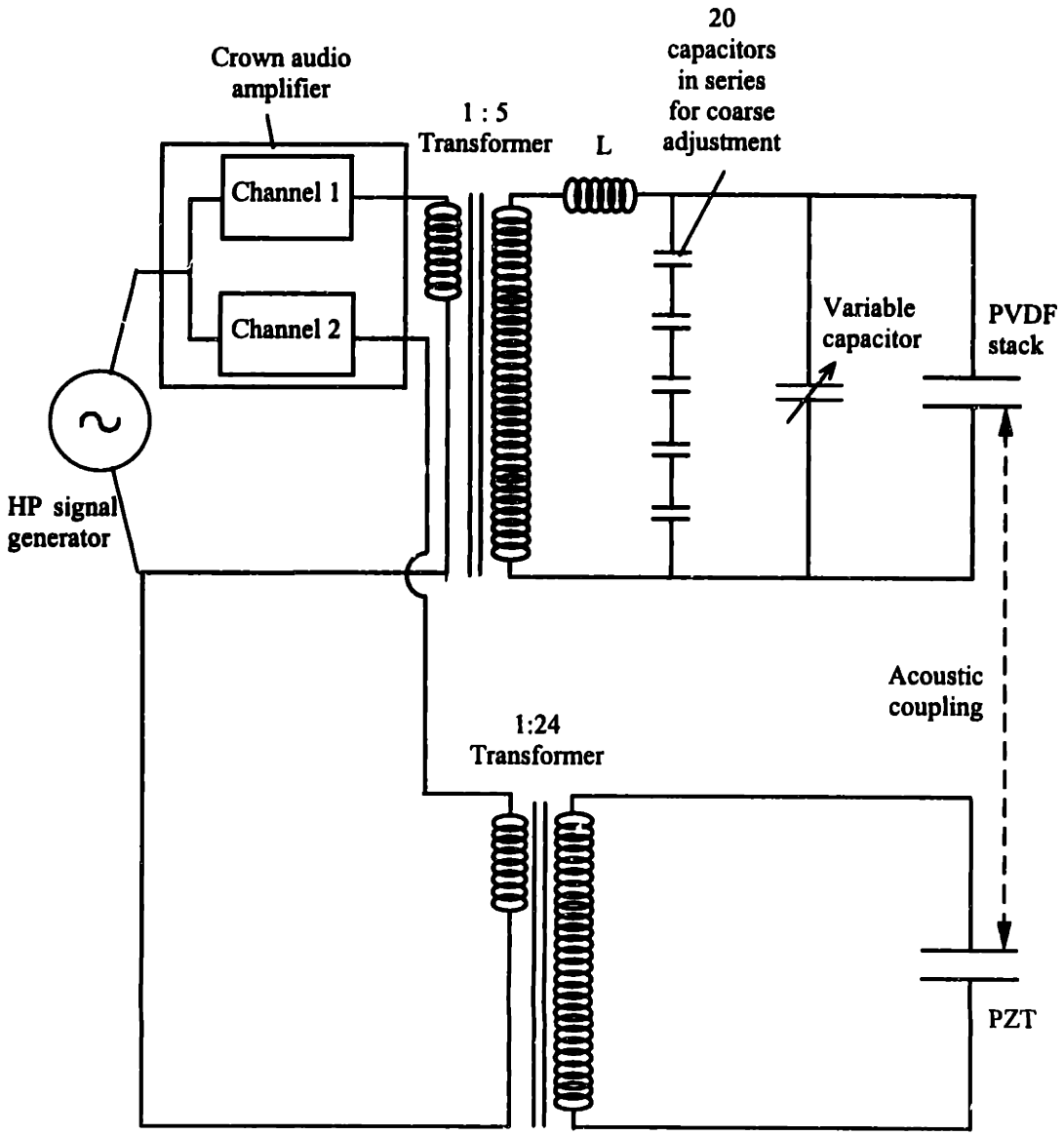

Figure 6.11. Schematic of the electrical circuit driving the stack.

6.4 Temperature Gradient Assembly

The schematic of the temperature gradient setup is shown in Figure 6.12. To provide temperature gradient across the stack a Minco HK 5255 R31.6 thermofoil heater, 25 mm × 13.5 mm × 0.3 mm is used as a hot temperature source. The thermofoil heater is mounted on the top of copper block 25 mm × 15 mm × 5 mm thick. A 0.05 mm thick mylar sheet is used to electrically insulate the PVDF stack from the copper block.

A copper block 25 mm × 15 mm × 5 mm thick with a passage for the cooling water is used as a cold temperature source. It is mounted on the bottom of the stack and is also separated from the PVDF stack by a thin layer of mylar. The cooling water is pumped through the reservoir filled with ice and the water volume flow rate is controlled with the Cole Parmer Masterflex model 7518-00 pump controller. Thermofoil heater, copper blocks, mylar sheets and PVDF stack are interleaved with thin layers of American Oil and Supply Company type HTC heat sink compound to provide for better thermal contact.

The temperatures of two copper blocks are measured with two type K thermocouples, inserted in the orifices specifically drilled in two copper blocks for that purpose and filled with the American Oil and Supply Company type HTC heat sink compound.

A 25 mm × 15 mm × 1 mm thick rubber padding is mounted on top of the thermofoil heater to provide thermal and mechanical insulation. A vertical clamping force is applied to the stack to help provide good thermal contact between the PVDF stack surfaces and cold and hot thermal sinks. The vertical force is applied by mounting a polyethylene spacer and 1.68 kg steel weight on the top of the temperature gradient assembly.

6.5 Experimental Setup

The PVDF stack is clamped in a precision machinist's vise, as shown in Figure 6.13. The vise is taped to the delrin baseplate using doublesided adhesive tape. A copper

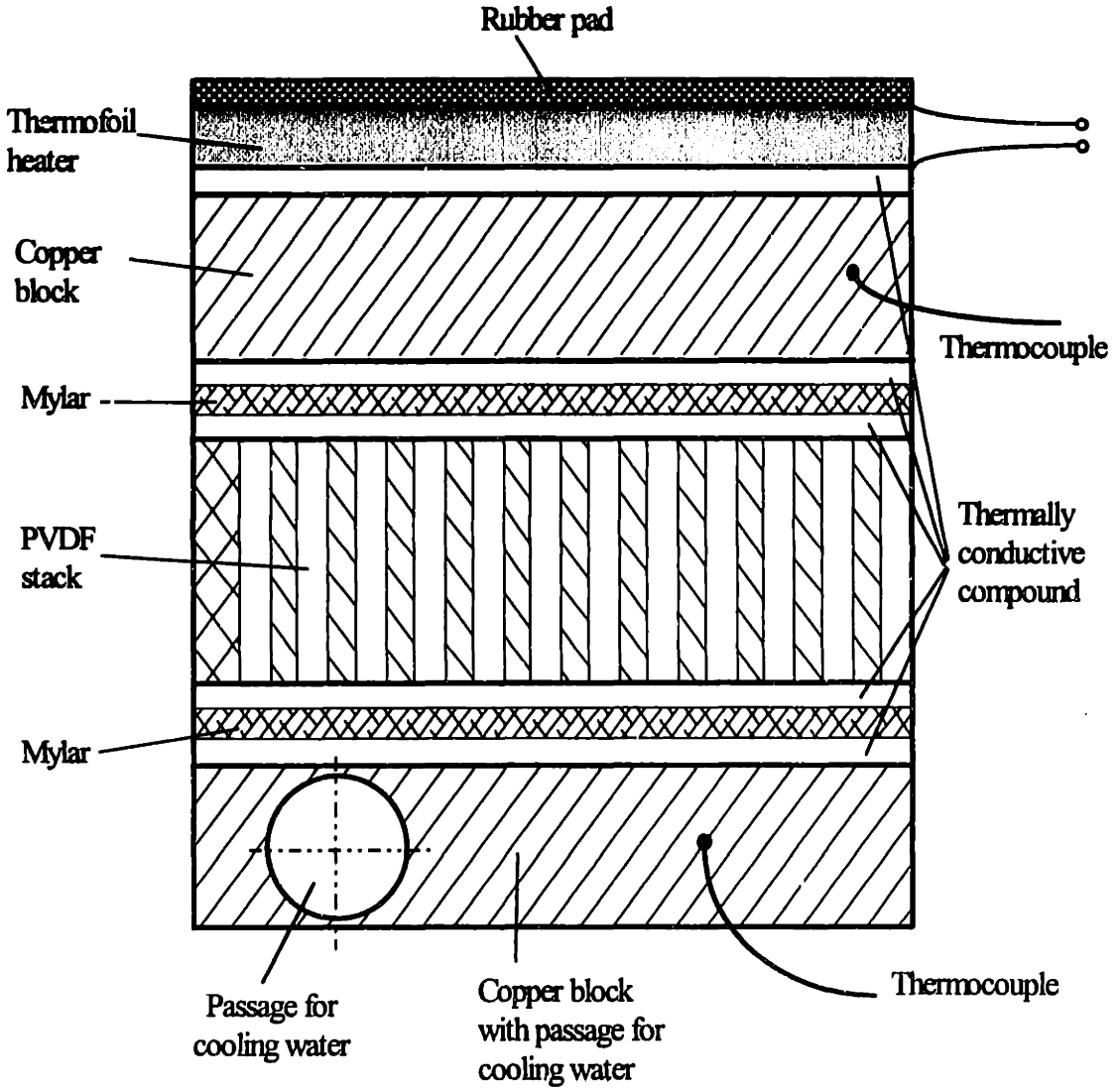

Figure 6.12 Schematic of the temperature gradient assembly.

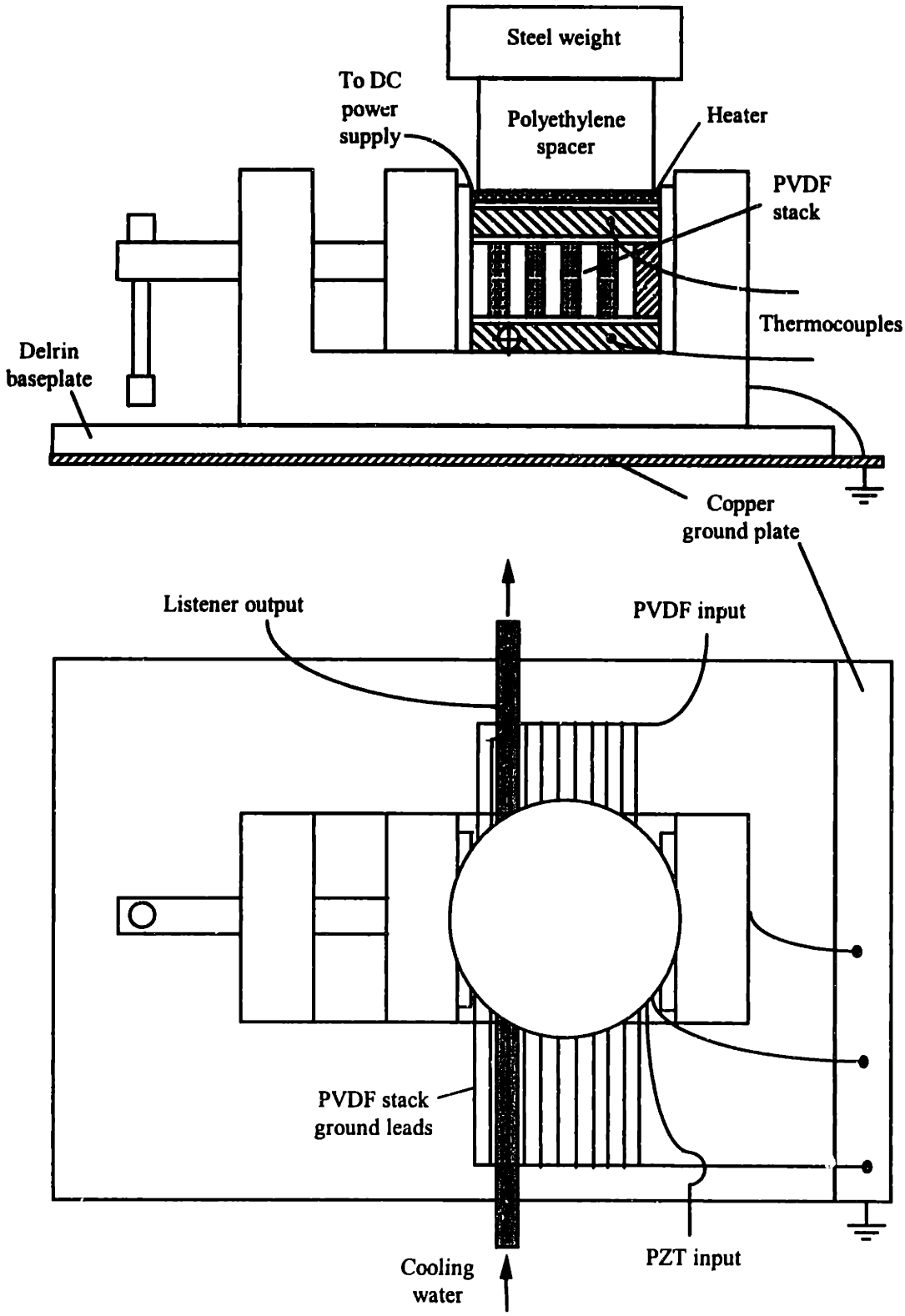

Figure 6.13. Schematic of the experimental setup

ground plate is attached to the bottom of the delrin plate and is connected to electrical ground. The vise and two copper blocks (heat sinks) are grounded by connecting them to the copper ground plate. To reduce the capacitive coupling between the listener stack and ten driver PVDF stacks, the positive leads are enclosed in electrically grounded copper tubings: one for the listener, and one for "drivers" (not shown in figure).

A Minco HK 5255 R31.6 thermofoil heater is connected to Thornton Associates, Inc., type 201B power supply. The power input is regulated by adjusting the voltage according to the required temperature level. The temperature of the cold heat sink is regulated by adjusting the cooling water volume flow rate.

The Hewlett Packard 33120A arbitrary waveform generator provides the input signal for the electrical circuit. The Crown DC 300A two channel audio amplifier is used to amplify the signal and separately regulate the gain on PZT and ten PVDF driver elements. The PZT is connected to the drive circuit through a 1 : 24 transformer board. The PVDF stack's input signal passes through the 1 : 5 transformer board and the L-C resonance circuit, described in section 6.3.

A Tektronix TDS 460A four channel digital oscilloscope is used to measure the amplitude and relative phase of the input signal on PZT and PVDF driver stacks and an output from the listener as a function of the driving frequency and applied temperature gradient.

6.6 Experimental Procedures and Results

All of the tests performed have a goal of searching for an anomalous response that might be related to the energy conversion mechanism. By varying the driving frequency and temperatures of cold and hot temperature sources it is hoped that the results of Strachan's experiments can be repeated and explained. The description of experimental procedures for different tests performed and results obtained during these tests are presented in this section.

Since for the half wave resonance the PVDF elements close to the ends of the stack experience higher strain and stress levels than those in the middle of the stack, element number 10 in generally taken to be a listener. The output signal amplitude and

relative phase measurements are performed by connecting the listener element to one of the channels of the Tektronix TDS 460A digital storage oscilloscope.

6.6.1. Low-Voltage Drive Testing

Low-voltage drive experiments are performed to measure the replica device performance and compare it with the predicted response. Two different test procedures are developed. One of these procedures, driving the stack with PZT only in the frequency range from 20 -75 kHz was described in Section 6.2.

The second testing procedure consists of driving both PZT and PVDF with low voltages, only up to 10 V, in wide frequency range with and without applied temperature gradient. A Hewlett Packard 33120A signal generator provides the drive signal in frequency range from 1 kHz - 2 MHz. The measurement of the output voltage drop on listener is performed for isothermal conditions (T = 23 °C) and with temperature gradient of 10.8 °C / mm. Several strong resonances are found at frequencies below 200 kHz. And the strongest resonance is found at 45 kHz. No significant differences are observed between frequency sweeps with an isothermal stack conditions and with the temperature gradient applied across the stack. The measured output voltage versus frequency for the stack with applied transverse temperature gradient of 10.8 °C/mm is shown in Figure 6.14.

6.6.2. Electrical Resonance Experiments

The experimental setup for electrical resonance experiments is shown in Figure 6.13. PZT and PVDF driver elements are connected to the drive circuit. The resonance frequency of the *L-C* circuit driving PVDF is adjusted to match the measured mechanical resonance frequency of the stack. The circuit assembled this way produces the constant input voltage on PZT independent of drive frequency and variable amplitude of the input signal on PVDF driver elements, while sweeping the frequency and passing through the resonance. The experiments are performed in frequency range from 35 - 70 kHz. The

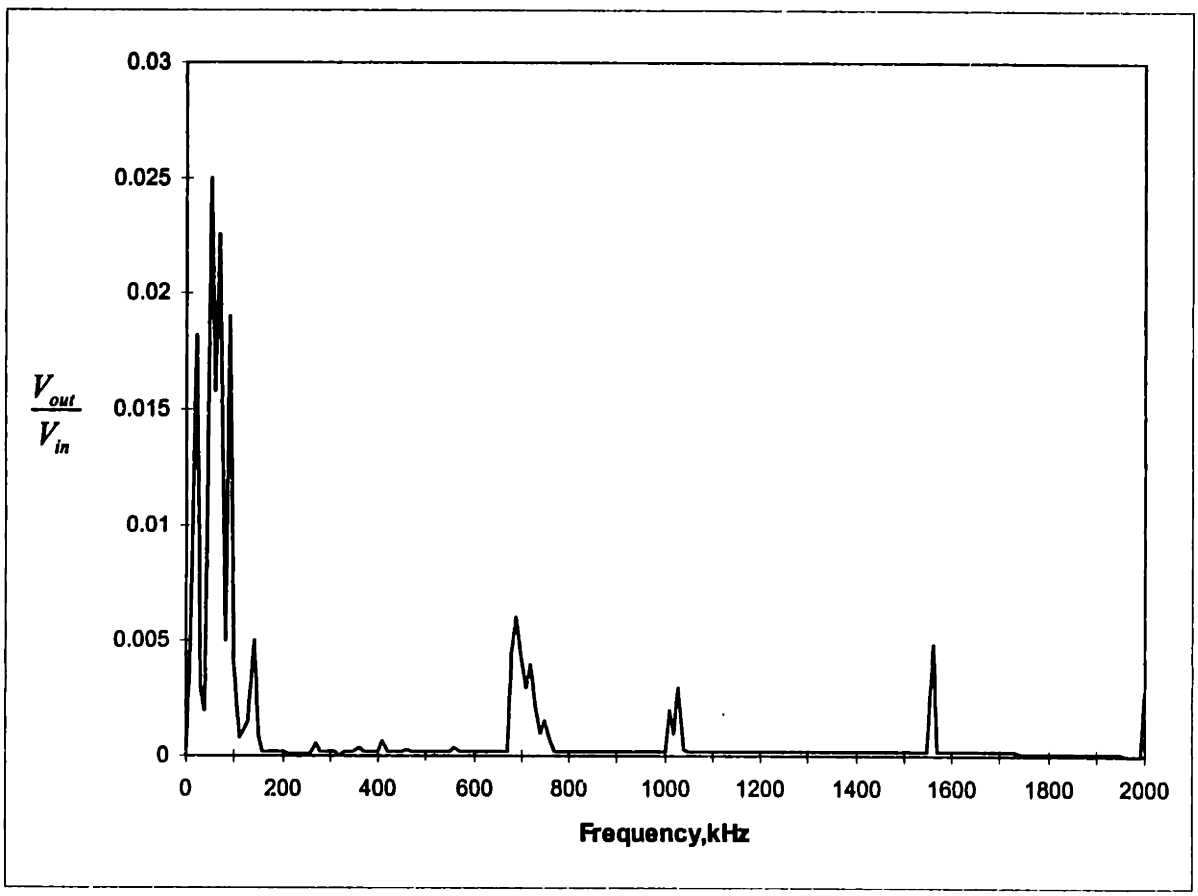

Figure 6.14 Measured $V_{listener} / V_{PZT}$ versus frequency for low voltage drive testing with applied transverse temperature gradient of 10.8 °C / mm.

stack is tested with isothermal conditions (T = 23 °C), and applied transverse temperature gradients of 26.8 °C /mm (T_C = 12.4 °C, T_H = 79.4 °C) and 10.8 °C/mm (T_C = 24.6 °C, T_H = 51.7 °C).

In addition, the measurements of the output voltage and phase angle are performed for the "shielded" listener (element 10). In this case, the two PVDF elements adjacent to the listener (elements 9 and 11) are grounded and not connected to the drive circuit, to reduce the capacitive coupling and electrical pickup by the listener. The results of these experiments are shown in Figures 6.15 and 6.16. The amplitude of the output signal in these figures is normalized with respect to voltage drop on PZT driver, since it can be kept approximately constant. The maximum voltage drop on PVDF driver elements, achieved in course of these experiments by introducing the resonance drive circuit, is $V_{PVDF,\ max}$ =1100 V and the maximum voltage drop on PZT after audio amplifier and transformer is $V_{PZT,\ max}$ = 520 V. No voltage spikes or other anomalous behavior in the PVDF stack is observed. No significant temperature dependence of the PVDF stack output voltage is found.

6.6.3 High-frequency testing

To test the replica device at higher frequency the high-voltage drive circuit consisting of Hewlett Packard model 33120A function generator, an Electronic Navigation Industries, Inc., model 310L RF power amplifier capable of working in frequency range from 250 kHz - 110 MHz and 1 : 24 custom made transformer is used to provide an input voltage up to 200 V. The measurements are performed at frequencies from 250 kHz-3 MHz . Several weak resonance are found in this range. The measured response is very similar to the response obtained using low-voltage drive setup, described in section 6.6.1. The biggest resonance at higher frequencies is found at f = 1.56 MHz, a frequency corresponding to a half-wave resonance in PZT driver.

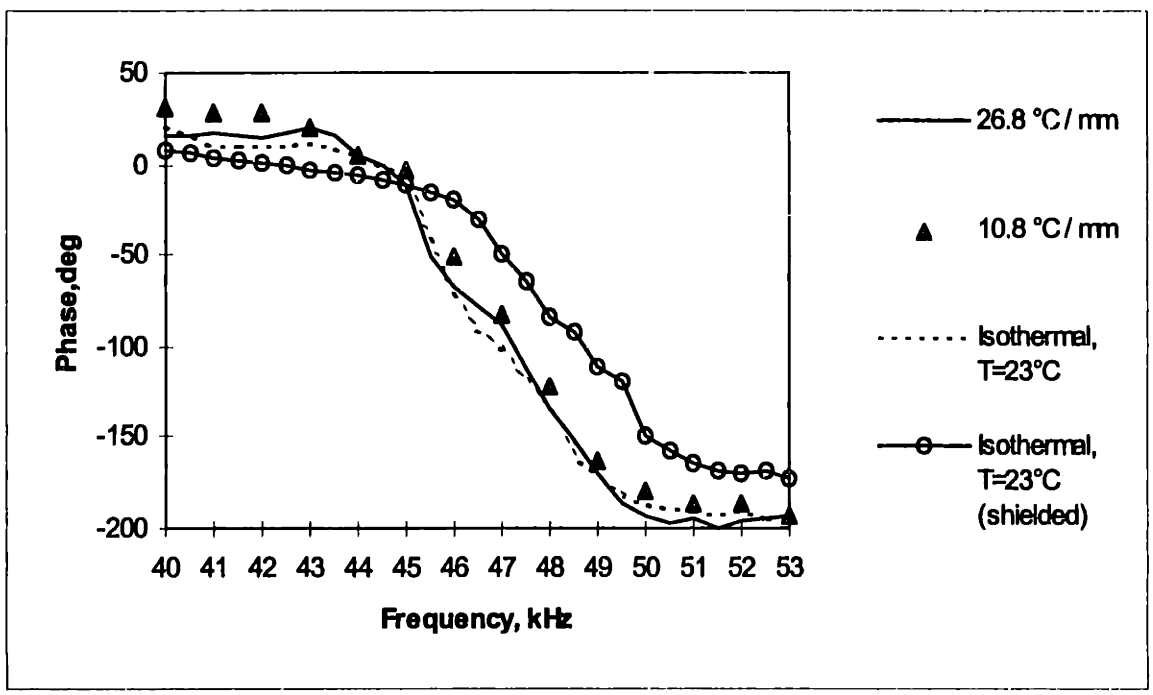

Figure 6.16. Measured phase difference between input and output signals versus frequency for different thermal boundary conditions

6.6.4 Measurement of Power Dissipation in Replica Device as Function of Applied Temperature Gradient

To find the temperature dependence of the dissipated power in the replica device the measurement setup similar to that used in electrical resonance tests, including the electrical circuit and temperature gradient assembly, is used. The driving frequency is adjusted to match the resonance frequency in the PVDF stack. The voltage drop across the stack is measured by Tektronix oscilloscope. The current is found by measuring the voltage drop across the 1 Ohm resistance included in circuit in series with the PVDF stack. The device dissipation power versus applied temperature gradient is shown in Figure 6.17. No significant temperature dependence of the replica device dissipation power is observed.

6.7. Summary

The simple one dimensional electro-mechanical model of the single PVDF layer behavior is constructed, completely ignoring thermal effects. The system response is calculated, based on this model. Series of experiments are performed, measuring the single PVDF layer response, and the results are compared with the response, given by piezoelectric model. A fairly good agreement of experimental results and the predicted response is observed. No significant difference between testing the PVDF layer with and without the temperature gradient is observed, which shows that thermal aspects have small impact on PVDF layer behavior.

The expected dynamic response of the device is calculated using one-dimensional mechanical model of the stack's behavior. The purpose of this model was to find the frequency range where the mechanical resonance in the stack combined with the electrical drive input would produce the highest excitation level in the stack. The measured and predicted primary resonance frequency are 45 and 46 kHz respectively.

A temperature gradient assembly is built to apply a transverse temperature gradient to the stack.

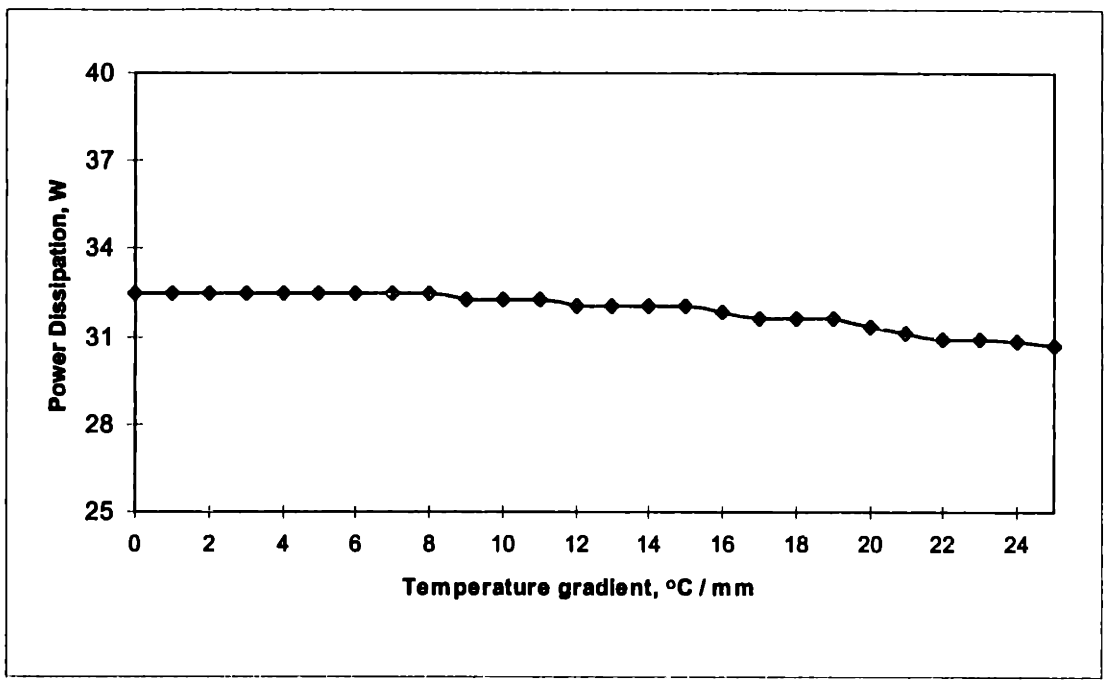

Figure 6.17 Measured dissipation power in the stack as function of applied temperature gradient

The low-voltage drive experiments are performed to measure stack's output voltage as function of frequency with and without applied temperature gradient. The results obtained from the low voltage tests are used to design the high amplitude voltage drive system, which is constructed in a way to be able to separately regulate the voltage and phase on PVDF stack and PZT driver in frequency range from 30 - 75 kHz.

High-voltage drive circuit is developed and a series of frequency sweeps are performed to test the performance of the Strachan-Aspden replica device, looking for the anomalous stack's behavior. The high-voltage drive circuit is designed in a way to provide for the separate regulation of the amplitude and phase angle of the input voltages on PVDF and PZT. The amplification of the input signal, driving PVDF, is made by matching the half wave acoustical resonance in the stack with the electrical resonance of *L-C* resonance circuit. The high-voltage drive circuit is capable of providing the input voltages on PVDF and PZT up to 1100 V and 520 V respectively in frequency range from 30 - 75 kHz. The device is tested at 23 °C and with 10.8 °C/mm and 26.8 °C/mm temperature gradients applied across the 2.5 mm stack dimension. No voltage spikes or other anomalous behavior is observed.

7. CONCLUSIONS

In this work the reported high efficiency energy conversion device of Strachan and Aspden was studied. The primary objective of the research was to build a replica of Strachan's device, find the evidence for the effect, investigate possible mechanisms and provide an explanation for the device operation.

For this thermo-elctro-mechanical device, there are two readily apparent mechanisms for energy conversion. The first is the thermoelectric action of the nickel-aluminum coating. The second is the energy conversion in the PVDF layers due to the piezo and pyroelectric qualities of the film. The orders of magnitude of these effects are estimated.

Aspden has attempted to explain the energy conversion phenomenon by postulating an "AC thermoelectric effect". His explanations are generally confusing and unconvincing. Calculations show that nickel-aluminum thermocouple in this temperature range can support the temperature difference of less then a degree between two junctions, although the results reported by Strachan and Aspden indicate the device performance with much higher temperature difference up to 70 °C.

The idea of the PVDF based engine or heat pump, utilizing the pyroelectric conversion cycle is theoretically possible. The pyroelectric energy conversion efficiency, however, is extremely low, typically less then 1%, and does not provide an explanation for energy conversion observed by Strachan.

Strachan and Aspden have also suggested that thermomagnetic or chemical effects might explain their observed effect. We have not considered these effects in this work.

The construction of the replica device was a result of numerous communications and correspondence with Strachan. The replica differed from first and third Strachan's devices in that it did not have a magnetic tape and a triggering circuit that would allow the device to self oscillate. Instead, it was powered by externally applied voltage. The structure of our stack and drive circuitry were similar to Strachan's second device. Our replica differed only from Strachan's second device in that it contained a PZT ceramic driver, a feature that was present in Strachan's first and third prototypes. All mechanical

connections in the stack were made with ethyl cyanoacrylate adhesive. We believe that the MIT replica device is a faithful reproduction of Strachan's prototypes.

The series of experiments performed with single PVDF layers and also with the two hundred layer PVDF stack did not show the energy conversion effect observed by Strachan. These tests showed that thermal effects seem to have little impact on PVDF device behavior.

If the Strachan-Aspden's energy conversion mechanism exists, then it is not clear why it could not be duplicated during the course of this study. We did not observe any of the high voltage pulses that Strachan reported. We also did not observe any effect that could not be explained by conventional theory. The models for the predicted response of the device based on thermoelectric, piezoelectric and pyroelectric effects in the stack and their influence on the device performance showed a good agreement with the experimental results.

No satisfactory explanation for the device operation has been revealed and none of the Strachan's results duplicated.

Appendix A. The Material Properties of the Device Componenets

Properties of Polyvinylidene Fluoride.

The relevant material properties of PVDF film are shown in Tables A.1 - A.2.

Symbol	Description	Numerical Value	Dimension
C	Capacitance	417	pF / cm^2
k	Thermal conductivity	0.13	W / m-K
Y	Young's modulus	2×10^9	N / m^2
Z_A	Acoustic impedance	2.7×10^6	kg / m^2-s
Z_E	Electrical impedance ($A=100cm^2$, $f=1$ kHz)	1000	Ohm
c_{11}	Elastic modulus	3×10^9	N / m^2
v_S	Velocity of sound	$1.5 - 2.2 \times 10^3$	m/s
ε	Permittivity	$(106\text{-}113) \times 10^{-12}$	F/m
$\varepsilon / \varepsilon_0$	Relative permittivity	12-13	-
μ	Dipole moment	6.9×10^{-30}	Coul-m
ρ	Density	1.78×10^3	kg / m^3
ρ_R	Volume resistivity	10^{13}	Ohm-meters
β	Volume thermal expansion	4.2×10^{-4}	1 / °C
tan δ	Loss tangent ($10 - 10^4$ Hz)	0.015-0.02	-
T_{max}	Maximum operating temperature	80 - 120	°C
V_{max}	Maximum operating voltage	30	V / μm
V_{break}	Breakdown voltage	100	V / μm

Table A.1. General Properties of PVDF (28 μm thick film).

Symbol	Description	Numerical Value	Dimension
d_{31}	Piezoelectric strain or charge constant	23×10^{-12}	$\frac{m/m}{V/m}$
d_{32}		3×10^{-12}	$\frac{m/m}{V/m}$
d_{33}		-33×10^{-12}	$\frac{m/m}{V/m}$
e_{31}	Piezoelectric stress or charge constant	69×10^{-3}	$\frac{Coul/m}{m//m}$
e_{32}		9×10^{-3}	$\frac{N/m^2}{V/m}$
e_{33}		-108×10^{-3}	$\frac{N/m}{V/m^2}$
g_{31}	Piezoelectric strain or voltage constant	216×10^{-3}	$\frac{N/m}{V/m^2}$
g_{32}		19×10^{-3}	$\frac{N/m}{V/m^2}$
g_{33}		-339×10^{-3}	$\frac{N/m}{V/m^2}$
k_{31}	Electromechanical coupling constant	12	%
k_{32}		1	%
k_{33}		19	%
p	Pyroelectric coefficient	-25×10^{-6}	$Coul/m^2{}^{\circ}K$

Table A.2. Piezoelectric and pyroelectric constants of PVDF

Properties of PZT ceramic.

The piezoelectric ceramic type PZT-5A is used as a mechanical driver. PZT-5A is a lead zirconate titanate with high sensitivity, permittivity and time stability.[26] It's typical thermoelectric properties are shown in Table A.3.

Symbol	Description	Numerical Value	Dimension
d_{31}	Piezoelectric strain or charge constant	-171	$\frac{m/m}{V/m}$
d_{33}		374	$\frac{m/m}{V/m}$
g_{31}	Piezoelectric strain or voltage constant	-11.4	$\frac{N/m}{V/m^2}$
g_{33}		24.8	$\frac{N/m}{V/m^2}$
k_{31}	Electromechanical coupling constant	-34	%
k_{33}		71	%
ρ	Density	7700	kg/m^3
ξ	Poisson's ratio	0.31	-
s^E_{11}	Elastic Constants, short circuit	16.4×10^{-12}	m^2/N
s^E_{33}		18.8×10^{-12}	m^2/N
s^D_{11}	Elastic Constants, open circuit	14.4×10^{-12}	m^2/N
s^D_{33}		9.4×10^{-12}	m^2/N

Table A.3. Electromechanical properties of PZT-5A. Adapted from Morgan Matroc, Inc.[26]

Acrylic Plates.

The cast acrylic sheet is used for the construction of the replica device. The acrylic material properties are shown in Table A.4.

Symbol	Description	Numerical Value	Dimension
T_{melt}	Melting temperature	95-110	°C
ρ	Density	1200	$\frac{kg}{m^3}$
v_s	Sound velocity	2700	$\frac{m}{s}$
Y	Young's modulus	3.1×10^3	$\frac{N}{m^2}$
β	Coefficient of linear thermal expansion	$50\text{-}90\times10^{-6}$	$\frac{1}{°C}$
K	Thermal conductivity	00.495	$\frac{W}{m\cdot K}$

Table A.4 Properties of cast acrylic .

Properties of Ethyl Cyanoacrylate adhesive.

The cyanoacrylate adhesives form strong bond with many materials without the need for heat or an added catalyst. They set very quickly when squeezed out to thin films between many types of adherents. The thinner the film, the stronger the bond and the faster the rate of bond formation. Most of cyanoacrylates are liquids of low viscosity which polymerize very easily in the presence of a slightly basic surface having on it absorbed water.[28]

ZAP CA super thin penetrating formula, from Pacers Technology, Inc. gave the thinnest and the strongest bond with PVDF. It's properties are shown in Table A.5.

Symbol	Description	Numerical Value	Dimension
μ	Viscosity range	$(2\text{-}5) \times 10^{-3}$	Pa-s
ρ	Density	1040	$\frac{kg}{m^3}$
T_{melt}	Melting Point	185	°C
n	Refractive Index	1.45	-
$\Delta L / L$	Elongation	2	%
t_C	Curing time	1-5	sec

Table A.5 Properties of ZAP CA ethyl cyanoacrylate adhesive.

Appendix B: Calculation of the Inductance for L-C Resonance Circuit

The inductance for L-C resonance circuit is made using series 6656 pot core assembly made of the series 3C8 ferrite material. The main advantages of the pot core assemblies are that because the wound coil is enclosed within the ferrite core, self - shielding prevents stray magnetic fields from entering or leaving the structure. They can be adjusted by moving a core in and out of the centerpost and the air gaps provide good thermal stability and high quality factor. The ferrite materials posses high resistivity that results in dense homogeneous magnetic medium with high permeability and extremely low eddy current losses over wide frequency range.

The mechanical and electrical characteristics of the series 6656 pot core are given in Table B.1.

The operating conditions of the inductance are limited by the values of PVDF stack resonance frequency and operation voltage, as given in Chapter 6. The inductance is designed for $f = 50$ kHz and $V = 1000$ V.

The dissipation power of the inductance is a strong function of the magnetic flux density. To have small value of the dissipation power and reasonable number of turns in the inductance the magnetic flux density is found to be B = 300 Gauss.

Core material		3C8	
Effective core area	A_e	7.15	cm^2
Effective core volume	V_e	88.3	cm^3
Magnetic path length	l_e	12.3	cm
Inductance index	A_L	0.0182 ± 25%	mH per $(\text{no. turns})^2$

Table B.1. Characteristics of the series 6656 pot core.

The number of turns is found from the Faraday law:

$$V = 4.44\, B\, A_e\, N f \times 10^{-8}, \qquad \text{(B.1)}$$

where 4.44 - coefficient for the sine wave,

A_e - effective core area in cm^2.

The number of turns found from (B.1):

$N = 210$

Then the lower limit of inductance with no air gap:

$$L = 0.75\, A_L\, N^2 = 601.96 \text{ mH} \qquad \text{(B.2)}$$

Increasing the air gap the inductance is adjusted to be L = 10 mH.

The impedance of the primary winding :

$$Z_{pri} = 2\pi f L = 3.142 \text{ Ohm}, \qquad \text{(B.3)}$$

that gives the current:

$$i_{pri} = \frac{V}{Z_{pri}} = 0.318 \text{ amp} \qquad \text{(B.4)}$$

To reduce eddy current losses in the primary winding 17 #32 gauge copper wires are used in parallel.

The resistance of the wires in the primary winding is

$$R_{pri} = \frac{N \cdot l_{mean} \cdot \rho_e}{17} = 0.81 \text{ Ohm} \qquad \text{(B.5)}$$

where l_{mean} = 0.13 m, is the mean length of the turn, and ρ_e = 0.531 Ohm / m is the resistivity of #32 gauge wire.

The dissipation in the primary winding :

$$P_{pri} = i_{pri}^2\, R_{pri} = 0.082 \text{ watt}$$

For the secondary winding the current is determined by the load capacitance:

$$i_{load} = 2\pi f C V = 0.314 \text{ amp}$$

The dissipation in the secondary winding :

$$P_{sec} = i_{load}^2\, R_{sec} = 0.4 \text{ watt}$$

To find the dissipation in the core material use the graph of the core loss vs. flux density for 3C8 ferrite material [31].

The core loss for f = 50 kHz and B = 300 Gauss is found to be 4 mW/cm^3, that corresponds to the dissipation power:

$$P_{core} = 4\frac{mW}{cm^3} \cdot V_e = 0.353 \text{ W}$$

The total dissipation power in the inductance:

$$P = P_{pri} + P_{sec} + P_{core} = 0.835 \text{ W},$$

which is small compared with the losses in the main circuit.

REFERENCES

1. Aspden, H., Strachan, J.S., 1993 " Solid State Thermoelectric Refrigeration ", *Proceedings of the 28th Intersociety Energy Conversion Engineering Conference,* August 8 - 13, 1993, Atlanta, Vol.1, pp. 891 - 896
2. Strachan, J.S., "A New Perspective on Thermoelectric Power Generation", *Speculations in Science and Technology,* Vol.13, No.4, pp. 289 - 293
3. Strachan, J.S., Private Communication to Charles Bullock, Carrier Corporation, February 9, 1994
4. Smith, J.L., Jr., 1994, Trip Report for Meeting with Harold Aspden and Scott Strachan on February 24,25, 1994.
5. Aspden H., Additional remarks supplementary to US Patent Application Serial No. 07 / 429,608, 15 October, 1990
6. Strachan, J.S., Private Communication to John G. Brisson, MIT, March 1, 1997
7. Smith, J.L., Jr., 1993, "Entropy Flow and Generation in Energy Conversion Systems", *Thermodynamics and the Design, Analysis and Improvement of Energy Systems,* AES - Vol.30, HTD - Vol.266, ASME Winter Annual Meeting, November 28 - December 3, 1993, New Orleans, LA, pp. 181 - 187.
8. Wang, H., Zhang,Q.M., Cross, L.E., Sykes, A.O., 1993, "Piezoelectric, Dielectric, and Elastic Properties of Poly(vinylidene Fluoride / Trifluoroethylene) ", *Journal of Applied Physics,* Vol.74, No.5, pp. 3394 - 3398
9. Marcus, M.A., 1981, "Ferroelectric Polymers and Their Applications", *Proceedings of the 5th International Meeting on Ferroelectricity at Pennsylvania State University,* August 17 - 21, 1981
10. Pollock, D.D., 1985, Thermoelectricity. Theory, Thermometry, Tool, ASTM Special Technical Publication 852.
11. Egli, P.H., 1960, Thermoelectricity, John Wiley & Sons, New York.
12. Rowe, D.M., ed., 1995, CRC Handbook of Thermoelectrics, CRC Press, Boca Raton, FL.

13 Aspden, H., 1993, "The Electronic Heat Engine", *Proceedings of the 27th Intersociety Energy Conversion Engineering Conference,* August 3-7, SanDiego, Vol. 4, pp. 357 - 363

14. Aspden, H., Strachan, J.S., 1992, "Electricity Without Magnetism", *Electronics World + Wireless World,* July 1992, pp. 540 - 542

15. Ikeda, Takuro, 1996, Fundamentals of Piezoelectricity, Oxford University Press, Oxford.

16. Goldsmid, H.J., 1960, Applications of Thermoelectricity, John Wiley & Sons, New York.

17. Goldsmid, H.J., 1986, Electronic Refrigeration, Pion Limited, London

18. Furukawa, T., Wen, J.X., Suzuki, K., Takashina, Y., Date, M., 1984, "Piezoelectricity and Pyroelectricity in Vinylidene Fluoride / Trifluoroethylene copolymers", *Journal of Applied Physics,* Vol.56, No.3, pp. 829-834

20. Mills A.F., 1995, Heat and Mass Transfer , Irwin, Inc., Chicago

21. Halliday D., Resnick R., 1962, *Physics for Students of Science and Engineering,* John Wiley and Sons, New York

22. Ohigashi, H., 1976, "Electromechanical Properties of Polarized Polyvinylidene Fluoride Films as Studied by the Piezoelectric Resonance Method", *Journal of Applied Physics,* Vol.47, No.3, pp. 949-955

23. Burkard, H., Pfister, G., 1974, "Reversible Pyroelectricity and Inverse Piezoelectricity in Polyvinylidene Fluoride", *Journal of Applied Physics,* Vol.45, No.8, pp. 3360-3364

24. Kepler, R.G., Anderson, R.A., 1978, "Piezoelectricity and Pyroelectricity in Polyvinylidene Fluoride", *Journal of Applied Physics,* Vol.49, No.8, pp. 4490-4494

25. KYNAR Piezo Film Technical Manual, Pennwalt, King of Prussia, PA

26. Das-Gupta, D.K., 1991, "Pyroelectricity in Polymers", *Ferroelectrics,* Vol.118, pp.165-189

27. *Guide to Modern Piezoelectric Ceramics,* Morgan Matroc, Inc., Bedford, OH

28. Landrock, A.H., 1985, Adhesives Technology Handbook, Noyes Publications, New Jersey.

29. Andreev, A.M., Donskaya, O.K., Kostenko, E.K., Mezenin, O.L., Sazhin, B.I., 1992, "Increasing the Energy Density of Capacitors by Introducing Polyvinylidene Fluoride in the Dielectric Structure", *Electrotechnika* , Vol.63, No1, pp. 52-54,

30. Linear Ferrite Materials and Components , 1984, Ferroxcube Facility, Division of Amperex Electronic Corporation, 7th edition.

31. Ferrite Cores for Power and Filter Applications , 1984, Magnetics, Division of Spang and Company.

32. Strachan, J.S., Aspden, H., 1991, "Thermoelectric Energy Conversion", US Patent No. 5,065,085

33. Strachan, J.S., Aspden, H., 1994, "Thermoelectric Energy Conversion", US Patent No. 5,288,336

34. MacBride, D.M., 1996, Investigations of a Potential High-Efficiency Thermo-electric Generator, M.S. Thesis, MIT

35. Lines, M.E., 1977, Principles and Applications of Ferroelectric and Related Materials, Clarendon Press, New York

36. Koga, K., Ohigashi, H., 1986, "Piezoelectricity and Related Properties of Vinylidene Fluoride and Trifluoroethylene Copolymers", *Journal of Applied Physics,* Vol. 59, No.6, pp. 2142 - 2150

37. Ohigashi, H., Koga, K., 1982, "Ferroelectric Copolymers of Vinylidenefluoride and Trifluoroethylene with a Large Electromechanical Coupling Factor", *Japanese Journal of Applied Physics,* Vol. 21, No.8, pp. L455 - L457

38. Brydson, J.A., 1989, Plastics Materials, 5th ed., Butterworths, London

39. Olsen, R.B., Evans B., 1983, "Pyroelectric Energy Conversion: Hysteresis loss and temperature Sensitivity of a Ferroelectric Material", *Journal of Applied Physics,* Vol. 54, No. 10 pp. 5941 - 5944

40. Bell, M.I., Tsuo, Y.H., 1979 Systematic Study of Pyroelectricity. Applications of Pyroelectric Materials, US Army Research & Development Command, Fort Monmouth, New Jersey.

41. Olsen, R.B., Bruno, D.A., Briscoe, J.M., Jacobs, E.W., 1985, "High Electric Resistivity and Pyroelectric Properties of Vinylidene Fluoride -Trifluoroethylene Copolymer", *Journal of Applied Physics,* Vol. 58, No. 8 pp. 5941 - 5944

42. Davis, G.T., 1993, "Piezoelectric and Pyroelectric Polymers", *Polymers For Electronic and Photonic Applications,* editor C.P. Wong, Academic Press, 1993

43. Jordan, R.C., Priester, G.B., 1948, Refrigeration and Air Conditioning, Prentice-Hall, Inc., New York

44. Heikes, R.R., Ure, R.W., Jr, 1961, *Thermoelectricity: Science and Engineering* , Interscience Publishers, New York - London

45. Ford, K.W., 1973, *Classical and Modern Physics , Vol 1-2* , Xerox College Publishing, Lexington, MA

46. Marks' Standard Handbook for Mechanical Engineers, 10th edition, editors Avalone E.A., T. Baumeister III, McGraw-Hill Inc., New York

47. Goldsmid, H.J., 1964, Thermoelectric Refrigeration, Plenum press, New York

48. Strachan, J.S., Aspden, H., "Strachan and Aspden Thermoelectric Device", Video.